THE PROCEEDINGS OF
THE PHYSICAL SOCIETY

Section A

VOL. 64, PART 8 | 1 August 1951 | No. 380 A

On θ Values in the Resistance of Metals

BY M. BLACKMAN
Physics Department, Imperial College, London

MS. received 13th April 1951

ABSTRACT. The θ value to be expected on the Bloch theory of the temperature dependence of the resistance of metals is shown to be much larger than that observed experimentally.

In a recent experimental work on the variation of the resistance of metals with temperature, MacDonald and Mendelssohn (1950) have determined the θ values, which we shall denote by θ_R, for the alkali metals using the Grüneisen (1933) function. For sodium, in particular, the T^5 law was found to hold at low temperatures as predicted by Bloch (1929). The θ_R value found is 202, while that derived from specific heat data, termed θ_D, is 150.

It is suggested that this θ_D value should be increased to 202 on the basis of Simon's (1926) theory of 'thermal quantum jumps'. The difference between the experimental θ_R value for lithium, 270, and that deduced by Simon, namely 512, is not considered. It should be pointed out that the elastic constants of sodium determined by Quimby and Siegel (1938) and by Bender (1937) lead to a θ value (termed θ_{el}) of about 140. This should equal the θ_D value at low temperatures, and the agreement between $\theta_D = 150$ and $\theta_{el} \simeq 140$ definitely disposes of the $\theta_D = 202$ value. In what follows we take $\theta_D = \theta_{el}$ as we shall be concerned with low temperatures.

An important point which needs emphasis is that *no agreement* is to be expected between the θ_D and θ_R values. The Bloch (1928) paper, and indeed all detailed accounts of Bloch's theory, make it perfectly clear that the only lattice vibrations which play a part in the resistance are the *longitudinal* waves. This is in marked contrast to what happens in specific heat theory, into which all vibrations enter. In fact, the θ_D value is determined in the main by the transverse vibrations.

It is surprising that, in experimental papers such as those of Grüneisen and others, it should be tacitly assumed that θ_D and θ_R should be identical. Even more surprising is that the same tacit assumption is made in theoretical papers, including, in some measure, Bloch's original paper.

On the Bloch theory we should expect $\theta_R = \theta_L$, where θ_L pertains to the longitudinal vibrations only. For an isotropic elastic medium this should be defined as

$$\theta_L = \frac{h}{k} c_L \left(\frac{3}{4\pi\Delta}\right)^{1/3},$$

where Δ is the volume per atom, c_L the 'longitudinal' velocity, h Planck's constant, and k Boltzmann's constant. For media with cubic symmetry $\rho c_L^2 = c_{11}$ where ρ is the density and c_{11} the 'longitudinal' elastic constant. This θ_L value is appreciably larger than the θ_D value. The latter, as mentioned above, can be calculated as θ_{el} from the elastic constants, where

$$\theta_D = \theta_{el} = \frac{h}{k}\bar{c}\left(\frac{9}{4\pi\Delta}\right)^{1/3}.$$

Here $\bar{c}$ is the mean wave velocity, which can be calculated from the elastic constants (see Born 1923). As examples we consider tungsten which is isotropic within experimental error, and aluminium which is nearly isotropic. In this latter case an average 'longitudinal' velocity is calculated, using the Born–von Karman (1913) method. The results of the calculation are: Al: $\theta_L = 707$, $\theta_D = 415$; W: $\theta_L = 636$, $\theta_D = 384$.

The Bloch theory assumes *inter alia* elastic isotropy and an isotropic Fermi distribution in momentum space. The latter assumption should be reasonably good for sodium, lithium and copper. The former does not hold at all well, though what is meant by 'elastic anisotropy' needs careful consideration. At any rate, we have to calculate, in these cases, an average c_L value.

A reasonable method of calculating an average c_L value would be

$$\frac{1}{\bar{c}_L^3} = \int \sum_j \frac{(\mathbf{S}_1 \cdot \mathbf{S}_2)^2}{c_j^3}\frac{d\Omega}{4\pi}, \qquad \ldots\ldots(1)$$

where $\mathbf{S}_1$ is a unit vector in the direction of the displacement associated with a wave in a crystal, and $\mathbf{S}_2$ a unit vector in the direction of propagation. The summation j is taken over the three types of waves, and $d\Omega$ is an infinitesimal solid angle. This form would be correct for the isotropic case, and also for the (purely hypothetical) special case of equal transverse and longitudinal velocities. Another method of averaging which is suggested by the Bloch T^5 low temperature law, is obtained by averaging c_j^{-5} instead of c_j^{-3}. These averages lead to θ_L values denoted by $\theta_L^{(3)}$, $\theta_L^{(5)}$ respectively.

Both methods of averaging were carried through for the three metals, sodium, lithium and copper, by solving numerically the cubic equation for the corresponding elastic media. The elastic constants used for sodium were those measured by Bender (1937), those for lithium and copper were taken from the work of Fuchs (1936). For symmetry reasons only an eighth of the total solid angle in (1) needs to be considered. This was divided into 90 equal sets. Each of these fixes a direction in space, and this, the three associated velocities. From these velocities the directions of the amplitude, associated with a wave travelling in the direction considered, are calculated.

Substance	$\theta_L^{(3)}$	$\theta_L^{(5)}$	θ_R
Na	282	260	202
Li	540	530	260
Cu	540	505	330

The disagreement is obvious, and is independent of the method of averaging. The detailed calculation shows that the main contribution to θ_L comes from only one of the three solutions of the elastic equations. This is mainly longitudinal in character and more isotropic (as the detailed calculations show) than the other two solutions which are mainly transverse in character. Further, the elastic

anisotropy (defined as the ratio of the maximum and the minimum value of the velocity for a particular type of solution), is smaller for copper than for sodium or lithium, yet the agreement between θ_L and θ_R is no better. When one remembers that the resistance of metals at low temperatures is proportional to θ_R^{-5}, the discrepancy shown above means a discrepancy of about five in the value of the resistance.

It appears from the above, that while there seems to be qualitative agreement between the Bloch theory and the experimental data, there are considerable quantitative discrepancies.

It is a rather curious empirical fact, established mainly by Grüneisen (see, for instance, Grüneisen 1933), that there is a remarkable correspondence between the θ_R and θ_D value for a large number of metals. It is true that the assumptions of the Bloch theory do not apply strictly to most of these cases; why the deviations from these assumptions should lead to $\theta_R \simeq \theta_D$ is a matter which is in great need of clarification. It has been one of the purposes of this paper to emphasize that this need exists.

ACKNOWLEDGMENT

I should like to express my thanks to Professor H. Jones for a number of very helpful discussions on the subject matter of this paper.

REFERENCES

BENDER, O., 1937, *Dissertation*, Marburg.
BORN, M., 1923, *Atomtheorie des festen Zustandes* (Berlin : Teubner).
BORN, M., and VON KARMAN, TH., 1913, *Phys. Z.*, **14**, 15.
BLOCH, F., 1928, *Z. Phys.*, **52**, 555; 1929, *Ibid.*, **59**, 208.
FUCHS, K., 1936, *Proc. Roy. Soc.* A, **153**, 622; **157**, 444.
GRÜNEISEN, E., 1933, *Ann. Phys., Lpz.*, **16**, 530.
MACDONALD, D. K. C., and MENDELSSOHN, K., 1950, *Proc. Roy. Soc.* A, **202**, 103.
QUIMBY, S. L., and SIEGEL, S., 1938, *Phys. Rev.*, **54**, 293.
SIMON, F., 1926, *S. B. Preuss. Akad. Wiss.*, **33**, 447.

Lattice Stability and Oriented Overgrowth

BY M. SMOLLETT AND M. BLACKMAN
Imperial College, London

MS. received 29th January 1951

ABSTRACT. The elastic constants of a two-dimensional ionic lattice, strained to fit on to the cube face of a substrate of the rocksalt type, are worked out. From these constants the stability conditions of the strained layer are deduced. These conditions are studied numerically in a number of selected cases where oriented overgrowth is observed in experiment. The calculations lead to conclusions which are in disagreement with a suggestion of Frank and van der Merwe as to the general mechanism of oriented overgrowth.

§ 1. INTRODUCTION

IN a series of papers Frank and van der Merwe (1949) have given a mathematical discussion of a theory of oriented overgrowth. In this theory oriented overgrowth is associated with an initial layer uniformly strained to fit the substrate; where this initial process is not possible the orientation is random.

The energy of a linear chain with quasi-elastic forces in a periodic potential field representing the substrate is compared in two cases: when the chain is strained

to fit the substrate, and when the chain contains dislocations. The authors find that the strained chain has the lower energy when the degree of misfit (defined by the relative difference in spacing) is less than 9%. Up to a larger critical misfit (about 14% in the above example) the monolayer can be deposited metastably in exact fit on the substrate at sufficiently low temperatures. Since according to Frank and van der Merwe the dislocated lattice is mobile on the surface, complete oriented overgrowth of one crystal on another is expected only if the first monolayer can be formed on the surface under 'sub-critical' conditions.

The above theory is claimed to be 'in general agreement' with experiment. The critical misfits of 9% or 14% are not strictly applicable to experimental cases, and it is assumed that a larger critical misfit can occur, for instance, in oxides. A particular case which is specifically quoted is that of zinc oxide (Cabrera and Mott 1949), where the misfit is 20%.

Such misfits involve remarkably high strains in the initial layer formed on the substrate. As it is known that strains of this order would be close to the theoretical elastic limit to which a crystal can be strained (see Zwicky 1923), it was decided to study the stability of a strained two-dimensional layer. In many cases the overgrowth consists of an alkali halide of the NaCl type, on a substrate of similar type. A two-dimensional ionic lattice, in arrangement similar to the (100) face of rocksalt, fitting on the (100) face of a selected alkali halide of the NaCl type, has therefore been chosen as a suitable model. To study the stability, the elastic constants of the two-dimensional layer are worked out in selected cases (Tables 2(*a*), 2(*b*)) where the layer is strained to fit the substrate. The effect of the substrate is taken into account. *In all these cases oriented overgrowth is observed in practice.* It will be shown that the strain leads to instability in all these cases, and hence the Frank–van der Merwe theory cannot account for these experimental results.

§ 2. THE STABILITY OF A TWO-DIMENSIONAL LATTICE

The equilibrium of two-dimensional lattices is considered in this work from the point of view of elastic stability with respect to small vibrations. The stability conditions which we shall use follow from the equations of motion of a two-dimensional 'regular' elastic medium, which can be written in the form

$$\left.\begin{aligned}[\rho\omega^2-\tau^2(c_{11}s_x^2+c_{44}s_y^2)]U_x-\tau^2(c_{12}+c_{44})s_xs_yU_y &= 0\\ -\tau^2(c_{12}+c_{44})s_xs_yU_x+[\rho\omega^2-\tau^2(c_{11}s_y^2+c_{44}s_x^2)]U_y &= 0.\end{aligned}\right\} \quad \ldots\ldots (1)$$

U_x, U_y are here the components of the amplitude $\mathbf{U}$ of a wave in the medium, the complete wave form being given by $\mathbf{U}\exp\{-i\tau(xs_x+ys_y)\}\exp(-i\omega t)$. The density of the medium is ρ, and its elastic constants are given by c_{11}, c_{12}, c_{44}, s_x, s_y are the components of a unit vector normal to the wave front, $\tau=2\pi/\lambda$ where λ is the wavelength, and ω is the angular frequency.

The conditions of stability may be deduced from (1), and these are (Blackman 1938) that $c_{11}>0$, $c_{11}-c_{12}>0$, $c_{44}>0$ for stability. If any of these expressions vanish or are negative, ω becomes imaginary and the medium is unstable. The stability problem reduces to the calculation of c_{11}, c_{12} and c_{44} for an ionic lattice of the type described in § 1, and then the determination of the vanishing points of $c_{11}-c_{12}$, c_{11} or c_{44}. Alternatively we can calculate for a specific case of a strained lattice, whether these quantities are positive, zero or negative, and hence deduce the stability.

§ 3. THE ELASTIC CONSTANTS

A method due to Born (1923) is used for the evaluation of the elastic constants. This proceeds by formulating the vibrational equation for the lattice and then specializing the equation for long wavelengths (and low frequencies). The limiting equations can then be identified with the equations of motion of the elastic continuum, and the elastic constants can then be calculated in terms of lattice sums. This procedure can be carried out for a uniformly strained lattice in the same way as for a lattice at equilibrium, and the equations of motion are formally the same. The only difference is that the Cauchy relation $c_{12}=c_{44}$ no longer holds in the case we are interested in, but we still obtain the equations (1) as the limiting equations.

The lattices we are dealing with contain, strictly speaking, two particles per cell. When the masses of the two particles are equal, we can work with one particle per cell if the repulsive forces between any pair of particles are taken to be independent of the type of particle. The equation of motion of the positively charged particle is then identical with that of the negatively charged particle. Further, as we are interested only in the long-wave limit of the equations of motion, and as these depend only on the mean mass of the particles (or the density), we can work with one particle per cell even when the masses are different, provided we use the mean mass M. The equations of motion will be correct in the limit we need, though not outside this limit.

We can now write the vibrational equations in a form similar to that given by Born (1923):

$$\left.\begin{aligned}(\omega^2 M+A_{xx})u_x+A_{xy}u_y &=0,\\ A_{xy}u_x+(\omega^2 M+A_{yy})u_y &=0,\end{aligned}\right\} \qquad \ldots\ldots(2)$$

where u_x, u_y are the components of the amplitude of a particle of mass M in the reference cell, and

$$A_{\alpha\beta}=\sum_{m_1 m_2}\phi_{\alpha\beta}^{m_1 m_2}\exp\{-i\tau(\mathbf{r}_{m_1 m_2}.\mathbf{s})\}. \qquad \ldots\ldots(3)$$

Here the summation m_1, m_2 extends over all cells, $\phi_{\alpha\beta}^{m_1 m_2}$ is the appropriate derivate of the potential energy ϕ of a pair of particles whose distance is $|\mathbf{r}_{m_1 m_2}|$. For the particular type of square lattice with which we are dealing $r_{m_1 m_2}^2=x_{m_1}^2+y_{m_2}^2$ with $x_{m_1}=m_1 r_0$, $y_{m_2}=m_2 r_0$ where r_0 is the lattice spacing and the m values are, of course, integral. The unit vector $\mathbf{s}$ specifies the direction of propagation of a plane wave in the lattice, ω is the angular frequency and $\tau=2\pi/\lambda$, where λ is the wavelength.

The coefficients $A_{\alpha\beta}$ are expanded for small values of τ. In equation (2) only the second order terms in s_x, s_y will be retained. The coefficients of these terms can then be directly related to the elastic constants in (1).

§ 4. LATTICE SUMS

The potential energy of a pair of particles in the lattice is written in the form $\phi(r)=\pm e^2/r+\beta/r^9$. The sign in the first term depends on whether the two particles have like or unlike charges. It is usual to split the lattice sums (3) into two parts, a 'Coulomb' part and one depending on the repulsive forces. These latter sums converge quickly and can be summed directly, while the Coulomb terms require a special technique.

A typical sum in (2) involving the Coulomb part of the potential has the form

$$A_{xx}^{(e)} = \sum_{m_1 m_2} (\phi^{(e)})_{xx}^{m_1 m_2} \exp[-i\tau(x_{m_1}s_x + y_{m_1}s_y)]$$

$$= \sum_{m_1 m_2} \pm \left(-\frac{e^2}{r_{m_1 m_2}^3} + \frac{3e^2 x_{m_1}^2}{r_{m_1 m_2}^5}\right) \exp[-i\tau(x_{m_1}s_x + y_{m_1}s_y)]. \quad \ldots\ldots(4)$$

Replacing x_{m_1} by $m_1 r_0$, y_{m_2} by $m_2 r_0$, and putting $\tau s_x r_0 = -2\pi h_1$, $\tau s_y r_0 = -2\pi h_2$, we can write the above in the form

$$A_{xx}^{(e)} = \frac{e^2}{r_0^3} \sum_{m_1 m_2} \frac{2m_1^2 - m_2^2}{(m_1^2 + m_2^2)^{5/2}} \exp[2\pi i\{m_1(h_1 + \tfrac{1}{2}) + m_2(h_2 + \tfrac{1}{2})\}], \quad \ldots\ldots(4a)$$

where the factor ± 1 is replaced by $\exp\{2\pi i(\frac{1}{2}m_1 + \frac{1}{2}m_2)\}$ and is incorporated into the exponential. Similarly

$$A_{xy}^{(e)} = \frac{3e^2}{r_0^3} \sum_{m_1 m_2} \frac{m_1 m_2}{(m_1^2 + m_2^2)^{5/2}} \exp[2\pi i\{m_1(h_1 + \tfrac{1}{2}) + m_2(h_2 + \tfrac{1}{2})\}]. \quad \ldots\ldots(4b)$$

Sums of the type given in (4 *a*) and (4 *b*) can be evaluated numerically with the help of the Epstein zeta functions (Epstein 1903, 1906) which are defined as

$$Z\begin{vmatrix} 0 & 0 \\ h_1 & h_2 \end{vmatrix}(s) = \sum_{m_1 m_2}{}' \frac{\exp\{2\pi i(m_1 h_1 + m_2 h_2)\}}{(m_1^2 + m_2^2)^{s/2}}, \quad \ldots\ldots(5)$$

where the prime indicates that the $(0, 0)$ term is excluded. It can then be shown that the zeta function we need can be expressed in the following form:

$$\pi^{-s/2}\Gamma\left(\frac{s}{2}\right) Z\begin{vmatrix} 0 & 0 \\ h_1 + \frac{1}{2} & h_2 + \frac{1}{2} \end{vmatrix}(s)$$

$$= -\frac{2}{s} + \int_1^\infty dz\, z^{(s-2)/2} \sum_{m_1 m_2}{}' \exp\{-\pi z[m_1^2 + m_2^2] + 2\pi i m_1(h_1 + \tfrac{1}{2}) + 2\pi i m_2(h_2 + \tfrac{1}{2})\}$$

$$+ \int_1^\infty dz\, z^{-s/2} \sum_{m_1 m_2} \exp\{-\pi z[(m_1 + h_1 + \tfrac{1}{2})^2 + (m_2 + h_2 + \tfrac{1}{2})^2]\} \quad \ldots\ldots(5a)$$

Here again the prime indicates that the $(0, 0)$ term is to be omitted; Γ denotes the usual gamma function; s is an integer, and the summation extends from $-\infty$ to $+\infty$. In the above form the summations are rapidly convergent.

The zeta function given above is not in the final form required for the sums occurring in (4 *a*), (4 *b*), which contain factors of the form $m_1^2, m_2^2, m_1 m_2$. These sums can be obtained by suitable partial differentiations with respect to h_1 or h_2. This is illustrated in (6):

$$\frac{\partial^2}{\partial h_1^2} Z\begin{vmatrix} 0 & 0 \\ h_1 + \frac{1}{2} & h_2 + \frac{1}{2} \end{vmatrix}(s) = -4\pi^2 \sum_{m_1 m_2}{}' \frac{m_1^2 \exp[2\pi i\{m_1(h_1 + \frac{1}{2}) + m_2(h_2 + \frac{1}{2})\}]}{(m_1^2 + m_2^2)^{s/2}}, \quad \ldots\ldots(6)$$

If we substitute $s = 5$ in equation (5 *a*) and carry out the differentiation as in (6) we find

$$\pi^{-5/2}\Gamma\left(\frac{5}{2}\right) \frac{\partial^2}{\partial h_1^2} Z\begin{vmatrix} 0 & 0 \\ h_1 + \frac{1}{2} & h_2 + \frac{1}{2} \end{vmatrix}(5)$$

$$= \int_1^\infty dz\, z^{3/2} \Sigma' - 4\pi^2 m_1^2 \exp[-\pi z(m_1^2 + m_2^2) + 2\pi i m_1(h_1 + \tfrac{1}{2}) + 2\pi i m_2(h_2 + \tfrac{1}{2})]$$

$$+ \int_1^\infty dz\, z^{-1/2} \Sigma 4\pi^2 (m_1 + h_1 + \tfrac{1}{2})^2 \exp[-\pi z\{(m_1 + h_1 + \tfrac{1}{2})^2 + (m_2 + h_2 + \tfrac{1}{2})^2\}]$$

$$+ \int_1^\infty dz\, z^{-3/2} \Sigma - 2\pi \exp[-\pi z\{(m_1 + h_1 + \tfrac{1}{2})^2 + (m_2 + h_2 + \tfrac{1}{2})^2\}]. \quad \ldots\ldots(7)$$

To obtain the terms needed in the approximation we need an expansion of this result up to the second order in h_1 and h_2. The terms which will interest us will be the second order terms. These are

$$\begin{aligned}
&h_1^2[\Sigma' 8\pi^4 m_1^4 \exp[\pi i(m_1+m_2)]F(\tfrac{3}{2};\ m_1;\ m_2)\\
&\quad+\Sigma 8\pi^4(m_1+\tfrac{1}{2})^4 F(\tfrac{3}{2};\ m_1+\tfrac{1}{2};\ m_2+\tfrac{1}{2})\\
&\quad+\Sigma -24\pi^3(m_1+\tfrac{1}{2})^2 F(\tfrac{1}{2};\ m_1+\tfrac{1}{2};\ m_2+\tfrac{1}{2})\\
&\quad+\Sigma 6\pi^2 F(-\tfrac{1}{2};\ m_1+\tfrac{1}{2};\ m_2+\tfrac{1}{2})]\\
&+h_2^2[\Sigma' 8\pi^4 m_1^2 m_2^2 \exp[\pi i(m_1+m_2)]F(\tfrac{3}{2};\ m_1;\ m_2)\\
&\quad+\Sigma 8\pi^4(m_1+\tfrac{1}{2})^2(m_2+\tfrac{1}{2})^2 F(\tfrac{3}{2};\ m_1+\tfrac{1}{2};\ m_2+\tfrac{1}{2})\\
&\quad+\Sigma -4\pi^3[(m_1+\tfrac{1}{2})^2+(m_2+\tfrac{1}{2})^2]F(\tfrac{1}{2};\ m_1+\tfrac{1}{2};\ m_2+\tfrac{1}{2})\\
&\quad+\Sigma 2\pi^2 F(-\tfrac{1}{2};\ m_1+\tfrac{1}{2};\ m_2+\tfrac{1}{2})], \qquad \ldots\ldots(7\,a)
\end{aligned}$$

where $F(n;\ x;\ y)=\int_1^\infty z^n \exp\{-\pi z(x^2+y^2)\}\,dz$.

We have indicated how to reduce a particular lattice sum to the required form. The integrals which occur in (7 *a*) can all be transformed to error functions, and the coefficients of h_1^2, h_2^2 are evaluated numerically without difficulty. In this way all the lattice sums can be dealt with.

§ 5. THE ELASTIC CONSTANTS

Collecting the electrostatic and repulsive terms together and comparing equation (2) with (1), the elastic constants are found to be

$$\left.\begin{aligned}
c_{11}&=-1{\cdot}45_6\frac{e^2}{r_0^3}+92{\cdot}0\frac{\beta}{r_0^{11}}, \qquad c_{12}=0{\cdot}22_5\frac{e^2}{r_0^3}+11{\cdot}7\frac{\beta}{r_0^{11}},\\
&\qquad c_{44}=1{\cdot}04_7\frac{e^2}{r_0^3}-7{\cdot}19\frac{\beta}{r_0^{11}}.
\end{aligned}\right\} \qquad \ldots\ldots(8)$$

These are valid for a stretched or compressed ionic lattice of the type described in § 1, where r_0 is the actual lattice spacing of the strained lattice.

The value of β has been calculated, where required, from the properties of the (three-dimensional) crystal, using the same assumption as above for the potential energy of a pair of particles. The equilibrium condition for the potential energy Φ of a crystal of the rocksalt type can then be expressed as

$$\frac{\partial\Phi}{\partial r}=0=N\left(\frac{Ae^2}{r^2}-\frac{9\beta B}{r10}\right) \quad \text{for} \quad r=d,$$

where N is the number of cells in the crystal, $A=1{\cdot}7476$, $B=6{\cdot}6288$. With the known equilibrium distance d, we find the value of β.

We next consider the effect of the substrate on the values of the elastic constants. In the calculation a positive ion in the strained lattice is assumed to be directly above a negative ion in the substrate, and a negative ion in the lattice to be above a positive ion in the substrate.

The method used for calculating the contribution of the substrate is similar to that given for the lattice. In this case, however, the summations in (2) are carried out between the particle in a reference cell in the lattice and those in all layers of the substrate. As far as the electrostatic part is concerned, the summation is carried out plane by plane, this summation being rapidly convergent. A brief account of the method is given in Appendix I. The distance of the lattice

from the substrate is found by working out the mutual potential energy and making this a minimum (Appendix II).

It should be noted that the substrate is treated as a fixed potential field. This may be justified by the fact that the contributions of the substrate are relatively small, as may be seen from Table 1. Only the Coulomb term contributions are considered, as the contributions to the repulsive terms are negligible in comparison.

In Table 1 $\Delta c_{44}^{(e)}$ and $\Delta(c_{11}-c_{12})^{(e)}$ are the contributions of the substrate to the value of c_{44} and of $(c_{11}-c_{12})$, these being electrostatic in nature, as explained above; $c_{44}^{(e)}$ and $(c_{11}-c_{12})^{(e)}$ are the electrostatic parts of the elastic constants given in (8). It should be noted that $\Delta c_{44}^{(e)}$ is always negative, so that it cannot assist the stability of the deposited layer. The contributions are given for various values of a where ar_0 is the distance of the strained lattice from the substrate, r_0 being the lattice spacing in the strained state. The values of a were chosen to suit experimental cases. It can be seen from the Table that the influence of the substrate diminishes rapidly as a becomes large.

Table 1

a	0·92	1·00	1·16	1·30	1·60	2·00
$\Delta c_{44}^{(e)}/c_{44}^{(e)}$	$-0{\cdot}22_4$	$-0{\cdot}18_8$	$-0{\cdot}12_9$	$-0{\cdot}08_2$	$-0{\cdot}06_1$	$-0{\cdot}00_8$
$\Delta(c_{11}-c_{12})^{(e)}/(c_{11}-c_{12})^{(e)}$	$+0{\cdot}13_1$	$+0{\cdot}10_1$	$+0{\cdot}05_6$	$+0{\cdot}03_1$	$+0{\cdot}02_3$	$+0{\cdot}00_5$

§ 6. LATTICE STABILITY

The effective elastic constants of the deposited layer (i.e. the strained lattice) are found by adding the contribution of the base to the ordinary elastic constants given in (8). These new constants are used in estimating the stability.

Calculations have been carried out for a number of cases where, in experiment, an alkali halide of the NaCl type is deposited on the cube face of an alkali halide substrate of this type. Whenever $(c_{44}+\Delta c_{44})$ or $(c_{11}-c_{12})+\Delta(c_{11}-c_{12})$ becomes negative, the deposit is unstable in accordance with the criteria given in § 2. It has been found that the c_{44} value vanishes first for a compression and the $(c_{11}-c_{12})$ value for an extension of the lattice, so that only those two expressions have been given in the tables. As will be seen below, in all the cases given in Tables 2(*a*) and 2(*b*), an oriented deposit is found in practice. The data on orientation are taken from van der Merwe (1949), except for the first case in Table 2(*a*), which was reported by Schulz (1950).

§ 7. DISCUSSION

We have evaluated above the elastic constants of a two-dimensional alkali halide layer strained to fit on to a substrate consisting of an alkali halide crystal. In each of the cases quoted in Tables 2(*a*) and 2(*b*) oriented growth is observed experimentally with the (100) face parallel to that of the cubic substrate.

Our theoretical calculations are designed to examine the dynamics of the uniformly strained lattice, treated statically by Frank and van der Merwe. In each of the examples investigated in Tables 2(*a*) and 2(*b*) instability is found in the initial deposited layer if this is strained to fit the substrate. We must therefore conclude that the orientation observed in experiment cannot arise from an initially uniformly strained layer. It seems reasonable therefore to suppose that orientation is associated with an initially 'distorted' lattice where by

'distortion' we mean any type of displacement of a lattice particle from its original position leaving the mean lattice spacing more or less constant.

Table 2 (*c*) has been included to show that our calculations will give dynamical stability in cases where orientation is found, and also in cases where orientation is not found. This should emphasize the point that stability of the type we have been discussing is a necessary but not a sufficient criterion. It is quite possible for a particular arrangement to be dynamically stable and yet to be far from the state of minimum free energy.

Table 2 (*a*)

S	D	C	a	c_{44}	Δc_{44}	Total	Stability	Θ
LiF	KBr	64	2·90	−12·21	0·00	−12·21	Unstable	+
NaCl	RbI	30	1·30	− 3·06	−0·42	− 3·48	Unstable	+
NaCl	KI	25	1·24	− 1·05	−0·45	− 1·50	Unstable	+

Table 2 (*b*)

S	D	E	a	$(c_{11}-c_{12})$	$\Delta(c_{11}-c_{12})$	Total	Stability	Θ
KCl	LiBr	13	0·96	−2·81	+0·65	−2·16	Unstable	+
KCl	AgCl	12	0·92	−2·65	+0·71	−1·94	Unstable	+
KCl	NaCl	10	0·93	−2·25	+0·68	−1·57	Unstable	+

Table 2 (*c*)

S	D	C	a	c_{44}	Δc_{44}	Total	Stability	Θ
NaCl	KBr	17	1·16	1·35	−0·59	0·76	Stable	+
KCl	RbI	17	1·16	1·14	−0·43	0·71	Stable	+
NaCl	NaI	15	1·17	1·86	−0·56	1·30	Stable	+
NaCl	RbCl	17	1·18	1·54	−0·59	0·95	Stable	−

S, substrate crystal; D, deposited growth; C, percentage misfit for a compression; E, percentage misfit for an extension. The elastic constants are given in units of $10^{22}e^2$ (dyne/cm.). Θ, orientation found in experiment; +, orientation present; −, no orientation.

It should further be pointed out that though Frank and van der Merwe (1949) claim agreement between theory and experiment on the basis of van der Merwe's review (1949), other reviews of the evidence on oriented growth (Thomson and Cochrane 1938, Thomson 1949) do not show any marked preference for the view that a critical degree of misfit is the deciding factor between complete and random orientation.

Nor is it clear how the idea of critical misfit explains the temperature dependence of the orientation of evaporated layers. For instance, in the case of silver evaporated on to rocksalt at low temperatures a random orientation is observed, while at about 150° c. silver will give a (100) orientation on the cube face of rocksalt (Bruck 1936). Further, in some cases orientation changes with temperature (see Thomson and Cochrane 1938); the orientation is definite above and below certain temperatures, but it passes through a partially oriented phase in the intermediate region. This again is difficult to reconcile with a critical misfit criterion.

The Frank–van der Merwe hypothesis has also been applied (Cabrera and Mott 1949) to chemical growth, using the idea that in oriented chemical growth the first layer (or layers) has the same spacing as the substrate. This concept is

applied particularly to oxide films, but presumably the theory is intended to be general. The main experimental evidence adduced is the pseudomorphic zinc oxide structure found on zinc by Finch and Quarrell (1933, 1934). However, a recent investigation (Raether 1950) has been made of the structure of the thin protective zinc oxide layer on the cleavage face of a single crystal of zinc. The oxide is found to have the normal structure, though this should be a very favourable case in which to observe the pseudomorphic form. The results of Raether are in agreement with independent work carried out at the Imperial College by Mr. L. N. D. Lucas.

A large number of investigations has been made on the growth of compounds on single crystals using the electron diffraction technique. The general rule is that the overgrowth has the normal crystal structure. This point could be studied in more detail if crystals with flat surfaces (produced by cleaving, electrolytic polishing or thermal etching) were used. With these surfaces layers of from five to ten atomic spacings should produce an observable pattern. It should then be possible to decide whether structures differing from the normal structure play a part in the mechanism of chemical growth or in the general process of oriented overgrowth.

ACKNOWLEDGMENTS

One of us (M.S.) wishes to thank the Department of Scientific and Industrial Research for a research grant. We should like to thank Professor Sir George Thomson for his interest and for his comments on this work.

APPENDIX I

When calculating the effect of the substrate, the additional contributions appear in the form given below. The expression for Δc_{11} is given as an example:

$$\Delta c_{11}=\frac{e^2}{2r_0{}^3}\sum_{m_1 m_2}\sum_{b}\frac{m_1{}^2\exp\{\pi i(m_1+m_2)\}}{(m_1{}^2+m_2{}^2+b^2)^{3/2}}-\frac{3e^2}{2r_0{}^3}\sum_{m_1 m_2}\sum_{b}\frac{m_1{}^4\exp\{\pi i(m_1+m_2)\}}{(m_1{}^2+m_2{}^2+b^2)^{5/2}}.$$

Here m_1 and m_2 refer to lattice points in the planes of the substrate; br_0 is the distance of a substrate plane from the particle in the cell which is taken as origin. The summation takes place over all m_1, m_2 and b. To evaluate the above sums which contain b we use a modified function which is defined by

$$Z\begin{vmatrix}0 & 0\\ h_1+\frac{1}{2} & h_2+\frac{1}{2}\end{vmatrix}(s,b)=\sum_{m_1 m_2}\frac{\exp[2\pi i\{m_1(h_1+\frac{1}{2})+m_2(h_2+1)\}]}{(m_1{}^2+m_2{}^2+b^2)^{s/2}}$$

and this zeta function can be expressed in the form

$$\pi^{-s/2}\Gamma\left(\frac{s}{2}\right)Z\begin{vmatrix}0 & 0\\ h_1+\frac{1}{2} & h_2+\frac{1}{2}\end{vmatrix}(s,b)$$

$$=\int_1^\infty dz\, z^{(s-2)/2}\exp(-\pi b^2 z)\sum_{m_1 m_2}\exp[-\pi z(m_1{}^2+m_2{}^2)+2\pi i\{m_1(h_1+\tfrac{1}{2})+m_2(h_2+1)\}]$$

$$+\int_1^\infty dz\, z^{-s/2}\sum_{m_1 m_2}\exp(-\pi b^2/z)\exp[-\pi z\{(m_1+h_1+\tfrac{1}{2})^2+(m_2+h_2+\tfrac{1}{2})^2\}].$$

This form enables us to compute the sums in the expression for Δc_{11}. The second integral cannot be reduced to an error function and must be calculated numerically.

APPENDIX II

To evaluate the distance of the stretched lattice from the substrate we form the potential energy of a representative particle in the lattice in the potential field of the substrate. The minimum value of this energy is found as a function of a. The form of the potential energy used for the Coulomb terms is (see Born 1923, p. 738)

$$-\frac{8e^2}{r_0}\sum_{m_1 m_2}\sum_{b}\frac{\exp\{-\pi b(m_1^2+m_2^2)^{1/2}\}}{(m_1^2+m_2^2)^{1/2}},$$

where the summation is over all positive odd values of m_1, m_2 and over all values of b which varies from plane to plane. The potential energy for the repulsive forces is

$$\frac{\beta}{r_0^9}\sum_{m_1 m_2}\sum_{b}(m_1^2+m_2^2+b^2)^{-9/2}$$

where the summation is over all integral values of m_1 and m_2 from $-\infty$ to $+\infty$. The quantity b takes the values a, $a+1$, $a+2$ etc. The value of β in the preceding equation is taken as the mean of the values for the substrate and the deposit.

REFERENCES

BLACKMAN, M., 1938, *Proc. Roy. Soc.* A, **164,** 62.

BORN, M., 1923, *Atomtheorie des festen Zustandes* (Berlin : Teubner).

BRUCK, L., 1936, *Ann. Phys., Lpz.*, **26,** 233.

CABRERA, N., and MOTT, N. F., 1949, *Rep. Prog. Phys.*, **12,** 163 (London : Physical Society).

EPSTEIN, P., 1903, *Math. Ann.*, **56,** 615; 1906, *Ibid.*, **63,** 205.

FINCH, G. I., and QUARRELL, A. G., 1933, *Proc. Roy. Soc.* A, **141,** 398; 1934, *Proc. Phys. Soc.*, **46,** 148.

FRANK, F. C., and VAN DER MERWE, J. H., 1949, *Proc. Roy. Soc.* A, **198,** 205, **200,** 125.

VAN DER MERWE, J. H., 1949, *Disc. Faraday Soc.*, **5,** 201.

RAETHER, H., 1950, *J. Phys. Radium*, **2,** 11.

SCHULZ, L. G., 1950, *Phys. Rev.*, **78,** 638.

THOMSON, G. P., 1948, *Proc. Phys. Soc.* A, **61,** 403.

THOMSON, G. P., and COCHRANE, W., 1938, *Theory and Practice of Electron Diffraction* (London : Macmillan).

ZWICKY, F., 1923, *Phys. Z.*, **24,** 131.

Some New Bitter Patterns on a Single Crystal of Nickel

BY L. F. BATES AND G. W. WILSON

Department of Physics, University of Nottingham

MS. received 9th April 1951

ABSTRACT. Some new Bitter figures have been obtained on a single crystal of nickel whose surface is a (111) plane when magnetized along a [110] direction, and a curve obtained of domain boundary spacing as a function of the effective magnetic field. Patterns of a complex nature, probably due to closure domains, were also obtained on a (112) plane.

§ 1. INTRODUCTION

THE present work was undertaken to extend our knowledge of the domain magnetization processes undergone by a single crystal of nickel when a magnetic field of varying intensity was applied to it. Much work has been done using the technique originated by Bitter (1932); most of it, however, has been

devoted to the magnetic properties and domain structures of crystals of silicon–iron, notably by Bozorth, Williams and Shockley (1949), and by Bates and Neale (1950). Nickel is of particular interest and difficulty because it possesses eight crystallographic directions—the [111] or trigonal axes, which are easy directions of magnetization, while iron and silicon–iron possess only six—the [100] or tetragonal axes.

Kaya and Sekiya (1935) published a paper containing some beautiful photographs showing powder patterns they had obtained on (100), (110) and (111) planes in nickel. Their method of preparation of the surface was, however, likely to result in strain, and as was found in the present work, this affects the nature of the powder patterns obtained very considerably. Indeed, on account of the large magnetostriction coefficient of nickel, the greatest care must be taken throughout the preparation and manipulation of the specimen to avoid distortion.

§2. PREPARATION OF THE SPECIMEN

The crystal was cut into the form of a slab having approximate dimensions 15 mm. × 5 mm. × 3 mm. Its main surface was approximately parallel to a (111) plane, and its sides roughly parallel to a [110] direction forming (112) planes.

It was mounted in a specially designed holder and the orientations of the required crystallographic planes and directions relative to the surfaces cut were found with an x-ray goniometer. The crystal surfaces were then carefully ground on a high-speed emery wheel so that they corresponded, within three degrees, to the required atomic planes. During this part of the preparation care was taken that the specimen never became unduly warm, in order to keep distortion and disturbance of the crystal to a minimum.

The surfaces were then polished mechanically on emery papers down to 0000. This removed the layer of disturbed metal produced during the cutting and grinding processes but left in its turn a thin polycrystalline Beilby layer which was covered with very fine scratches. To remove both and expose the true crystal surface, the specimen was polished electrolytically (Bates and Mee 1950) in a solution consisting of 100 cm^3 of orthophosphoric acid, 25 cm^3 of sulphuric acid and 75 cm^3 of distilled water. This electrolyte was best used at a temperature of 40–50° c. in an inverted-bottle type of cell. The specimen formed the anode and was surrounded by a cylindrical iron cathode. A current density of 1 amp/cm^2 of anode surface was employed, and a polishing time of from three to four minutes was required to remove the scratches.

To remove strains the specimen was annealed *in vacuo* at 900° c. for about two hours and then cooled slowly at the rate of 120° c/hour. The importance of doing this is shown by the unusual 'maze' pattern, obtained on the surface before annealing, shown in Figure 1 (*a*) (Plate *).

The crystal specimen was placed in a horizontal field between the pole pieces of a small electromagnet of special design, giving but little stray field in a vertical direction. The pole-pieces were of similar shape to those used by Bozorth, Williams and Shockley (1949) in their work on silicon–iron. The figures were made manifest with a colloidal suspension of magnetite in soap solution, developed by Elmore (1938).

* For Plates see end of issue.

§ 3. EXPERIMENTAL PROCEDURE

To remove the effect of stray magnetic fields encountered during the preparation of the specimen it was first saturated by passing a heavy current through the electromagnet coils and then carefully demagnetized by reversals. On placing colloid on the crystal, no pattern was observed while it was in a demagnetized state, but on applying magnetic fields of gradually increasing intensity powder patterns were obtained. Preliminary experiments on a single crystal disc whose equatorial plane was a (111) surface showed that patterns were only obtained when a field was applied along a [110] direction (face diagonal).

The patterns obtained were straight lines perpendicular to the direction of the applied field. Examples of these patterns are given in Figures 1 (*b*), (*c*) and (*d*). The spacing of these lines was sufficiently regular to enable some quantitative measurements of the line spacing to be made. The spacing varied in a regular manner as the applied field was altered. Before each measurement of a spacing the crystal was carefully demagnetized by reversals and then put into the cyclic state corresponding to the required field value.

Graph (*a*) of Figure 2 shows the variation of line spacing with strength of the effective magnetic field, measured by a magnetic potentiometer. It will be seen that it bears a marked resemblance to the Néel (1944) case for a single crystal of iron, in the form of a slab bounded by (100) and (110) planes with a magnetic field applied along a [110] direction. No useful patterns of any regularity were observed when a magnetic field was applied in a vertical direction.

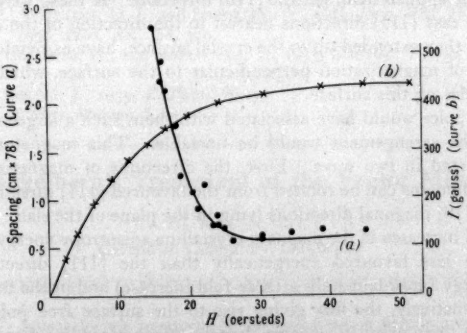

Figure 2. (*a*) Graph of line spacing against applied magnetic field. (*b*) *I*, *H* curve for nickel crystal strip, (111) plane, [110] direction of magnetization.

Colloid was also applied to a polished (112) plane on the side of the above crystal and patterns obtained. These were rather more complex in nature (Figure 1 (*e*)). As can be seen from some of the accompanying photographs, at relatively low values of the applied magnetic field the lines appear very broad, with side branches parallel to the field. As the field is increased the lines become more definite and also move closer together, following the lines on the (111) plane. A peculiar branching of the powder lines can be seen at a crystal boundary on one of the photographs, Figure 1 (*f*), and it is thought that this may be due to surface closure domains. If this is correct, closure domains will be formed on both (111) and (112) planes; that these closure domains are likely

from the energetic point of view can be shown by energy considerations given below.

The magnetization curve for the crystal was obtained experimentally. The effective field acting on the crystal was measured directly by a very small magnetic potentiometer in series with a sensitive Tinsley galvanometer, a standard mutual inductance being used for calibration purposes. The intensity of magnetization was found by using a search coil wound directly on the specimen itself. As can be seen by comparing graph (*b*) of Figure 2 obtained in this way with that of Honda *et al.* (1935), the measured intensity of magnetization is somewhat lower than that generally accepted. This may perhaps be explained by assuming that the most stable domain configuration corresponding to any particular value of the magnetic field takes time to form.

§ 4. DISCUSSION OF RESULTS

Nickel has eight directions of easy magnetization—the [111] body diagonals of the face-centred cubic lattice. The portion of the magnetization curve over which the patterns appear suggests that it is a two-phase region (Néel 1944). This will extend from the main knee of the magnetization curve towards saturation. Now the (111) plane has no easy direction of magnetization in it: the nearest makes an angle of approximately 20° with the surface and an angle of 35° with the applied magnetic field. Thus if the crystal is divided into domains, as the powder patterns suggest, these will be in the form of sheets perpendicular to the direction of the applied field, i.e. the [110] direction. If these were magnetized along the two easy [111] directions nearest to the direction of the applied field, they would, if they extended up to the crystal surface, have associated with them a component of magnetization perpendicular to the surface, which would give rise to free poles on this surface.

Such free poles would have associated with them such a large magnetostatic energy that the arrangement would be unstable. This magnetostatic energy can be eliminated in two ways. First, the directions of magnetization of the fundamental domains can be rotated from the favoured [111] directions into two of the three [110] diagonal directions lying in the plane of the slab. This would result in small increases in the magneto-crystalline anisotropy energy as the [110] directions are less favoured energetically than the [111] directions in the boundary energy (approximately a three-fold increase) and in the magnetic field energy. Alternatively, the flux giving rise to the surface free poles could be closed through small prismatic closure domains magnetized in a direction parallel to the applied field. The latter suggestion is more in agreement with observation, for reversal of the field direction does not seem to affect the position of the patterns. The rotation of the magnetization vector involved in traversing the boundary between a fundamental domain and a closure domain is small and the wall energy of such a domain is also small.

As can be seen from the photographs, the patterns formed on nickel are rather thin and diffuse compared with those found on cobalt or iron. For this there may be two reasons. First, the magneto-crystalline anisotropy constant of nickel is small ($-5{\cdot}1 \times 10^4$ ergs/cm^3 as compared with $4{\cdot}2 \times 10^5$ ergs/cm^3 and $4{\cdot}1 \times 10^6$ ergs/cm^3 for iron and cobalt respectively). Consequently a domain boundary is considerably thicker and the gradient of H_s^2 (where H_s is the stray surface field) is less and the attraction on the colloid particles is much reduced.

Secondly, the intensity of magnetization of nickel is less than that of iron or cobalt (500 against 1,700 and 1,400 E.M.U/cm^3), and, as it is the component of the magnetization in a vertical direction at the domain interface which gives rise to the stray field H_s, this results in a further reduction of the forces attracting the colloid to the domain boundaries.

Unfortunately, because of the weakness of the stray fields existing at the surface of a nickel crystal, none of the techniques so far used to ascertain the directions of magnetization of the surface domains, e.g. the scratch, colloid striation or magnetic probe techniques, gave conclusive results. Hence at the moment one cannot safely decide which of the two domain arrangements suggested above is the more correct.

ACKNOWLEDGMENTS

We are indebted to Dr. H. H. Potter for the kind provision of nickel crystals and to Mr. S. C. Wallwork for help with the x-ray measurements. We are greatly indebted to the British Electrical and Allied Industries Research Association for the financial support which has made this work possible, and we record our thanks to the Director for permission to publish.

REFERENCES

BATES, L. F., and MEE, C. D., 1950, *J. Sci. Instrum.*, **27**, 317.
BATES, L. F., and NEALE, F. E., 1950, *Proc. Phys. Soc.* A, **63**, 374.
BITTER, F., 1932, *Phys. Rev.*, **41**, 507.
BOZORTH, R. M., WILLIAMS, H. J., and SHOCKLEY, W., 1949, *Phys. Rev.*, **75**, 155.
ELMORE, W. C., 1938, *Phys. Rev.*, **54**, 309.
HONDA, K., MASUMAOTO, H., and SHIRAKAWA, Y., 1935, *Sci. Rep. Tôhoku Imp. Univ.*, **24**, 291.
KAYA, S., and SEKIYA, J., 1935, *Z. Phys.*, **96**, 53.
NÉEL, L., 1944, *J. Phys. Radium*, **5**, 241.

On Stueckelberg's Treatment of the Vector Meson Field

BY SURAJ N. GUPTA*
Cavendish Laboratory, Cambridge

Communicated by N. Kemmer; *MS. received* 22nd *March* 1951

ABSTRACT. Stueckelberg's treatment of the vector meson field is investigated, and is found to involve difficulties similar to those of Fermi's treatment of the radiation field. It is shown that these difficulties may be removed by the same procedure as has already been applied to the radiation field in an earlier paper, which involves the use of an indefinite metric and a modification of the supplementary condition.

§1. INTRODUCTION

IT has been shown by Stueckelberg (1938) that vector mesons may be treated in very much the same way as the radiation field. Stueckelberg's treatment seems to have some advantages, but it involves the same difficulties as appear in Fermi's treatment of the radiation field, according to which one cannot find a normalized state satisfying the supplementary condition, and

* State Scholar of the Government of India.

therefore one cannot define the state of vacuum in an entirely satisfactory way (Ma 1949, Belinfante 1949). Recently the present writer (Gupta 1950) has shown that the difficulties in the quantization of the radiation field may be removed by using an indefinite metric and modifying the supplementary condition, and here it is proposed to show that the same procedure may also be applied to Stueckelberg's form of the meson theory. It must, however, be admitted that the difficulties to be treated in this paper are by no means as serious as those of the radiation field. For, instead of Stueckelberg's treatment one can always use the usual form of the theory given by Kemmer and others (Kemmer 1938), which does not involve any such difficulty.

We shall throughout follow the same treatment as has been applied to the radiation field in the earlier paper (Gupta 1950), which will here be referred to as I. Moreover, we shall consider only the neutral meson field, for the charged field may be treated in a similar way.

§2. FIELD EQUATIONS FOR THE VECTOR MESONS

According to Stueckelberg (see Pauli 1941) vector mesons may be described by means of two auxiliary fields $A_\mu(x)$ and $B(x)$ satisfying the field equations

$$(\Box^2-\kappa^2)A_\mu(x)=0, \quad (\Box^2-\kappa^2)B(x)=0, \qquad \ldots\ldots(1)$$

and subject to the supplementary condition

$$\left(\frac{\partial A_\mu}{\partial x_\mu}+\kappa B\right)\Psi=0. \qquad \ldots\ldots(2)$$

The field equations (1) can be derived from the Lagrangian density

$$L=-\frac{1}{2}\left\{\left(\frac{\partial A_\mu}{\partial x_\nu}\right)^2+\kappa^2 A_\mu{}^2+\left(\frac{\partial B}{\partial x_\nu}\right)^2+\kappa^2 B^2\right\}, \qquad \ldots\ldots(3)$$

which gives for the Hamiltonian density

$$H=\frac{\partial A_\mu}{\partial t}\frac{\partial A_\mu}{\partial t}+\frac{\partial B}{\partial t}\frac{\partial B}{\partial t}-L. \qquad \ldots\ldots(4)$$

One also obtains for the commutation relations in the usual way:

$$[A_\mu(x),\ A_\nu(x')]=i\delta_{\mu\nu}\Delta(x-x') \qquad \ldots\ldots(5)$$

$$[B(x),\ B(x')]=i\Delta(x-x'), \qquad \ldots\ldots(6)$$

where the function $\Delta(x-x')$ has been defined by Schwinger (1949).

If we now define a field operator U_μ as

$$U_\mu=A_\mu+\frac{1}{\kappa}\frac{\partial B}{\partial x_\mu}, \qquad \ldots\ldots(7)$$

the supplementary condition (2) may be written as

$$\frac{\partial U_\mu}{\partial x_\mu}\Psi=0, \qquad \ldots\ldots(8)$$

and the commutation relations for U_μ will be given by

$$[U_\mu(x),\ U_\nu(x')]=i\left(\delta_{\mu\nu}-\frac{1}{\kappa^2}\frac{\partial^2}{\partial x_\mu \partial x_\nu}\right)\Delta(x-x'). \qquad \ldots\ldots(9)$$

In the present treatment we shall retain all the above equations, except that the supplementary condition (2) or (8) will be replaced by a weaker condition.

§3. QUANTIZATION OF THE MESON FIELD

Following I, we regard A_μ and B as self-adjoint quantities, and expand them as:

$$\left.\begin{aligned} A_\mu(x) &= \sum_{\mathbf{k}}(2k_0)^{-1/2}\{a_\mu(\mathbf{k})\exp[i(\mathbf{k}\cdot\mathbf{r}-k_0t)]+a_\mu^\dagger(\mathbf{k})\exp[-i(\mathbf{k}\cdot\mathbf{r}-k_0t)]\} \\ B(x) &= \sum_{\mathbf{k}}(2k_0)^{-1/2}\{b(\mathbf{k})\exp[i(\mathbf{k}\cdot\mathbf{r}-k_0t)]+b^\dagger(\mathbf{k})\exp[-i(\mathbf{k}\cdot\mathbf{r}-k_0t)]\} \end{aligned}\right\} \quad \ldots(10)$$

with
$$k_0^2 = k^2+\kappa^2, \qquad \ldots(11)$$

where a dagger denotes an adjoint. Substituting the Fourier expansions (10) in (5) and (6), we get

$$[a_\mu(\mathbf{k}),\ a_\nu^\dagger(\mathbf{k})]=\delta_{\mu\nu},\quad [b(\mathbf{k}),\ b^\dagger(\mathbf{k})]=1. \qquad \ldots(12)$$

Also, substituting the above Fourier expansions in (4), using the commutation relations (12), and omitting the zero-point energy, we obtain for the Hamiltonian of the meson field:

$$\int H dv = \sum_{\mathbf{k}} k_0\{a_1^\dagger(\mathbf{k})a_1(\mathbf{k})+a_2^\dagger(\mathbf{k})a_2(\mathbf{k})+a_3^\dagger(\mathbf{k})a_3(\mathbf{k})-a_0^\dagger(\mathbf{k})a_0(\mathbf{k})+b^\dagger(\mathbf{k})b(\mathbf{k})\}. \qquad \ldots(13)$$

We now choose our z axis along the vector $\mathbf{k}$, so that the operators $a_1(\mathbf{k})$, $a_2(\mathbf{k})$ and their adjoints correspond to the transverse mesons. Moreover, for the present purpose it is more convenient to replace the operators $a_3(\mathbf{k})$ and $a_0(\mathbf{k})$ by $a_L(\mathbf{k})$ and $c(\mathbf{k})$, which are given by

$$a_L(\mathbf{k})=\frac{k_0}{\kappa}a_3(\mathbf{k})-\frac{k}{\kappa}a_0(\mathbf{k}),\quad c(\mathbf{k})=\frac{-ik}{\kappa}a_3(\mathbf{k})+\frac{ik_0}{\kappa}a_0(\mathbf{k}). \qquad \ldots(14)$$

It may be verified from (11), (12) and (14) that

$$a_L^\dagger(\mathbf{k})a_L(\mathbf{k})-c^\dagger(\mathbf{k})c(\mathbf{k})=a_3^\dagger(\mathbf{k})a_3(\mathbf{k})-a_0^\dagger(\mathbf{k})a_0(\mathbf{k}), \qquad \ldots(15)$$

$$[a_L(\mathbf{k}),\ a_L^\dagger(\mathbf{k})]=1,\quad [c(\mathbf{k}),\ c^\dagger(\mathbf{k})]=-1,\quad [a_L(\mathbf{k}),\ c^\dagger(\mathbf{k})]=0. \qquad \ldots(16)$$

Thus, the operators $a_L(\mathbf{k})$ and $c(\mathbf{k})$ have properties similar to those of $a_3(\mathbf{k})$ and $a_0(\mathbf{k})$, and the Hamiltonian (13) may be written as

$$\int H dv = \sum_{\mathbf{k}} k_0(a_1^\dagger(\mathbf{k})a_1(\mathbf{k})+a_2^\dagger(\mathbf{k})a_2(\mathbf{k})+a_L^\dagger(\mathbf{k})a_L(\mathbf{k})-c^\dagger(\mathbf{k})c(\mathbf{k})+b^\dagger(\mathbf{k})b(\mathbf{k})). \qquad \ldots(17)$$

Besides the transverse mesons corresponding to $a_1(\mathbf{k})$ and $a_2(\mathbf{k})$, and the longitudinal mesons corresponding to $a_L(\mathbf{k})$, we have two more types of mesons, which we shall refer to as the b- and c-mesons. Since according to (16) the c-mesons have a negative commutator, we use an indefinite metric for these mesons as explained in I, while we treat the other types of mesons in the usual way. Thus, all the operators $a_1(\mathbf{k})$, $a_2(\mathbf{k})$, $a_L(\mathbf{k})$, $b(\mathbf{k})$, and $c(\mathbf{k})$ appear as absorption operators, while their adjoints are all emission operators. Moreover, now all the mesons have positive energy, though the states containing an odd number of c-mesons have a negative normalization.

§4. THE SUPPLEMENTARY CONDITION

It can be easily seen that according to the present treatment the supplementary condition (2) or (8) cannot be satisfied by any state of the meson field. Therefore, following I, we choose our supplementary condition as

$$\frac{\partial U_\mu^{(+)}}{\partial x_\mu}\Psi=0, \qquad \ldots(18)$$

where $U_\mu^{(+)}$ is the positive frequency part of U_μ. It follows from (18) and its adjoint equation that the expectation value of $\partial U_\mu/\partial x_\mu$ vanishes, so that our supplementary condition agrees with the usual one in the classical limit.

Substituting the Fourier expansions (10) in (18), and noting that we have chosen our z axis along $\mathbf{k}$, we obtain:

$$\left(i\frac{k}{\kappa}a_3(\mathbf{k})-i\frac{k_0}{\kappa}a_0(\mathbf{k})+b(\mathbf{k})\right)\Psi=0, \qquad \ldots\ldots(19)$$

which, on account of (14), may be written as

$$\{b(\mathbf{k})-c(\mathbf{k})\}\Psi=0. \qquad \ldots\ldots(20)$$

Since $b(\mathbf{k})$ and $c(\mathbf{k})$ are both absorption operators, (20) is evidently satisfied by any state not containing any b- and c-mesons. In general, as shown in I, a solution of (20) will consist of a normalized state containing no b- and c-mesons, and a superposition of a series of 'redundant states' with *arbitrary coefficients, zero normalization, and zero energy*. However, these redundant states do not give rise to any physical effect.* Thus, for all practical purposes we may ignore such states, and regard the b- and c-mesons as entirely absent in a non-interacting meson field.

Now the state of vacuum may be defined as that containing no transverse and longitudinal mesons, because the b- and c-mesons will be automatically excluded by the supplementary condition as explained above. Moreover, since the use of an indefinite metric for the c-mesons ensures that all the components of $A_\mu^{(+)}$ contain the absorption operators, the state of vacuum will satisfy the relations

$$A_\mu^{(+)}\Psi_0=0, \quad B^{(+)}\Psi_0=0, \quad U_\mu^{(+)}\Psi_0=0. \qquad \ldots\ldots(21)$$

It must be observed that if one does not use an indefinite metric for the c-mesons, the operator $c(\mathbf{k})$ occurring in (20) will have to be treated as an emission operator, and it will not be possible to find a normalized state satisfying (20). But we have seen that no such difficulty arises in the present treatment.

§ 5. TREATMENT OF INTERACTION

For the treatment of interaction, it is very convenient to use the interaction representation, which has already been used by Miyamoto (1948) and Matthews (1949) for Stueckelberg's formulation. We shall, therefore, add only a few remarks to indicate the points of difference.

It should first be observed that in the interaction representation our supplementary condition retains the form (18), which may easily be seen to satisfy the usual requirements of consistency. This situation is different from that arising in the treatment of the electromagnetic field. For Bleuler (1950) has extended the theory, given in I, to the interaction representation, and he has shown that the appropriate supplementary condition for the electromagnetic field in the interaction representation is given by

$$\left[\frac{\partial A_\mu^{(+)}(x)}{\partial x}-\int_\sigma D^{(+)}(x-x')j_\mu(x')d\sigma_\mu'\right]\Psi[\sigma]=0, \qquad \ldots\ldots(22)$$

which is obtained by replacing $A_\mu(x)$ and $D(x-x')$, occurring in the usual supplementary condition (Schwinger 1948), by their positive frequency parts $A_\mu^{(+)}(x)$ and $D^{(+)}(x-x')$. The physical significance of this difference in the two situations is as follows: The 'charge term' in the supplementary condition (22) allows

* It should be noted that a redundant state will always remain redundant, because the normalization is conserved in course of time.

virtual longitudinal and scalar photons to appear in the presence of interaction. But, since there is no corresponding term in the supplementary condition for the meson field, *the b- and c-mesons cannot appear even in virtual states.* Thus, these mesons play no part at all in the present theory, which is therefore completely identical with the usual theory, involving only transverse and longitudinal mesons.

For the invariant perturbation theory based on the interaction representation, we require, in addition to the commutators (5) and (6), the vacuum expectation values of the anticommutators. Using the vacuum condition (21), we find by following Schwinger (1949):

$$\left.\begin{aligned} &\langle\{A_\mu(x),\ A_\nu(x')\}\rangle_0=\delta_{\mu\nu}\Delta^{(1)}(x-x'), \qquad \langle\{B(x),\ B(x')\}\rangle_0=\Delta^{(1)}(x-x'),\\ &\langle\{U_\mu(x),\ U_\nu(x')\}\rangle_0=\left(\delta_{\mu\nu}-\frac{1}{\kappa^2}\frac{\partial^2}{\partial x_\mu\partial x_\nu}\right)\Delta^{(1)}(x-x'). \end{aligned}\right\} \quad \ldots\ldots(23)$$

It is to be noted that the use of an indefinite metric does not make any difference to the calculation of the vacuum expectation values, for the indefinite metric operator η, defined in I, contributes a factor $(-1)^n$ to a state containing n c-mesons. Therefore, for the state of vacuum η is just equal to unity.

§ 6. LORENTZ-INVARIANCE

In conclusion, we discuss the Lorentz-invariance of the present formulation. It will be observed that in I a preferred direction was introduced in our treatment, viz. the direction of the time-like anti-Hermitian component of the electromagnetic potential, and the Lorentz-invariance of the theory was ensured by the fact that the results of physical interest were independent of this direction. But, in the present case we do not have to introduce any preferred direction. For, one can split the vector field $A_\mu(x)$ into two parts, $A_\mu^{(1)}(x)$ and $A_\mu^{(2)}(x)$, such that

$$A_\mu^{(1)}(x)=\frac{1}{\kappa^2}\frac{\partial^2 A_\nu(x)}{\partial x_\mu\partial x_\nu}, \quad A_\mu^{(2)}(x)=A_\mu(x)-\frac{1}{\kappa^2}\frac{\partial^2 A_\nu(x)}{\partial x_\mu\partial x_\nu}. \quad \ldots\ldots(24)$$

Following the interaction representation and using (10) and (14), one can also find separately the contributions of $A_\mu^{(1)}(x)$ and $A_\mu^{(2)}(x)$ to the Hamiltonian of the meson field. In this way, one can see that $A_\mu^{(1)}(x)$ just corresponds to the c-mesons, while $A_\mu^{(2)}(x)$ corresponds to the transverse and longitudinal mesons. Since one can separate the c-mesons from the transverse and longitudinal ones in a Lorentz-invariant way, the use of an indefinite metric for the c-mesons does not conflict with the requirements of relativity.

ACKNOWLEDGMENT

I wish to express my thanks to Dr. N. Kemmer for valuable comments.

REFERENCES

Belinfante, F. J., 1949, *Phys. Rev.*, **76**, 226.
Bleuler, K., 1950, *Helv. phys. Acta*, **23**, 567.
Gupta, S. N., 1950, *Proc. Phys. Soc.* A, **63**, 681.
Kemmer, N., 1938, *Proc. Roy. Soc.* A, **166**, 127.
Ma, S. T., 1949, *Phys. Rev.*, **75**, 535.
Matthews, P. T., 1949, *Phys. Rev.*, **76**, 1657.
Miyamoto, Y., 1948, *Progr. Theor. Phys.*, **3**, 124.
Pauli, W., 1941, *Rev. Mod. Phys.*, **13**, 203.
Schwinger, J., 1948, *Phys. Rev.*, **74**, 1439; 1949, *Ibid.*, **75**, 651.
Stueckelberg, E. C. G., 1938, *Helv. phys. Acta*, **11**, 225, 299.

Polarized Nuclear Reactions

By R. J. BLIN-STOYLE
The Clarendon Laboratory, Oxford

MS. received 5th February 1951

ABSTRACT. Using properties of states of quantized angular momentum, general formulae are obtained for the angular distribution in nuclear reactions and scattering processes in which the bombarding particles and target nuclei are polarized. A simple symmetrical formula for use in specific calculations is given. The following cases are considered in detail : (*a*) polarized bombarding particles only, (*b*) target nuclei polarized in a magnetic field and bombarded by polarized particles. Finally, general predictions are made concerning the polarization of particles resulting from any reaction or scattering process and the results applied to the D–D reaction which is suggested as a source of fast polarized neutrons and protons.

§1. INTRODUCTION

THE spin dependence of nuclear reactions and scattering processes might be effectively investigated by observing the effect of polarization of the target nuclei and bombarding particles on the angular distribution of the outgoing particles.

Several methods have been suggested for the production of a beam of polarized elementary particles, the most successful being the polarization of thermal neutrons by scattering in magnetized iron (Bloch 1936, Hughes *et al.* 1948). The polarization of fast neutrons has been discussed by various authors (Schwinger 1946, 1948, Lepore 1950), whilst Wolfenstein (1949) has proposed methods for the production of polarized protons.

Partial alignment of the spins of the target nuclei can be effected at low temperatures by direct coupling of the nuclear magnetic moments with a large external magnetic field, or, in the case of a paramagnetic substance, by using a smaller field merely to align the moment due to the orbital electrons. In this latter case, the magnetic field at the nucleus due to the electron shells is then usually sufficient to produce appreciable nuclear polarization (Rose 1949).

The form of the angular distribution in the unpolarized case has been discussed by Eisner and Sachs (1947) using the theorem of vector addition of angular momentum and by Yang (1948) who considers the properties of states of quantized angular momentum under rotation and inversion.

Wolfenstein has extended the former method and investigated the case of polarized bombarding particles, but, like the preceding authors, confines himself to obtaining general limitations on the angular distribution rather than obtaining formulae which may be used in specific cases.

In this present paper use is made of the above methods in order to obtain a general expression for the angular distribution when both the bombarding particles and the target nuclei are polarized. This expression is then reduced to a simpler symmetrical form, use of which considerably facilitates calculations in specific cases.

The formulae are then used to obtain more detailed results in two particular cases: (*a*) bombarding particles of spin $\frac{1}{2}$ polarized in an arbitrary direction and

target nuclei unpolarized; (*b*) target nuclei polarized in a magnetic field and bombarded by polarized particles of spin $\frac{1}{2}$, the axis of polarization being parallel to the direction of incidence.

Finally, the general predictions made by Wolfenstein concerning the polarization of particles of spin $\frac{1}{2}$ resulting from any reaction or scattering process are obtained in a form suitable for calculation in actual cases. As an example, the results are applied to the D–D reaction which is suggested as a source of fast polarized neutrons and protons.

§ 2. POLARIZATION

A spin function representing a state of polarization of a nucleus of spin s, will be of the form

$$\psi = \sum_m U_m \psi_s^m, \quad \text{where} \quad \sum_m |U_m|^2 = 1, \qquad \ldots\ldots(1)$$

m is the component of spin along the axis of quantization (z axis) and $|U_m|^2$ represents the probability of the nucleus being in the spin state ψ_s^m.

If the axis of polarization is defined by the spherical polar angles Θ, Φ and if the probability of the nucleus having a 'spin orientation' m' referred to this axis is proportional to $\alpha_{m'}$, then since a spin function $\psi_s^{m'}$ quantized with respect to this axis is related to ψ_s^m by

$$\psi_s^{m'} = \sum_m D_{m'm}^s(\Phi - \pi, -\Theta, 0)\psi_s^m, \qquad \ldots\ldots(2)$$

where the matrix elements $D_{m'm}^s$ form an irreducible representation of order s of the group of real rotations of space, it follows that U_m is given by

$$U_m = \left(\sum_{m'} \epsilon_{m'}(\alpha_{m'})^{1/2} D_{m'm}^s\right) \Big/ \left(\sum_{m'} \alpha_{m'}\right)^{1/2}. \qquad \ldots\ldots(3)$$

$\epsilon_{m'}$ is a statistical variable indicating that for a given 'spin orientation' m' there will be a random distribution of spins about the axis of polarization. It possesses the property $\langle \epsilon_{m'} \epsilon_m^* \rangle = \delta_{m'm}$, where $\langle\ \rangle$ indicates a statistical average.

In order to describe the magnitude and direction of the polarization, it is convenient to introduce a polarization vector $\mathbf{P}$ defined by

$$\mathbf{P} = \mathbf{r}P = \mathbf{r}\left(\sum_m m\alpha_m\right) \Big/ \left(s\sum_m \alpha_m\right), \qquad \ldots\ldots(4)$$

where $\mathbf{r}$ is a unit vector in the direction of polarization and P (referred to as the polarization factor) can be regarded as the ratio of the mean spin of the nucleus along the axis of polarization to its actual spin.

Thus in the case of polarization of nuclei by a magnetic field H, α_m has the form $\exp(\gamma m)$, where $\gamma = \mu H/ksT$ and μ = nuclear magnetic moment, k = Boltzmann's constant, T = temperature of the substance polarized.

It then follows that (Rose 1949)

$$P = [(2s+1)\coth \tfrac{1}{2}(2s+1)\gamma - \coth \tfrac{1}{2}\gamma]. \qquad \ldots\ldots(5)$$

In most practical cases, $\gamma \ll 1$ and P then reduces to the form $P = \frac{1}{3}(s+1)\gamma$.

§ 3. THE ANGULAR DISTRIBUTION

(i) *The Nuclear Process*

For a nuclear process represented symbolically by $A + P \rightarrow B + Q$ in which the target nuclei A and the bombarding particles P are polarized, the angular distribution of the outgoing particles in the centre-of-mass system can be written

$$I(\theta\phi) = \sum_{bq} \Big| \sum_{Llap} (2L+1)^{1/2} i^L U_p V_a F_{bqlm}^{apLO} \psi_l^m(r\theta\phi) \Big|^2, \qquad \ldots\ldots(6)$$

the direction of incidence being along the z axis. Here a, p, b and q represent the z components of the spins s_A, s_P, s_B and s_Q of the nuclei A, P, B and Q, and L and l are the incoming and outgoing angular momenta respectively. $\psi_l^m(r\theta\phi)$ is a normalized wave function representing the relative orbital motions of B and Q in terms of the spherical polar variables r, θ, ϕ measured in the centre-of-mass system.

No summation is taken over m, since, by conservation of the z component of angular momentum $m=a+p-b-q$.

F_{bqlm}^{apLM} is related to the probability of the nuclear process proceeding from an initial state $\psi_i=\psi_{s_A}^a\psi_{s_P}^p\psi_L^M$ to a final state $\psi_f=\psi_{s_B}^b\psi_{s_Q}^q\psi_l^m$.

Equation (6) has a similar form to that given by Yang (1948) except that since it is concerned with polarized incident particles, their spins are not orientated at random so that factors U_p and V_a dependent on the nature of the polarization have to be introduced and the summation over p and a kept inside the square modulus.

Since $\psi_l^m(r\theta\phi)$ involves θ and ϕ in the form of a normalized spherical harmonic $Y_l^m(\theta\phi)$, it follows that, as in the unpolarized case, the maximum degree spherical harmonic that may occur in the angular distribution is $2l_{\max}$, subject to any other limitation that may be imposed.

In Appendix I, by using the theorem of vector addition of angular momenta, it is shown that, in terms of the well-known transformation coefficients

$$F_{bqlm}^{apLM}=\sum_{SsJ}\rho_{lsJ}^{LSJ}(s_A,a;s_P,p|S)(S,a+p;LM|J)(s,b+q;l,m|J)(s_B,b;s_Q,q|s),$$

where ρ_{lsJ}^{LSJ} is a function of the energy of the incident particles and is related to the probability of the reaction proceeding through different eigen-states of the total angular momentum J of the whole system. S and s are the total initial and final spins.

It is also shown in Appendix I from parity conservation arguments that

$$F_{-b\ -q\ l-m}^{-a-p\ L-M}=\pm F_{bqlm}^{apLM}, \qquad \ldots\ldots(7)$$

only one of the signs holding for a particular process.

(ii) *Rotational Properties of* $I(\theta\phi)$

Following the procedure used by Yang and obtaining a transformation equation for $F_{bqlm}^{apLM}\psi_l^m(r\theta\phi)$ under an arbitrary rotation of axes through the Eulerian angles χ_0, θ_0, ϕ_0 it is then easy to show that

$$I(\theta'\phi')=\sum_{bq}\Big|\sum_{LLMa'ap'p}(2L+1)^{1/2}i^L U_{p'}V_{a'}D_{0M}^{L}(\chi_0\theta_0\phi_0)D_{p'p}^{s_P}(\chi_0\theta_0\phi_0)D_{a'a}^{s_A}(\chi_0\theta_0\phi_0)\times F_{bqlm}^{apLM}\psi_l^m(r\theta\phi)\Big|^2,$$

where θ' and ϕ' are measured in the orientated system of axes and are functions of θ, ϕ, χ_0, θ_0, ϕ_0.

If $\theta=\phi=0$, then $\theta'=\theta_0$, $\phi'=\pi-\phi_0$ and, since $\psi_l^m(r\theta\phi)$ involves θ and ϕ as $Y_l^m(\theta\phi)$, it will only take a non-zero value when $m=0$, i.e. when $M=b+q-a-p$.

Writing

$$(2L+1)^{1/2}i^L F_{bql}^{apL}{}_{0}^{b+q-a-p}\psi_l^0(r00)=f_{bql}^{apL} \qquad \ldots\ldots(8)$$

and $\theta_0=\theta$, $\phi_0=\pi-\phi$, a final expression for the angular distribution is obtained:

$$I(\theta\phi)=\sum_{bq}\Big|\sum_{Lla'ap'p}U_{p'}V_{a'}D_{0\ b+q-a-p}^{L}(\theta,\pi-\phi)D_{p'p}^{s_P}(\theta,\pi-\phi)D_{a'a}^{s_A}(\theta,\pi-\phi)f_{bql}^{apL}\Big|^2. \qquad \ldots\ldots(9)$$

χ_0 has been omitted since it only occurs as $\exp[-i(b+q)\chi_0]$ and therefore disappears since the summation over b and q is taken outside the square modulus.

The maximum degree spherical harmonic that can occur in (9) is $2(L_{\max}+s_A+s_P)$ or $2(L_{\max}+s_A+s_P-\frac{1}{2})$ whichever is even. This results from the form of the rotation group elements and standard parity conservation arguments. If the particles A and P are unpolarized, the maximum degree is $2L_{\max}$ since, in this case, $U_{p'}$ and $V_{a'}$ are replaced by $\epsilon_{p'}/(2s_P+1)^{1/2}$ and $\epsilon_{a'}/(2s_A+1)^{1/2}$ so that the summations over p' and a' come outside the square modulus and the corresponding rotation group elements disappear because of the orthogonality property

$$\sum_m D^s_{mm'} D^{s*}_{mm''} = \delta_{m'm''}. \qquad \ldots\ldots(10)$$

Using (8) and (7) an expression for f^{apL}_{bql} is obtained and if this is used in (9), then two applications of the theorem given in Appendix II enable $I(\theta\phi)$ to be written in the following symmetrical form:

$$I(\theta\phi) = \sum_{bq} \Big| \sum_{Jap} U_p V_a H^J_{ap} D^J_{a+p,\, b+q}(\theta, \pi-\phi) G^J_{bq} \Big|^2, \qquad \ldots\ldots(11)$$

where $$H^J_{ap} = \sum_{SL} (2L+1)^{1/2} i^L (s_A, a;\ s_P, p \,|\, S)(S, a+p;\ L, 0 \,|\, J) \rho^{LSJ}$$

and $$G^J_{bq} = \sum_{sl} \psi^0_l(r00)(s_B, b;\ s_Q, q \,|\, s)(s, b+q;\ l, 0 \,|\, J) \rho_{lsJ},$$

the factor ρ^{LSJ}_{lsJ} being written as $\rho^{LSJ} \times \rho_{lsJ}$.

Consideration of (11) shows that the complexity of the angular distribution is further limited by the maximum value taken by the angular momentum J of any compound state, the maximum degree being $2J_{\max}$. In the particular case of the reaction proceeding through one compound state only, this state having angular momentum $J=\frac{1}{2}$, the angular distribution is spherically symmetrical. This arises because $G^J_{-b,\,-q} = \pm G^J_{bq}$ for a given J value (following from a similar argument to that resulting in (7)), so that on summing over b and q, all rotation group elements disappear by (10).

If the reaction results in the emission of a gamma-ray photon, care must be taken in interpreting the wave function of the outgoing particle. Goertzel (1946) has shown that a photon may be treated as a particle of spin 1 having total angular momentum j (z component m) and z component of spin μ, if the wave function $\psi^m_j(r\theta\phi\mu)$ is replaced by $A_{jm}(r\theta\phi\mu)$. Here $\mu=\pm 1$ corresponds to $(A^x \pm iA^y)_{jm}$ and $\mu=0$ to A^z_{jm}, the Cartesian indices referring to the three components of the vector potential of a spherical wave decomposition of the electromagnetic field corresponding to a photon of total angular momentum quantum numbers j and m.

Using this interpretation of the wave function of the out-going particle and an analysis similar to that already given, it is found that the same limits on the complexity of the angular distribution are effective. The limit $2l_{\max}$ arising in the particle case, however, is now replaced by $2j_{\max}$.

Thus, collecting results, the following general statement can be made about the complexity of the angular distribution of the outgoing particles in a nuclear reaction or scattering process in which the initial particles are polarized.

If x is the maximum degree spherical harmonic occurring in the angular distribution, then the following inequalities hold: $x \leqslant 2(L_{\max}+s_A+s_P)$ if $2(L_{\max}+s_A+s_P)$ is even, $x \leqslant 2(L_{\max}+s_A+s_P-\frac{1}{2})$ if $2(L_{\max}+s_A+s_P)$ is odd, $x \leqslant 2J_{\max}$, $x \leqslant 2l_{\max}$ (or $2j_{\max}$ in the case of gamma-emission). $x=0$ if only one compound state is involved, this state having $J=\frac{1}{2}$.

These inequalities should be compared with those concerning unpolarized particles. The latter can in fact be obtained from the above expressions by putting $s_A = s_P = 0$.

Calculations of the angular distribution in specific cases can be made using any of the general forms that have been obtained for $I(\theta\phi)$. In practice, however, the symmetrical formula (11) is found to simplify such calculations considerably.

So far, then, general forms for the angular distribution have been obtained and limits on its complexity imposed. In subsequent calculations use is made of these forms and detailed results obtained for cases in which the bombarding particles have spin $\frac{1}{2}$. It should be stressed that these results do *not* apply in general (i.e. for bombarding particles having spin greater than $\frac{1}{2}$).

§ 4. POLARIZATION OF THE BOMBARDING PARTICLES ONLY

Suppose that only the bombarding particles P are polarized and that the axis of polarization is defined by the spherical polar angles Θ and Φ. Then by (3)

$$U_{p'} = \left(\sum_{p''} \epsilon_{p''}(\alpha_{p''})^{1/2} D^{\frac{1}{2}}_{p'',p'}(\Phi - \pi, -\Theta, 0)\right) \Big/ \left(\sum_{p''} \alpha_{p''}\right)^{1/2}.$$

Since the nuclei A are unpolarized, $V_{a'}$ can be replaced by $\epsilon_{a'}/(2s_A+1)^{1/2}$. Then substituting for $U_{p'}$ and $V_{a'}$ in (9), there results

$$I(\theta,\phi) = I_{un}(\theta) - \frac{iP_P}{(2s_A+1)} \sin\Theta \sin(\Phi - \phi) \sum_{abq} (R^{a\frac{1}{2}}_{bq}(\theta))^* (R^{a-\frac{1}{2}}_{bq}(\theta)), \quad \ldots\ldots(12)$$

where

$$R^{ap}_{bq}(\theta) = \sum_{Ll} f^{apL}_{bql} D^L_{0,\,b+q-a-p}(\theta), \quad \ldots\ldots(13)$$

$I_{un}(\theta)$ is the unpolarized angular distribution and P_P is the polarization factor for the particles P.

The following properties of R^{ap}_{bq} are used in the deduction of (12):

$$|R^{ap}_{bq}(\theta)|^2 = |R^{a-p}_{b-q}(\theta)|^2 \quad \text{and} \quad \sum_{abq} [(R^{a\frac{1}{2}}_{bq}(\theta))^* (R^{a-\frac{1}{2}}_{bq}) + \text{c.c.}] = 0.$$

They result from (7) and the fact that

$$D^J_{M'M}(\theta) = (-1)^{2J+M'-M} D^J_{M'-M}(\theta). \quad \ldots\ldots(14)$$

Now if $\mathbf{n}$ is a unit vector defined by the vector equation

$$\mathbf{k}_0 \wedge \mathbf{k} = \mathbf{n} \sin\theta, \quad \ldots\ldots(15)$$

where $\mathbf{k}_0$ is a unit vector in the direction of incidence and $\mathbf{k}$ a unit vector in the direction of the outgoing particle, then (12) can be written in the vector form

$$I(\theta\phi) = I_{un}(\theta) + \mathbf{n} \cdot \mathbf{P}_P \sum_{LL'M} g^M_{LL'} Y^M_L(\theta) Y^{M+1}_{L'}(\theta), \quad \ldots\ldots(16)$$

where $\mathbf{P}_P$ is the polarization vector for the particles P. $g^M_{LL'}$ is real and is defined by

$$g^M_{LL'} = \frac{-i}{(2s_A+1)} \sum_{bql'} \frac{4\pi}{\{(2L+1)(2L'+1)\}^{1/2}} (f^{b+q-M-\frac{1}{2},\frac{1}{2},L}_{b,\,q,\,l})^* (f^{b+q-M-\frac{1}{2},-\frac{1}{2},L'}_{b,\,q,\,l}).$$

In (16) use has been made of the property $D^L_{0-M}(\theta) = \{4\pi(2L+1)\}^{1/2} Y^M_L(\theta)$, where $Y^M_L(\theta)$ is a normalized spherical harmonic.

Since $\mathbf{n}$ is perpendicular to the axis of incidence, it follows at once that polarization parallel to this axis produces no change in the angular distribution. Further, a reaction induced only by S waves still maintains a spherically symmetrical angular distribution when the bombarding particles are polarized.

The maximum effect is to be expected when the polarization is perpendicular to the axis of incidence, for example along the y axis, in which case an asymmetry of the form

$$I(\theta\phi) = I_{\text{un}}(\theta) + P_{\text{P}} \cos\phi \sum_{LL'M} g^{M}_{LL'} Y^{M}_{L}(\theta) Y^{M+1}_{L'}(\theta), \qquad \ldots\ldots(17)$$

is obtained as predicted by Wolfenstein who considers this particular case only.

The results of this section may of course be restricted by any of the other limitations given at the end of § 3.

§ 5. BOMBARDING PARTICLES AND TARGET NUCLEI POLARIZED

In this section the case of polarization about the axis of incidence is considered, the polarization of the target nuclei being accomplished by means of an external magnetic field. The polarization factor for these nuclei is then given by (5). The z axis is defined by $\Theta = 0$, so that by (3)

$$U_{p'} = \epsilon_{p'}(\alpha_{p'})^{1/2} \Big/ \Big(\sum_{p'} \alpha_{p'}\Big)^{1/2}; \quad V_{a'} = \epsilon_{a'}(\beta_{a'})^{1/2} \Big/ \Big(\sum_{a'} \beta_{a'}\Big)^{1/2}. \qquad \ldots\ldots(18)$$

Also for polarization in a magnetic field, $\beta_{a'} = \exp(\gamma a')$ (see § 2).

Substituting (18) into (9) gives

$$I(\theta) = \Big\{ \sum_{ap} \alpha_p \exp(\gamma a) I_{ap}(\theta) \Big\} \Big/ \Big\{ \sum_{ap} \alpha_p \exp(\gamma a) \Big\}, \qquad \ldots\ldots(19)$$

where $I_{ap}(\theta)$ is the angular distribution to be expected when the particles A and P have 'spin orientations' denoted by a and p respectively, and is given by

$$I_{ap}(\theta) = \sum_{b'q'} \Big| \sum_{La'p'} D^{L}_{0b'+q'-a'-p'}(\theta) D^{\frac{1}{2}}_{pp'}(\theta) D^{s_{\text{A}}}_{aa'}(\theta) f^{a'p'L}_{b'q'i} \Big|^2. \qquad \ldots\ldots(19a)$$

The rotation group elements have been written as functions of θ only, since, by the nature of the summation, it is obvious that ϕ is not involved and that the angular distribution is therefore symmetrical about the z axis.

$I_{ap}(\theta)$ is found to be a polynomial in powers of $\cos\theta$, only even powers occurring if L is confined to either all odd or all even values. Further, by (7) and (14), it possesses the property $I_{ap}(\theta) = I_{-a-p}(\theta)$. Using this property, (19) may be written

$$I(\theta) = \Big\{ \sum_{a} [\cosh(\gamma a) + P_{\text{P}} \sinh(\gamma a)] I_{a\frac{1}{2}}(\theta) \Big\} \Big/ \Big\{ \sum_{a} \exp(\gamma a) \Big\}, \qquad \ldots\ldots(20)$$

where P_{P} is the polarization factor for the particles P.

In most practical cases $\gamma \ll 1$, so that it is of interest to consider the form of (20) for such low values of γ. In Appendix III it is shown that to order γ^2, the angular distribution may be written

$$I(\theta) = I_{\text{un}}(\theta) + \gamma \sum_{n=0}^{2(L_{\max}+1)} (a_n P_{\text{P}} + \gamma b_n) \cos^n\theta, \qquad \ldots\ldots(21)$$

i.e. the maximum power of $\cos\theta$ involved is $2(L_{\max}+1)$ independent of the spin of the nucleus A. As further powers of γ are considered, then higher powers of $\cos\theta$ will enter the expression up to the maximum permitted by the general limitations given in § 3.

It is at once obvious that if $\gamma = 0$, then the angular distribution is unchanged. This bears out the result of the preceding section that polarization of bombarding particles of spin $\frac{1}{2}$ along the axis of incidence has no effect on the angular distribution. This fact also implies that if $s_{\text{A}} = \frac{1}{2}$, all $b_n = 0$.

If the bombarding particles are unpolarized, then $P_{\text{P}} = 0$ and the change in the angular distribution is of the second order in γ. In particular for a reaction

induced only by S waves, the angular distribution, which would normally be spherically symmetrical, has the asymmetrical form $I(\theta)\propto 1+A\gamma^2(1-3\cos^2\theta)$, where

$$A=\left\{\sum_{ap}\left(\frac{s_A(s_A+1)-3a^2}{12}\right)I_{ap}(\theta=0)\right\}\Big/\left\{\Sigma I_{ap}(\theta=0)\right\}_{ap}.$$

For the case of a resonance reaction (one compound state only) induced by S waves and resulting in the emission of a gamma-ray photon, the following simple expression for $I_{ap}(\theta)$ is obtained by using the concept introduced in §3 for the 'wave function' of the photon:

$$I_{ap}(\theta)\propto|(s_P,p;s_A,a|J)|^2\sum_\lambda\{|D^J_{a+p,\lambda}(\theta)|^2[|(j,1;s_B,\lambda-1|J)|^2+|(j,-1;s_B,\lambda+1|J)|^2]\}.$$

Here J is the angular momentum of the resonance level and j is the multipole order of the transition resulting in the emission of the gamma-ray.

Calculations for particular reactions using this expression for $I_{ap}(\theta)$ indicate that with $\gamma=\frac{1}{2}$ and $P_P=\frac{1}{2}$, asymmetries of up to 25% might be expected. The observation of such effects however would in many cases be masked by gamma-rays from accompanying cascade transitions.

§6. PRODUCTION OF POLARIZED PARTICLES

(i) *Nature of the Polarization*

Methods suggested by the authors referred to in §1 for the polarization of fast nuclear particles consist mainly of scattering processes in which there is strong spin–orbit coupling. Any nuclear reaction or scattering process in which such coupling plays a part might be expected to result in polarization of the outgoing particles, and in this section general results relating to the nature of this polarization are given.

In the process represented symbolically by A + P → B + Q, consider the polarization of the particles Q (assumed to be of spin $\frac{1}{2}$). If the initial particles A and P are unpolarized, the final state of the process can be represented by

$$\psi_I=\frac{1}{\sqrt{(2s_A+1)}\sqrt{(2s_P+1)}}\sum_{Llapbq}(2L+1)^{1/2}i^L\epsilon_{a^0p}F^{apLQ}_{bqlm}\psi^b_{s_B}\psi^q_{s_Q}\psi^m_l(r\theta\phi). \quad \ldots\ldots(22)$$

The polarization of the particles Q is defined by

$$(\psi^*_f,\psi_f)\mathbf{P}=(\psi^*_f,\boldsymbol{\sigma}\psi_f), \quad \ldots\ldots(23)$$

where $\boldsymbol{\sigma}$ is a vector representing the three components of the Pauli spin operator for the particles Q. (It is easily shown that this definition of $\mathbf{P}$ is consistent with that given in (4) when applied to particles of spin $\frac{1}{2}$.)

Substitution of (22) into (23) and use of the well-known properties of $\boldsymbol{\sigma}$ gives

$$I(\theta)[P_x(\theta\phi)+iP_y(\theta\phi)]=\frac{2}{(2s_A+1)(2s_P+1)}\sum_{apb}\left(\sum_{Ll}(2L+1)^{1/2}i^LF^{apLQ}_{b\frac{1}{2}lm}\psi^m_l(r\theta\phi)\right)^*\times\left(\sum_{Ll}(2L+1)^{1/2}i^LF^{apLQ}_{b-\frac{1}{2}lm'}\psi^{m'}_l(r\theta\phi)\right),$$

$$I(\theta)P_z(\theta\phi)=\frac{1}{(2s_A+1)(2s_P+1)}\sum_{apb}\left(\left|\sum_{Ll}(2L+1)^{1/2}i^LF^{apLQ}_{b\frac{1}{2}lm}\psi^m_l(r\theta\phi)\right|^2-\left|\sum_{Ll}(2L+1)^{1/2}i^LF^{apLQ}_{b-\frac{1}{2}lm'}\psi^{m'}_l(r\theta\phi)\right|^2\right),$$

where $I(\theta)$ is the angular distribution of the particles Q in the centre-of-mass system.

From (7) it follows at once that $P_z(\theta\phi)=0$.

By investigating the behaviour of the quantity $[P_x(\theta\phi)+iP_y(\theta\phi)]$ under an arbitrary rotation of axes and adapting the procedure of § 3 to this case, there results

$$I(\theta)[P_x(\theta\phi)+iP_y(\theta\phi)]=\frac{2}{(2s_A+1)(2s_P+1)}\sum_{apb}\left(\sum_q D^{\frac{1}{2}}_{\frac{1}{2}q}(\theta)R^{ap}_{bq}(\theta)\right)^*\left(\sum_q D^{\frac{1}{2}}_{-\frac{1}{2}q}(\theta)R^{ap}_{bq}(\theta)\right) \quad \ldots\ldots(24)$$

where $R^{ap}_{bq}(\theta)$ is defined in (13).

Using the properties of $R^{ap}_{bq}(\theta)$ given in § 4, (24) reduces to

$$I(\theta)[P_x(\theta\phi)+iP_y(\theta\phi)]=i\exp(i\phi)\sum_{LL'M}k^M_{LL'}Y^M_L(\theta)Y^{M+1}_{L'}(\theta), \quad \ldots\ldots(25)$$

where the coefficients $k^M_{LL'}$ are real and are given by

$$k^M_{LL'}=\frac{-2i}{(2s_A+1)(2s_P+1)}\sum_{bpl'}\frac{4\pi}{\{(2L+1)(2L'+1)\}^{1/2}}(f^{b+\frac{1}{2}-M-p,\ p,\ L}_{b\qquad\ \frac{1}{2},\ l})^*(f^{b+\frac{1}{2}-M-p,\ p,\ L'}_{b\qquad\ -\frac{1}{2},\ l'}).$$

If a vector $\mathbf{n}$ is defined as in (15), then (25) can be written in the vector form

$$I(\theta)\mathbf{P}(\theta)=\mathbf{n}\sum_{LL'M}k^M_{LL'}Y^M_L(\theta)Y^{M+1}_{L'}(\theta), \quad \ldots\ldots(26)$$

i.e. if the outgoing particles are polarized, the axis of polarization is perpendicular to the plane containing their direction of motion and the axis of incidence. Also, for $\mathbf{P}(\theta)$ to have a non-zero value, P waves at least must be effective in the reaction.

(ii) *Example*: *Application to the D–D Reaction*

Analysis of the D–D reaction (Konopinski and Teller 1948, Beiduk, Pruett and Konopinski 1950) shows that in order to explain the observed angular distribution up to deuteron energies of about 0·5 MEV., it is necessary to introduce strong spin–orbit coupling and P wave effect. As indicated in the previous section, these are the necessary conditions for the production of polarized particles and it might therefore be expected that the outgoing neutrons and protons are polarized.

Assuming that only S and P waves are effective in the reaction (26) gives $I(\theta)\mathbf{P}(\theta)=\mathbf{n}[(k^0_{01}-k^{-1}_{10})Y^0_0(\theta)Y^1_1(\theta)+(k^0_{11}-k^{-1}_{11})Y^0_1(\theta)Y^1_1(\theta)]$. If in the reaction the transitions taking place are ${}^1S_0\rightarrow{}^1S_0$, ${}^3P\rightarrow{}^3P$, ${}^3P_1\rightarrow{}^1P_1$ then in f^{apL}_{bql} the following have non-zero values: ρ^{000}_{000}, ρ^{110}_{110}, ρ^{111}_{111}, ρ^{112}_{112}, ρ^{111}_{101}.

To conform to the notation used by Beiduk *et al.*, the following substitutions for matrix elements are made:

$$\sigma_0|\alpha_0|^2=\tfrac{1}{2}|\rho^{000}_{000}|^2,\quad \sigma_1|\alpha_{1J}|^2=\tfrac{3}{2}|\rho^{11J}_{11J}|^2,\quad \sigma_1|\beta_{11}|^2=\tfrac{3}{2}|\rho^{111}_{101}|^2,$$

$$\gamma^m_{1,M-m}=\sum_J\alpha_{1J}(L,0;\ 1,M|J)(L,M-m;\ 1,m|J).$$

The energy dependence of the reaction is taken to enter only through the approach cross sections σ_L (for definition see the references given above).

In the above substitutions, M represents the initial z component of total spin and m the final z component, so that matrix elements having $M\neq m$ are those arising from spin–orbit coupling.

Then, with these substitutions,

$$k_{01}^0 - k_{10}^{-1} = 0, \quad k_{11}^0 - k_{11}^{-1} = -i4\sqrt{2}\sigma_1 \operatorname{Im}\{\gamma_{10}^{1*}(\gamma_{11}^0 + \beta_{11}/\sqrt{2}) + \gamma_{10}^{0*}\gamma_{11}^{-1}\}$$

and

$$I(\theta) = |\alpha_0|^2\sigma_0\left\{1 + \frac{\sigma_1}{\sigma_0}\left[\left(\frac{6|\gamma_{10}^1|^2 + 3|\gamma_{10}^0|^2}{|\alpha_0|^2}\right)\cos^2\theta + \left(\frac{3|\beta_{11}|^2 + 6|\gamma_{11}^0|^2 + 6|\gamma_{11}^{-1}|^2}{2|\alpha_0|^2}\right)\sin^2\theta\right]\right\}.$$

If $I(\theta)$ is written in the form $I(\theta) \propto 1 + A(E)\cos^2\theta$, where E represents the deuteron energy, then the expression for the polarization is easily shown to be $\mathbf{P}(E,\theta) = \mathbf{n}Bp(E,\theta)$, where $p(E,\theta) = A(E)\sin\theta\cos\theta/(1 + A(E)\cos^2\theta)$ and $B = -4i\operatorname{Im}[\gamma_{10}^{1*}(\gamma_{11}^0 + \beta_{11}/\sqrt{2}) + \gamma_{10}^{0*}\gamma_{11}^{-1}]/[4|\gamma_{10}^1|^2 + 2|\gamma_{10}^0|^2 - |\beta_{11}|^2 - 2|\gamma_{11}^0|^2 - 2|\gamma_{11}^{-1}|^2]$.

The coefficient B is energy independent but cannot be evaluated without a knowledge of the relative phases of the various matrix elements. * If there is no spin–orbit coupling $\gamma_{11}^0 = \gamma_{11}^{-1} = \beta_{11} = 0$ and it takes the value zero; otherwise to be consistent with experimental results for the angular distribution, its value must lie within the approximate range $1 > B > -1$.

The maximum value taken by $p(E,\theta)$ for a given value of E is readily shown to be $p_{\max}(E) = A(E)/2(A(E)+1)^{1/2}$ at $\theta = \cos^{-1}[(A(E)+2)^{-1/2}]$. Using values of $A(E)$ obtained from fitting a curve of the form $I(\theta) \propto 1 + A(E)\cos^2\theta$ to the observed angular distribution of outgoing protons for deuteron energies up to 0·5 MeV. (Huntoon *et al.* 1940) we see that $p_{\max}(E)$ varies continuously from zero, at zero energy, to 0·54 at 0·5 MeV. At this latter energy, then, the polarization may take any value in the approximate range 0–50%.

§ 7. SUMMARY

From the foregoing work we see that polarization of the initial particles in a nuclear reaction or scattering process leads to an increase in the complexity of the angular distribution of the outgoing particles. This increase, however, is limited by a series of inequalities referring to the maximum degree spherical harmonic that can occur in the angular distribution.

If the bombarding particles have spin $\frac{1}{2}$ and if only they are polarized, then the azimuthal variation of the angular distribution can be given exactly (§ 4). In particular, polarization parallel to the axis of incidence produces no effect on the angular distribution; also, a process induced only by S waves will result in a spherically symmetrical angular distribution for any direction of polarization.

The target nuclei may be polarized by means of an external magnetic field, and if they are bombarded by polarized particles of spin $\frac{1}{2}$, the axis of polarization in both cases being parallel to the direction of incidence, then the resulting angular distribution is symmetrical about this axis and is in the form of a polynomial in powers of $\cos\theta$, the maximum permissible power being $2[L_{\max} + s_A(+\frac{1}{2})]$. If the field is 'small', then the maximum power that may occur is $2[L_{\max} + 1]$ whatever the spin of the target nucleus A (§ 5).

The increase in complexity of the angular distribution is thus dependent on the form of the polarization. It is also related to the spin dependence of the nuclear

* *Note added in proof.* Beiduk *et al.* (1950) have attempted to calculate these matrix elements assuming that the spin orbit coupling may be attributed to tensor forces only, and to their approximation $\beta_{11} = 0$ and $\gamma_{11}^{-1} = -\gamma_{11}^0$, so that B is identically zero. However, their calculated results for the angular distribution show considerable disagreement with experiment and indicate that other spin orbit forces are probably acting.

forces that are effective in the process considered and should therefore give some information about the nature of these forces. (Bhatia (1950) has discussed in detail the information that could be obtained from an experimental investigation of the scattering of fast polarized neutrons by protons.) The multipolarity of transitions resulting in gamma-emission might also be deduced from this dependence of the angular distribution on polarization, but normally, experimental procedure would be complicated by accompanying cascade transitions.

General considerations (§ 6) show that a nuclear reaction or scattering process resulting in polarized outgoing particles must necessarily be induced by at least P waves and must involve strong spin–orbit coupling, the polarization then being perpendicular to the plane containing the axis of incidence and the direction of motion of the outgoing particle. The D–D reaction satisfies the above conditions and it seems probable that the outgoing protons and neutrons are polarized although the exact magnitude of the polarization cannot be predicted without performing detailed calculations assuming some theory of nuclear forces. Measurement of the polarization, of course, will give information about the nature of such forces.

APPENDIX I

An expression for F^{apLM}_{bqlm} can be obtained by applying the theorem of vector addition of angular momenta to an initial wave function of the form $\psi^M_L \psi^a_{s_A} \psi^p_{s_P}$.

The product $\psi^a_{s_A}\psi^p_{s_P}$ can be expressed in terms of eigenfunctions ψ^{a+p}_S of the total spin S, and the product $\psi^{a+p}_S \psi^M_L$ in terms of eigenfunctions ${}^{L,S}\psi^{a+p+M}_J$ of the total angular momentum J. The indices L and S indicate the mode of formation of the eigenfunctions. Then

$$\psi_i = \sum_{SJ} (s_A, a;\ s_P, p\,|\,S)(S, a+p;\ L, M|J)\,{}^{L,S}\psi^{a+p+M}_J,$$

where the coefficients of ${}^{L,S}\psi^{a+p+M}_J$ are the well-known transformation coefficients.

The effect of the nuclear reaction is to transform the states ${}^{L,S}\psi^{a+p+M}_J$ of the incoming particles to $\sum_{ls} \rho^{LSJ}_{lsJ}\,{}^{l,s}\psi^{a+p+M}_J$ where ${}^{l,s}\psi^{a+p+M}_J$ is one of the states of the outgoing particles. An interpretation of the factors ρ^{LSJ}_{lsJ} has been given in the text.

ow the state ${}^{l,s}\psi^{a+p+M}_J$ can be written as a linear superposition of the individual states $\psi^m_l(r,\theta,\phi)$, $\psi^b_{s_B}$ and $\psi^q_{s_Q}$ where $m = M+a+p-b-q$, so that

$$\psi_f = \sum_{lsSJbq} \rho^{LSJ}_{lsJ}(s_A, a;\ s_P, p\,|\,S)(S, a+p;\ L, M|J)(s, b+q;\ l, m|J) \times (s_B, b;\ s_Q, q\,|\,s)\psi^q_{s_Q}\psi^b_{s_B}\psi^m_l(r,\theta,\phi),$$

i.e.

$$F^{apLM}_{bqlm} = \sum_{SsJ} \rho^{LSJ}_{lsJ}(s_A, a;\ s_P, p\,|\,S)(S, a+p;\ L, M|J)(s, b+q;\ l, m|J)(s_B, b;\ s_Q, q\,|\,s).$$

Also $(S, M;\ s, m|J)$ possesses the property that

$$(S, -M;\ s, -m|J) = (-1)^{S+s-J}(S, M;\ s, m|J)$$

so that $F^{a-p\ L-M}_{-b-q\ l-m} = \sum_{SsJ} (-1)^n \rho^{LSJ}_{lsJ}(s_A, a;\ s_P, p\,|\,S)(S, a+p;\ L, M|J) \times (s, b+q;\ l, m|J)(s_B, b;\ s_Q, q\,|\,s),$

where $n = s_A + s_P + s_B + s_Q + L + l - 2J$.

But in a nuclear reaction in which the parities of the initial and final nuclei are fixed, it readily follows from parity conservation considerations that the integer quantity $(L+l-2J)$ cannot have both odd and even values, and since $s_A+s_P+s_B+s_Q$ is fixed for the reaction, n can take only odd or even values but not both. Then, $F^{-a-p\ L-M}_{-b-q\ l-m} = \pm F^{apLM}_{bqlm}$, only one of the signs holding for a particular reaction.

APPENDIX II

Consider two states $\psi^{a'}_{s_A}$ and $\psi^{p'}_{s_P}$ quantized with respect to a set of axes $0x'$, $0y'$, $0z'$, obtained from the set $0x$, $0y$, $0z$, by rotation through the Eulerian angles χ, θ, ϕ.

The product state $\psi^{a'}_{s_A}\psi^{p'}_{s_P}$ can be written as a superposition of eigenfunctions $\psi^{a'+p'}_J$ of the total angular momentum J:

$$\psi^{a'}_{s_A}\psi^{p'}_{s_P} = \sum_J (s_A, a';\ s_P, p'|J)\psi^{a'+p'}_J = \sum_{JM} (s_A, a';\ s_P, p'|J) D^J_{a'+p',M}(\chi,\theta,\phi)\psi^M_J,$$

where ψ^M_J is a state quantized in the initial set of axes. But the product state $\psi^{a'}_{s_A}\psi^{p'}_{s_P}$ can also be written as

$$\psi^{a'}_{s_A}\psi^{p'}_{s_P} = \sum_{ap} D^{s_A}_{a'a}(\chi\theta\phi) D^{s_P}_{p'p}(\chi\theta\phi)\psi^a_{s_A}\psi^p_{s_P},$$

and then $\psi^a_{s_A}\psi^p_{s_P}$ can be expressed as a superposition of eigenfunctions of the total angular momentum J to give

$$\psi^{a'}_{s_A}\psi^{p'}_{s_P} = \sum_{apJ} D^{s_A}_{a'a}(\chi\theta\phi) D^{s_P}_{p'p}(\chi\theta\phi)(s_A, a;\ s_P, p|J)\psi^{a+p}_J.$$

Comparing the two expressions for $\psi^{a'}_{s_A}\psi^{p'}_{s_P}$ and equating coefficients of ψ^M_J gives

$$(s_A, a';\ s_P, p'|J) D^J_{a'+p',M}(\chi\theta\phi) = \sum_p D^{s_A}_{a',M-p}(\chi\theta\phi) D^{s_P}_{p'p}(\chi\theta\phi)(s_A, M-p;\ s_P, p|J),$$

which is the required theorem.

APPENDIX III

To order γ^2 (20) can be written

$$I(\theta) = \frac{1}{2s_A+1}\left\{\left(1-\gamma^2\frac{s_A(s_A+1)}{6}\right)\sum_a I_{a\frac{1}{2}}(\theta) + \gamma P_P \sum_a a I_{a\frac{1}{2}}(\theta) + \tfrac{1}{2}\gamma^2\sum_a a^2 I_{a\frac{1}{2}}(\theta)\right\}.$$

$\{1/(2s_A+1)\}\sum_a I_{a\frac{1}{2}}(\theta)$ is just an expression for the unpolarized angular distribution $I_{un}(\theta)$. Consider $\sum_a a I_{a\frac{1}{2}}(\theta)$. By (19 a) the summation over a involves terms of the form $\sum_a a D^{s_A}_{aa_1}(\theta) D^{s_A}_{aa_2}(\theta)$ which can be written $\sum_{aa'} (D^{s_A}_{a_1a}(\theta))^{-1} a\delta_{aa'} (D^{s_A}_{a'a_2}(\theta))$, since the matrices $[D^{s_A}_{aa_1}(\theta)]$ are unitary and also real. This expression represents the elements (a_1a_2) of the transform by the matrix $D^{s_A}_{aa_1}(\theta)$ of the diagonal matrix $a\delta_{aa'}$.

But $D^{s_A}_{aa_1}(\theta)$ represents a rotation about the y axis through an angle θ, so that in terms of rotation operators the above expression becomes, using an obvious notation for Cartesian components of angular momentum operators and matrix elements,

$$\langle s_A a_1 | e^{-i\alpha\gamma\beta} a_x e^{i\alpha\gamma\beta} | s_A a_2 \rangle = \langle s_A a_1 | a_x \cos\theta + a_z \sin\theta | s_A a_2 \rangle,$$
$$= a\cos\theta \text{ if } a_1 = a_2 = a;$$
$$= \tfrac{1}{2}[(s_A - a)(s_A + a + 1)]^{1/2} \sin\theta \text{ if } a_1 = a;\ a_2 = a+1;\ \text{or if } a_1 = a+1;\ a_2 = a$$
$$= 0 \text{ otherwise.}$$

θ therefore enters $\sum_a I_{a\frac{1}{2}}(\theta)$ through terms of the form

$$D^{L_1}_{0,b+q-a-p_1}(\theta) D^{L_2}_{0,b+q-a-p_2}(\theta) D^{\frac{1}{2}}_{\frac{1}{2}p_1}(\theta) D^{\frac{1}{2}}_{\frac{1}{2}p_2}(\theta) \cos\theta$$

and

$$D^{L_1}_{0,b+q-a-p_1}(\theta) D^{L_2}_{0,b+q-a-1-p_2}(\theta) D^{\frac{1}{2}}_{\frac{1}{2}p_1}(\theta) D^{\frac{1}{2}}_{\frac{1}{2}p_2}(\theta) \sin\theta.$$

By inspection it can be seen that both terms may be expressed in powers of $\cos\theta$ and that the maximum power occurring is $2(L_{\max}+1)$.

The term $\sum_a a^2 I_{a\frac{1}{2}}(\theta)$ can be treated by the same method and is also found to involve powers of $\cos\theta$ up to $2(L_{\max}+1)$.

Collecting results then leads to equation (21).

ACKNOWLEDGMENT

The author would like to express his thanks to Dr. J. A. Spiers for the many helpful suggestions he has made concerning this work.

REFERENCES

Beiduk, F. M., Pruett, J. R., and Konopinski, E. J., 1950, *Phys. Rev.*, **77,** 622.
Bhatia, A. B., 1950, *Proc. Phys. Soc.* A, **63,** 502.
Bloch, F., 1936, *Phys. Rev.*, **50,** 259.
Eisner, E., and Sachs, R. G., 1947, *Phys. Rev.*, **72,** 680.
Goertzel, G., 1946, *Phys. Rev.*, **70,** 897.
Hughes, D. J., Wallace, J. R., and Holtzmann, R. H., 1948, *Phys. Rev.*, **73,** 1277.
Huntoon, R. D., Ellett, A., Bayley, D. S., and Van Allen, J. A., 1940, *Phys. Rev.*, **58,** 97.
Konopinski, E. J., and Teller, E., 1948, *Phys. Rev.*, **73,** 822.
Lepore, J. V., 1950, *Phys. Rev.*, **79,** 137.
Rose, M. E., 1948, *Nucleonics*, **3,** No. 6, 23; 1949, *Phys. Rev.*, **75,** 213.
Schwinger, J., 1946, *Phys. Rev.*, **69,** 681; 1948, *Ibid.*, **73,** 407.
Wolfenstein, L., 1949, *Phys. Rev.*, **75,** 1664.
Yang, C. N., 1948, *Phys. Rev.*, **74,** 764.

The Scattering Phase Shifts of Two-Nucleon Systems

By S. A. KUSHNERIUK * and M. A. PRESTON
Physics Department, University of Toronto

Communicated by R. E. Peierls; MS. received 23rd February 1951

ABSTRACT. Energy expansions for simple functions of the scattering phase shifts are given for all relative angular momenta for central forces in neutron–proton and proton–proton scattering and for non-central static forces in proton–proton scattering including the coupling of P and F states. The differential scattering cross section for this latter case is given in an appendix.

INTRODUCTION

THE recent papers of Blatt and Jackson (Blatt and Jackson 1949, Jackson and Blatt 1950) have demonstrated the importance for the analysis of nucleon scattering experiments of the expansion of certain functions of the phase shifts as power series in the energy. Such expansions have been derived by a number of authors using various techniques (Landau and Smorodinsky 1944, Schwinger 1947, Hatcher, Arfken and Breit 1949, Peierls and Barker 1949, Chew and Goldberger 1949, Christian 1949, Bethe 1949). In this paper, the techniques used by Bethe (1949) are extended to the cases of general orbital angular momentum states and of tensor forces for both neutron–proton and proton–proton systems.

§1. NEUTRON–PROTON CENTRAL INTERACTIONS

The radial wave function multiplied by r satisfies the differential equation

$$\frac{d^2y}{dr^2}+\left[k^2-\frac{l(l+1)}{r^2}-P_l(r)\right]y=0 \qquad \ldots\ldots(1.1)$$

with the boundary conditions $y(0,k)=0$ and

$$y(r,k)\sim A_l[\sin(kr-l\pi/2)+\tan\delta^{(l)}\cos(kr-l\pi/2)]. \qquad \ldots\ldots(1.2)$$

In the above $P_l(r)$ represents a central, short range nuclear potential for states with angular momentum $l\hbar$. The remainder of the notation is standard, $\delta^{(l)}$ being the corresponding phase shift. The subscript l will in future be dropped where no confusion arises.

Expressions for the phase shifts are readily derived by converting (1.1), along with the boundary conditions, into an integral equation. Let v_R and v_I be regular and irregular solutions of (1.1) in the absence of the nuclear potential, i.e.

$$v_R=krj_l(kr)\sim\sin(kr-l\pi/2), \quad v_I=-krn_l(kr)\sim\cos(kr-l\pi/2). \qquad \ldots\ldots(1.3)$$

The Wronskian of v_R and v_I is $W=-1$. Then, by variation of parameters, it is readily established that

$$y(r)=Av_R(r)+\frac{1}{kW}\left\{v_R(r)\int_r^\infty v_I(s)P(s)y(s)\,ds+v_I(r)\int_0^r v_R(s)P(s)y(s)\,ds\right\} \ldots(1.4)$$

$$\sim A\sin(kr-l\pi/2)+\cos(kr-l\pi/2)\frac{1}{kW}\int_0^\infty v_RPy\,ds. \qquad \ldots\ldots(1.5)$$

* Now at Atomic Energy Project, Chalk River, Ontario, Canada.

Comparison of (1.2) and (1.5) gives

$$kWA=\cot\delta\int_0^\infty v_R(r)P(r)y(r)\,dr. \qquad \ldots\ldots(1.6)$$

The normalization of y is still arbitrary. A formula for the phase shift independent of the normalization may be readily derived. Substituting the value of A from (1.6) into (1.4), multiplying through by yP and integrating throughout the range of r yields

$$\cot\delta=kW\frac{\int_0^\infty P(r)y^2(r)\,dr-\int_0^\infty dr\,P(r)y(r)\int_0^\infty G(r,s)P(s)\,ds}{\left[\int_0^\infty v_R(r)P(r)y(r)dr\right]^2}. \qquad \ldots\ldots(1.7)$$

$G(r,s)$ is Green's function given by

$$\left.\begin{aligned} kWG(r,s)&=v_R(r)v_I(s), \qquad s<r,\\ &=v_I(r)v_R(s), \qquad s>r.\end{aligned}\right\} \qquad \ldots\ldots(1.8)$$

This is the Schwinger variational form. Other expressions for the phase shifts may be deduced by specializing the normalization. A convenient choice, particularly if y is determined by applying the iteration procedure to (1.4), would be $A=1$. In this case by (1.7)

$$\tan\delta=\frac{1}{kW}\int_0^\infty v_R Py\,dr. \qquad \ldots\ldots(1.9)$$

The expansions for the phase shifts may now be obtained using relationships of the type (1.7) and (1.9) directly. Alternatively, Bethe's (1949) methods may be generalized to the case of general orbital angular momentum. We derive below the expansion for $k^{2l+1}\cot\delta_l$ using Bethe's techniques. In this instance we choose $A\equiv\cot\delta$ so that the solution of (1.1) with $P=0$ is

$$v=\cot\delta[v_R(r,k)+\tan\delta v_I(r,k)] \qquad \ldots\ldots(1.10)$$

and for large r, y is identical with v.

Let $y=y(r,k)$ and $y_0=y(r,k_0)$ be the two solutions of (1.1) corresponding to the wave numbers $k=k$ and $k=k_0$. The corresponding solutions (1.10) are then labelled v and v_0. Then, following Bethe (1949), we have

$$[vv_0'-v_0v']_{r_0}=(k^2-k_0^2)\int_{r_0}^\infty(yy_0-vv_0)\,dr \qquad \ldots\ldots(1.11)$$

where r_0 implies the limit $r\to0$. Substituting for v from (1.10), equation (1.11) reduces to

$$\begin{aligned}-k^{l+1}k_0^{-l}\cot\delta^{(l)}+k_0^{l+1}k^{-l}\cot\delta_0{}^{(l)}&\\ =(k^2-k_0^2)\int_{r_0}^\infty(yy_0-vv_0)\,dr-[v_Iv_{I0}'-v_{I0}v_I']_{r_0}.&\end{aligned} \qquad \ldots\ldots(1.12)$$

Noting that

$$\frac{d}{dr}[v_Iv_{I0}'-v_{I0}'v_I']=(k^2-k_0^2)v_Iv_{I0}, \qquad \ldots\ldots(1.13)$$

it is easy to see that the square bracket in (1.12) just cancels the singularities arising in the integral. We can then write

$$k^{2l+1}\cot\delta^{(l)}=k_0{}^{2l+1}\cot\delta_0{}^{(l)}+k^lk_0{}^l(k^2-k_0^2)\int_0^\infty\{(vv_0-yy_0)-\text{singularities at } r=0\}\,dr. \qquad \ldots\ldots(1.14)$$

We now expand

$$Y(r,k)=k^{l}y(r,k), \qquad V(r,k)=k^{l}v(r,k) \qquad \text{.....(1.15)}$$

into the power series

$$Y=Y_0+(k^2-k_0^2)Y_1+(k^2-k_0^2)^2Y_2+\dots. \qquad \text{.....(1.16)}$$

$$V=V_0+(k^2-k_0^2)V_1+(k^2-k_0^2)^2V_2+\dots. \qquad \text{.....(1.17)}$$

Substituting into (1.14), we have

$$k^{2l+1}\cot\delta^{(l)}=\beta_0(k_0)+(k^2-k_0^2)\beta_1(k_0)+(k^2-k_0^2)^2\beta_2(k_0)+\dots. \qquad \text{.....(1.18)}$$

in which $\beta_0=k_0^{2l+1}\cot\delta_0^{(l)}$,

$$\beta_n=\int_0^\infty (V_0V_{n-1}-Y_0Y_{n-1}-\text{singularities at } r=0)\,dr \qquad \text{.....(1.19)}$$

β_0 is thus determined by the asymptotic form of y_0 which must be obtained, perhaps numerically from its differential equation, perhaps by iteration in a formula like (1.5).

From (1.10) and (1.17), we have

$$V_0=\beta_0k_0^{-l-1}v_{R0}+k_0^{l}v_{I0}, \qquad \text{.....(1.20)}$$

$$V_1=\left[\frac{d}{dk^2}V(k)\right]_{k=k_0}=\beta_1(k_0)k_0^{-l-1}v_{R0}+\beta_0\left[\frac{d}{dk^2}\frac{1}{k^{l+1}}v_R\right]_{k=k_0}+\left[\frac{d}{dk^2}k^{l}v_I\right]_{k=k_0} \qquad \text{.....(1.21)}$$

$$V_2=\frac{1}{2}\left[\frac{d^2}{d(k^2)^2}V(k)\right]_{k=k_0}=\beta_2(k_0)k_0^{-l-1}v_{R0}+\beta_1\left[\frac{d}{dk^2}k^{-l-1}v_R\right]_{k=k_0}+\tfrac{1}{2}\beta_0\left[\frac{d^2}{d(k^2)^2}k^{-l-1}v_R\right]_{k=k_0}+\frac{1}{2}\left[\frac{d^2}{d(k^2)^2}k^{l}v_I\right]_{k=k_0} \qquad \text{.....(1.22)}$$

etc. The coefficients Y_n in the expansion (1.16) may also be defined as

$$Y_0=Y(r,k_0) \qquad Y_n=\frac{1}{n!}\left[\frac{d^n}{d(k^2)^n}Y(k)\right]_{k=k_0} \qquad \text{.....(1.23)}$$

or alternatively through the set of differential equations

$$\frac{d^2Y_0}{dr^2}+\left[k_0^2-\frac{l(l+1)}{r^2}-P(r)\right]Y_0=0, \qquad \text{.....(1.24)}$$

$$\frac{d^2Y_n}{dr^2}+\left[k_0^2-\frac{l(l+1)}{r^2}-P(r)\right]Y_n=-Y_{n-1} \qquad \text{.....(1.25)}$$

as may readily be established by substituting (1.16) into (1.1) and equating the coefficients of each power of $(k^2-k_0^2)$ to zero. Keeping in mind that $Y_n\sim V_n$, one can also write the solution of (1.25) as a solution (perhaps by iteration) of an integral equation, namely

$$Y_n=\beta_nk_0^{-l-1}v_{R0}+(1/kW)\left[v_{R0}\int_r^\infty v_{I0}(s)P(s)Y_n(s)\,ds+v_{I0}\int_0^r v_{R0}\{P(s)Y_n(s)-Y_{n-1}(s)\}\,ds+v_{R0}\int_0^r v_{I0}(s)Y_{n-1}(s)\,ds\right]. \qquad \text{.....(1.26)}$$

The most useful energy about which to develop these expansions is zero, in which case $k_0=0$. From the series expansion for $j_l(kr)$ and $n_l(kr)$ we deduce that in this limit

$$V_0=\beta_0B_lr^{l+1}+[(2l+1)B_lr^{l}]^{-1} \qquad \text{.....(1.27)}$$

where $1/B_l = 1.3.5. \ldots (2l+1)$. Also Y_0 is that solution of

$$d^2Y_0/dr^2 - [l(l+1)/r^2 + P(r)]Y_0 = 0 \qquad \ldots\ldots(1.28)$$

which is asymptotically equal to V_0. The higher order functions V_n and Y_n are obtained by taking similar limits.

Since β_0 has the appropriate dimensions, we can write $\beta_0 = -a_l^{-2l-1}$, where a_l is a generalized scattering length for zero energy. Then β_1 may be written $\beta_1 = \frac{1}{2}a_l^{-2l}r_l$, where r_l is the 'range' of forces in the state with angular momentum $l\hbar$. Thus for $k_0 = 0$, (1.18) becomes

$$a_l^{2l}k^{2l+1}\cot\delta^{(l)} = -1/a_l + \tfrac{1}{2}r_lk^2 - r_l^3P_lk^4 + r_l^5Q_lk^6 - \ldots \qquad \ldots\ldots(1.29)$$

In this notation (1.19) may be rewritten

$$r_0 = 2\int_0^\infty [(1+r/a_0)^2 - Y_0^2]\,dr, \qquad \ldots\ldots(1.30)$$

$$r_l = 2\int_0^\infty [B_l^2(r/a_l)^{2l+2} + 2(r/a_l)/(2l+1) - a_l^{2l}Y_0^2]\,dr, \quad l>0, \qquad \ldots\ldots(1.31)$$

$$P_0 = \int_0^\infty \left[\tfrac{1}{8}\mu_0^2x^4 - \tfrac{2}{3}\mu_0x^3 + \tfrac{1}{2}(1+\mu_0)x^2 - \tfrac{1}{2}x + \frac{1}{r_0^2}Y_0Y_1\right]dx, \qquad \ldots\ldots(1.32)$$

$$P_1 = -\int_0^\infty \left[\tfrac{1}{90}\mu_1^4x^6 + \tfrac{1}{18}\mu_1^3x^4 + \tfrac{2}{15}\mu_1x^3 - \tfrac{1}{6}x - \frac{1}{2\mu_1^2} + \frac{1}{\mu_1^2}Y_0Y_1\right]dx, \qquad \ldots\ldots(1.33)$$

$$P_l = \int_0^\infty [\mu_l^{2l+2}B_l^2x^{2l+4}/2(2l+3) + \tfrac{1}{2}B_l^2\mu_l^{2l+1}x^{2l+2} + 2\mu_lx^3/(2l-1)(2l+1)(2l+3) - x/2(2l+1) + (a_l^{2l}/r_l^2)Y_0Y_1]\,dx, \quad l>1, \qquad \ldots\ldots(1.34)$$

where $\mu_l = r_l/a_l$.

Before leaving the neutron–proton system, it is desirable to consider the normalization $A \equiv 1$. Then

$$y \sim \sin(kr - l\pi/2) + \tan\delta^{(l)}\cos(kr - l\pi/2) \qquad \ldots\ldots(1.35)$$

and $\tan\delta^{(l)}$ is given by (1.9). We see that as $k \to 0$

$$\gamma_0 \equiv -\lim_{k\to 0} k^{-2l-1}\tan\delta^{(l)} \to \int_0^\infty B_lr^{l+1}P(r)y_0(r)\,dr, \qquad \ldots\ldots(1.36)$$

where $y_0(r)$ is the solution of (1.31) with the asymptotic form corresponding to (1.36), viz.

$$y_0 \sim B_lr^{l+1} - \gamma_0[(2l+1)B_lr^l]^{-1}. \qquad \ldots\ldots(1.37)$$

Alternatively, y_0 is the solution of

$$y_0(r) = B_lr^{l+1} - r^{l+1}\int_r^\infty s^{-1}P(s)y_0(s)\,ds/(2l+1) - r^{-l}\int_0^r s^{l+1}P(s)y_0(s)\,ds/(2l+1) \qquad \ldots\ldots(1.38)$$

The phase shift for general k may be expanded about $k_0 = 0$ in the form

$$k^{-2l-1}\tan\delta^{(l)} = -(\gamma_0 + \gamma_1k^2 + \gamma_2k^4 + \ldots). \qquad \ldots\ldots(1.39)$$

Then

$$\gamma_n = \int_0^\infty (x_0y_n + \ldots + x_{n-1}y_1 + x_ny_0)P(r)\,dr, \qquad \ldots\ldots(1.40)$$

where x_n and y_n are the coefficients in the series $k^{-l-1}y = y_0 + y_1k^2 + y_2k^4 + \ldots$ and $k^{-l-1}v_R = x_0 + x_1k^2 + x_2k^4 + \ldots$, i.e. $x_n = (-)^n\pi^{1/2}r^{2n+l+1}/2^{2n+l+1}\Gamma(l+3/2+n)n!$, from (1.3).

§ 2. PROTON-PROTON CENTRAL INTERACTION

The radial wave function times r satisfies the differential equation

$$\frac{d^2y}{dr^2} + [k^2 - l(l+1)/r^2 - 2\alpha k/r - P(r)]y = 0 \qquad \ldots\ldots(2.1)$$

and the boundary conditions

$$y(0,k) = 0, \qquad y(r,k) \sim A_l[\sin\{kr - l\pi/2 + \delta^{(l)}(r)\} + \tan\delta^{(l)}\cos\{kr - l\pi/2 + \delta^{(l)}(r)\}], \qquad \ldots\ldots(2.2)$$

where $\alpha = 1/2kr$, $R = \hbar^2/Me^2$, $2\alpha k/r$ is the Coulomb potential, $P(r)$ is the short range nuclear potential, $\delta^{(l)}(r)$ the Coulombian phase shift

$$\delta^{(l)}(r) = \gamma^{(l)} - \alpha\log 2kr, \qquad \gamma^{(l)} = \arg\Gamma(i\alpha + l + 1), \qquad \ldots\ldots(2.3)$$

$\delta^{(l)}$ is the nuclear phase shift and A_l is fixed by the normalization of y.

If we denote by F_R and F_I the regular and irregular solutions of equation (2.1) in the absence of the nuclear potential, with the asymptotic behaviour indicated below, then $y(r,k)$ is alternatively the solution of the integral equation

$$y(r,k) = A_lF_R(r,k) + \frac{1}{kW}F_R(r,k)\int_r^\infty F_I(s,k)P(s)y(s,k)\,ds + \frac{1}{kW}F_I(r,k)\int_0^r F_R(s,k)P(s)y(s,k)\,ds \qquad \ldots\ldots(2.4)$$

$$\sim A_l\sin\{kr - l\pi/2 + \delta^{(l)}(r)\} + \cos\{kr - l\pi/2 + \delta^{(l)}(r)\}\frac{1}{kW} \times \int_0^\infty F_R(s,k)P(s)y(s,k)\,ds, \quad kr \gg 1. \qquad \ldots\ldots(2.5)$$

It follows in the same way as in the n–p case that

$$A_l = \frac{\cot\delta^{(l)}}{kW}\int_0^\infty F_R(r,k)P(r)y(r,k)\,dr \qquad \ldots\ldots(2.6)$$

and for arbitrary normalization

$$\cot\delta^{(l)} = kW\frac{\int_0^\infty P(r)y^2(r,k)\,dr - \int_0^\infty y(r,k)P(r)\,dr\int_0^\infty G(r,s)P(s)y(r,s)\,ds}{\left[\int_0^\infty F_R(r,k)P(r)y(r,k)\,dr\right]^2}. \qquad \ldots(2.7)$$

To derive an energy expansion for the phase shifts we again use Bethe's methods. We choose for A_l

$$A_l \equiv C_l\cot\delta^{(l)}, \qquad \ldots\ldots(2.8)$$

in which C_l is the Coulomb barrier penetration factor, shortly to be defined explicitly. Further, let $F(r,k)$ be the complete solution of the auxiliary equation such that $F(r,k)$ is identical with $y(r,k)$ outside the range of nuclear forces, i.e.

$$F(r,k) = C_l\cot\delta^{(l)}[F_R(r,k) + \tan\delta^{(l)}F_I(r,k)]. \qquad \ldots\ldots(2.9)$$

It then follows as in the n–p case that

$$[FF_0' - F_0F']_{r_e} = (k^2 - k_0^2)\int_{r_e}^{\infty} [yy_0 - FF_0]\,dr. \qquad \ldots\ldots(2.10)$$

The solutions F_R and F_I have been investigated in some detail by Yost, Wheeler and Breit (1936). Using their results and substituting for F from (2.9) into (2.10) we have

$$\begin{aligned} k^{2l+1}C_l^2 \cot\delta^{(l)} + \frac{k^{2l+1}}{(2l+1)^2}[(2l+1)(q - p\ln\alpha) + p] &= g_l(k,k_0) + k_0^{2l+1}C_l^{(0)2}\cot\delta_0^{(l)} \\ &+ k_0^{2l+1}[(2l+1)(q_0 - p_0\ln\alpha_0) + p_0]/(2l+1)^2 \\ &+ k^l k_0^l (k^2 - k_0^2)\rho_l(k,k_0), \qquad \ldots\ldots(2.11) \end{aligned}$$

in which $g_l(k,k_0)$ is a known function of the energy:

$$\begin{aligned} g_l(k,k_0) = &-k^l k_0^l/(2l+1)^2\{(2l-1)a_l k^l a_{-l+1}^{(0)} k_0^{-l+1} \\ &+ a_{l-1}k^{l-1}a_{-l+2}^{(0)}k_0^{-l+2}(2l-3) + \ldots + a_{-l+1}k^{-l+1}(1-2l)a_l^{(0)}k_0^l\}, \\ &\qquad \ldots\ldots(2.12) \end{aligned}$$

$$(2l+1)!\,C_l = 2^l[l^2+\alpha^2]^{1/2}[(l-1)^2+\alpha^2]^{1/2}\ldots[1+\alpha^2]^{1/2}(2\pi\alpha)^{1/2}(e^{2\pi\alpha}-1)^{-1/2}, \qquad \ldots\ldots(2.13)$$

$$p = (2l+1)(e^{2\pi\alpha}-1)C_l^2/\pi, \qquad \ldots\ldots(2.14)$$

$$\begin{aligned} q = p\left\{\sum_{s=1}^{l} s/(s^2+\alpha^2) - \sum_{s=1}^{2l+1} s^{-1} + \mathrm{Re}\,\frac{\Gamma'(-i\alpha)}{\Gamma(-i\alpha)}\right\} \\ + (-)^{l+1}2^l/(2l)!\sum_{n=-l}^{l}\mathrm{Im}\,\frac{2^n(i\alpha+n-1)\ldots(i\alpha-l)}{(l+n+1)!} \qquad \ldots\ldots(2.15) \end{aligned}$$

and a_n are coefficients defined by Yost, Wheeler and Breit (1936) by certain recurrence formulae. In (2.11)

$$\rho_l(k,k_0) = \int_0^{\infty}[FF_0 - yy_0 - \text{singularities at } r=0]\,dr. \qquad \ldots\ldots(2.16)$$

The singularities referred to in (2.16) arise in a manner similar to those in the n–p considerations; that these singularities are subtracted out may be readily established.

Explicitly, for $l=0$, formulae (2.11) and (2.12) become

$$\frac{1}{R}\left[\frac{\pi\cot\delta^{(0)}}{\exp(2\pi\alpha)-1} + h_0(\alpha)\right] = \frac{1}{R}\left[\frac{\pi\cot\delta_0^{(0)}}{\exp(2\pi\alpha_0)-1} + h_0(\alpha_0)\right] + (k^2-k_0^2)\rho_0(k,k_0). \qquad \ldots\ldots(2.17)$$

$g_0(k,k_0)=0$, and $h_0(\alpha)$ is defined by

$$h_0(\alpha) = \mathrm{Re}\,\frac{\Gamma'(-i\alpha)}{\Gamma(-i\alpha)} - \ln\alpha. \qquad \ldots\ldots(2.18)$$

For $l=1$, this formula is

$$\begin{aligned} \frac{1}{R}\left[\frac{\pi k^2(1+\alpha^2)\cot\delta^{(1)}}{\exp(2\pi\alpha)-1} + k^2h_1(\alpha)\right] &= \frac{1}{R}\left[\frac{\pi k_0^2(1+\alpha_0^2)\cot\delta_0^{(1)}}{\exp(2\pi\alpha_0)-1} + k_0^2h_1(\alpha_0)\right] \\ &+ \frac{1}{2R}(k^2-k_0^2) + 9k^2k_0^2(k^2-k_0^2)\rho_1(k,k_0), \qquad \ldots\ldots(2.19) \end{aligned}$$

$g_1(k,k_0) = \dfrac{1}{18R}(k^2-k_0^2)$, and $h_1(\alpha)$ is given by

$$h_1(\alpha) = -1 + (1+\alpha^2)\{\mathrm{Re}\,\Gamma'(-i\alpha)/\Gamma(-i\alpha) - \ln\alpha - 3/2\}. \qquad \ldots\ldots(2.20)$$

The expression for $g_2(k, k_0)$ has also been derived, and is

$$25g_2(k,k_0)=13(k^2-k_0^2)/576R^3+3(k^4-k_0^4)/96R. \quad \ldots\ldots(2.21)$$

We now perform the expansion of (2.11) in the special case $k_0=0$. For this purpose we denote

$$\lim_{k\to 0} k^{2l+1}C_l^2\cot\delta^{(l)}=a^{-2l-1} \quad \ldots\ldots(2.22)$$

and also write

$$\lim_{k\to 0} Rk^{2l}[(2l+1)(q-p\ln\alpha)+p]=h_l(R). \quad \ldots\ldots(2.23)$$

In particular

$$h_0(R)=\lim_{k\to 0}h_0(\alpha)=0, \qquad h_1(R)=\lim_{k\to 0}k^2h_1(\alpha)=-3/8R^2. \quad \ldots\ldots(2.24)$$

Similarly, let

$$\lim_{k\to 0}g_l(k,k_0)=g_l(k)=\gamma_1k^2+\gamma_2k^4+\ldots.\gamma_lk^{2l} \quad \ldots\ldots(2.25)$$

where the coefficients γ_n are defined explicitly for $l=0$, 1, 2 by (2.17), (2.19) and (2.21) respectively. Choosing also an expansion for $k^lF(r,k)$ and $k^ly(r,k)$ as

$$\left.\begin{aligned} k^lF(r,k)&=X_0(r)+k^2X_1(r)+k^4X_2(r)+\ldots.\\ k^ly(r,k)&=y_0(r)+k^2y_1(r)+k^4y_2(r)+\ldots.,\end{aligned}\right\} \quad \ldots\ldots(2.26)$$

we have, on substituting into (2.11)

$$\begin{aligned} k^{2l+1}C_l^2\cot\delta^{(l)}&+k^{2l+1}/(2l+1)^2[(2l+1)(q-p\ln\alpha)+p]\\ &=a_l^{-2l-1}+h_l(R)/(2l+1)^2R+(\gamma_1+\beta_1)k^2+(\gamma_2+\beta_2)k^4+\ldots.\\ &\quad+(\gamma_l+\beta_l)k^{2l}+\beta_{l+1}k^{2l+2}+\ldots. \quad \ldots\ldots(2.27)\end{aligned}$$

in which

$$\beta_n=\int_0^\infty (X_0X_{n-1}-y_0y_{n-1})\,dr. \quad \ldots\ldots(2.28)$$

The coefficients X_n are now defined in more detail. We recall that

$$k^lF(r,k)=C_l^2k^{2l+1}\cot\delta^{(l)}[F_R(r,k)/C_lk^{l+1}]+k^lC_lF_l(r,k). \quad \ldots\ldots(2.29)$$

In Appendix A the power series development for $F_R(r,k)/C_lk^{l+1}$ and $k^lC_lF_l(r,k)$ is outlined. Using these developments together with the development for $C_l^2k^{2l+1}\cot\delta^{(l)}$ given by (2.27) we get

$$X_0(r)=a_l^{-2l-1}S_0^{(l)}(r)+N_0^{(l)}(r), \quad \ldots\ldots(2.30)$$

$$\begin{aligned} X_1(r)=a_l^{-2l-1}S_1^{(l)}(r)+\left\{\gamma_1+\beta_1-\left\langle\frac{d}{d(k^2)}\frac{k^{2l+1}}{(2l+1)^2}\right.\right.\\ \left.\left.\times[(2l+1)(q-p\ln\alpha)+p]\right\rangle_{k=0}\right\}S_0^{(l)}(r)+N_1^{(l)}(r) \quad \ldots\ldots(2.31)\end{aligned}$$

$$\begin{aligned} X_2(r)=a^{-2l-1}S_2^{(l)}(r)+\left\{\gamma_1+\beta_1-\left\langle\frac{d}{d(k^2)}\frac{k^{2l+1}}{(2l+1)^2}[(2l+1)(q-p\ln\alpha)+p]\right\rangle_{k=0}\right\}\\ \times S_1^{(l)}(r)+\left\{\gamma_2+\beta_2-\left\langle\frac{d^2}{d(k^2)^2}\frac{k^{2l+1}}{(2l+1)^2}[(2l+1)(q-p\ln\alpha)+p]\right\rangle_{k=0}\right\}\\ \times S_0^{(l)}(r)+N_2^{(l)}(r) \quad \ldots\ldots(2.32)\end{aligned}$$

etc,

The coefficients y_n may generally be written down as solutions of either the set of differential equations

$$\frac{d^2y_n}{dr^2}-[l(l+1)/r^2+2\alpha k/r+P(r)]y_n=-y_{n-1}, \; n\geqslant 1 \quad \ldots\ldots(2.33)$$

or the integral equation

$$y_n = A_n^{(l)} S_0^{(l)}(r) + \frac{1}{kW(S,N)} S_0^{(l)}(r) \int_r^\infty N_0^{(l)}(s) P(s) y_n(s)\, ds$$
$$+ \frac{1}{kW(S,N)} N_0^{(l)}(r) \int_0^r S_0^{(l)}(s)[P(s) y_n(s) - y_{n-1}(s)]\, ds$$
$$+ \frac{1}{kW(S,N)} S_0^{(l)}(r) \int_0^r N_0^{(l)}(s) y_{n-1}(s)\, ds, \qquad n \geqslant 1 \quad \ldots\ldots (2.34)$$

in which

$$A_n^{(l)} = \gamma_n + \beta_n - \left\langle \frac{d^n}{d(k^2)^n}[(2l+1)(q - p\ln\alpha) + p] \right\rangle_{k=0}. \quad \ldots\ldots (2.35)$$

§ 3. NON-CENTRAL PROTON-PROTON INTERACTION

We derive the contribution to the triplet differential scattering cross section taking into account the P state and the coupling of the F state to the P state, having assumed a tensorial (axial dipole dependence) interaction. The relation of the phase shifts to the interaction potential in this instance is also derived and the expansions in the energy are also indicated for quantities closely related to the phase shifts.

In the non-relativistic Schrödinger equation for the wave function of the two protons in the centre-of-mass system, viz.

$$[\Delta + (M/\hbar^2)(E - V)]\psi = 0, \quad \ldots\ldots (3.1)$$

we choose an interaction of the form

$$V = J(r) + K(r)\boldsymbol{\sigma}^{(1)} \cdot \boldsymbol{\sigma}^{(2)} + L(r) D_{12} + e^2/r \quad \ldots\ldots (3.2)$$

in which D_{12} is an axial dipole coupling

$$D_{12} = 3(\boldsymbol{\sigma}^{(1)} \cdot \mathbf{x}_0)(\boldsymbol{\sigma}^{(2)} \cdot \mathbf{x}_0) - \boldsymbol{\sigma}^{(1)} \cdot \boldsymbol{\sigma}^{(2)}. \quad \ldots\ldots (3.3)$$

The notation used is standard; $J(r)$, $K(r)$ and $L(r)$ are radial functions, $\boldsymbol{\sigma}^{(1)}$ the Pauli spin operator for particle (1), etc., $\mathbf{x}_0$ a unit vector in the direction of the line joining the two particles, e^2/r the Coulomb potential.

The states of the system separate, in the usual way, into two classes: the singlet states for l even, triplet states for l odd. In the singlet state, $J^2 = l^2$, $J_z = L_z$ and the complete spin, angular momentum and radial dependence of ${}^1\psi$ for a given j and m is

$${}^1\psi_j^m = (1/r)\,{}^1R_j^{(l)}(r)\,{}^1Z_l^m(\theta, \phi) \quad \ldots\ldots (3.4)$$

in which ${}^1R_j^{(l)}(r)$ is the solution of the equation

$$[d^2/dr^2 + k^2 - l(l+1)/r^2 - 2\alpha k/r - {}^1P(r)]\,{}^1R_j^{(l)}(r) = 0 \quad \ldots\ldots (3.5)$$

and, for an interaction of the form (3.2),

$${}^1P(r) = (M/\hbar^2)[J(r) - 3K(r)]. \quad \ldots\ldots (3.6)$$

In the singlet state, then, the definition of the phase shifts, the energy expansions and the differential scattering cross section are identical in form to the case when the potential (3.2) is purely central.

In the triplet state, pertaining to the possibilities $j = l$ and $j = l \pm 1$, for l odd, the wave function ${}^3\psi_j^m$ may be generally written as

$${}^3\psi_j^m = \Sigma_l (1/r)\,{}^3R_j^{(l)}(r)\,{}^3Z_j^{(l)m} \quad \ldots\ldots (3.7)$$

in which the summation is $l=j$ for j odd, $l=j\pm1$ for j even. The radial wave functions ${}^3R_j^{(l)}$ are now solutions of the equations

$$l=j: \quad [d^2/dr^2-j(j+1)/r^2-2\alpha k/r+k^2]{}^3R_j^{(l)} - (M/\hbar^2)[J(r)+K(r)+2L(r)]{}^3R_j^{(l)}=0 \qquad \ldots\ldots(3.8)$$

and the coupled set

$$l=j-1: \quad \left[\frac{d^2}{dr^2}-\frac{(j-1)j}{r}-\frac{2\alpha k}{r}+k^2-P(r) + \frac{2(j-1)}{2j+1}Q(r)\right]u_j+\frac{6[j(j+1)]^{1/2}}{2j+1}Q(r)v_j=0, \qquad \ldots\ldots(3.9)$$

$$l=j+1: \quad \left[\frac{d^2}{dr^2}-\frac{(j+1)(j+2)}{r}-\frac{2\alpha k}{r}+k^2-P(r) + \frac{2(j+2)}{2j+1}Q(r)\right]v_j+\frac{6[j(j+1)]^{1/2}}{2j+1}Q(r)u_j=0. \qquad \ldots\ldots(3.10)$$

In the above we have set

$$u_j\equiv{}^3R_j^{(j-1)}, \qquad v_j\equiv{}^3R_j^{(j+1)}, \qquad P(r)=(M/\hbar^2)[J(r)+K(r)], \qquad Q(r)=(M/\hbar^2)L(r). \qquad \ldots\ldots(3.11)$$

We note here that for $l=j$, j odd, the radial wave function is uncoupled; the definition of the nuclear phase shift and the expansion in energy may again be performed as outlined in § 2.

As for the coupled set (3.10) and (3.11), we note first that the solutions u_j and v_j are to be regular at the origin, i.e. $u_j(0,k)=v_j(0,k)=0$, and outside the range of nuclear forces they are equivalent to the solution of (3.10) and (3.11) with $P(r)\equiv Q(r)\equiv0$, having the asymptotic behaviour

$$\left.\begin{aligned} u_j &\sim A_j(\cos\delta_j{}^u)^{-1}\sin(kr-\tfrac{1}{2}(j-1)\pi+\delta^{(j-1)}(r)+\delta_j{}^u),\\ v_j &\sim B_j(\cos\delta_j{}^v)^{-1}\sin(kr-\tfrac{1}{2}(j+1)\pi+\delta^{(j+1)}(r)+\delta_j{}^v). \end{aligned}\right\} \qquad \ldots\ldots(3.12)$$

Furthermore, we see that there are four linearly independent functions, regular at the origin, satisfying these conditions. Call these $u_j{}^{\alpha,\gamma}$ and $v_j{}^{\alpha,\gamma}$ and the corresponding nuclear phase shifts $\delta_j{}^{u,\alpha,\gamma}$ and $\delta_j{}^{v,\alpha,\gamma}$. The triplet wave functions, defined by (3.7), will be labelled ${}^3\psi_j{}^{\alpha,m}$ and ${}^3\psi_j{}^{\gamma,m}$, viz.

$${}^3\psi_j{}^{\alpha,m}=(1/r)[u_j{}^{\alpha}{}^3Z_j{}^{(j-1)m}+v_j{}^{\alpha}{}^3Z_j{}^{(j+1)m}], \qquad \ldots\ldots(3.13)$$

etc.

By a slight generalization of the phase shift concept, we rewrite (3.13) and its counterpart with α replaced by γ, so that

$${}^3\psi_j{}^{\alpha,m}\sim(1/r\cos\delta_j{}^{\alpha})\sin[kr-(j-1)\pi/2+\delta^{(j-1)}(r)+\delta_j{}^{\alpha}] \times\{{}^3Z_j{}^{(j-1)m}+\omega_j{}^{\alpha}{}^3Z_j{}^{(j+1)m}\}, \qquad \ldots\ldots(3.14)$$

$${}^3\psi_j{}^{\gamma,m}\sim(1/r\cos\delta_j{}^{\gamma})\sin[kr-(j+1)\pi/2+\delta^{(j+1)}(r)+\delta_j{}^{\gamma}] \times\{{}^3Z_j{}^{(j-1)m}+\omega_j{}^{\gamma}{}^3Z_j{}^{(j+1)m}\}. \qquad \ldots\ldots(3.15)$$

$\omega_j{}^{\alpha}$ and $\omega_j{}^{\gamma}$ measure respectively the extent of the admixture of the state with orbital angular momentum number $l=j+1$ to that state with $l=j-1$ and vice versa. We are here following the methods given for neutron–proton tensor forces by Rohrlich and Eisenstein (1949). By substituting (3.12) into (3.13) we find that (3.14) and (3.15) may be arrived at by setting

$$\delta_j{}^{\alpha}\equiv\delta_j{}^{u,\alpha}=\delta_j{}^{v,\alpha}+\gamma^{(j-1)}-\gamma^{(j+1)}-\pi, \qquad \ldots\ldots(3.16)$$

$$\delta_j{}^{\gamma}\equiv\delta_j{}^{u,\gamma}=\delta_j{}^{v,\gamma}+\gamma^{(j+1)}-\gamma^{(j-1)}+\pi \qquad \ldots\ldots(3.17)$$

and setting

$$\omega_j^{\alpha} = \frac{B_j^{\alpha}}{A_j^{\alpha}} \cos\delta_j^{\alpha}[\cos(\delta^{\alpha}{}_j + \gamma^{(j-1)} - \gamma^{(j+1)} - \pi)]^{-1} \quad \ldots\ldots(3.18)$$

$$\omega_j^{\gamma} = \frac{B_j^{\alpha}}{A_j^{\alpha}} \cos\{\delta_j^{\gamma} + \gamma^{(j+1)} - \gamma^{(j-1)} + \pi\}[\cos\delta_j^{\gamma}]^{-1}. \quad \ldots\ldots(3.19)$$

It also follows from the orthogonality conditions on the wave functions ${}^3\psi_j^{\alpha,m}$ and ${}^3\psi_j^{\gamma,m}$ that

$$\omega_j^{\alpha}\omega_j^{\gamma} = -1. \quad \ldots\ldots(3.20)$$

The total triplet wave function for a fixed j and m, j even, is then a linear combination of the functions ${}^3\psi_j^{\alpha,m}$ and ${}^3\psi_j^{\gamma,m}$. Call this ${}^3\psi_j^{m(2)}$. If we denote by ${}^3\psi_j^{m(1)}$ the triplet wave function for fixed j and m, j odd, then the total triplet wave function for a fixed polarization, ${}^3\psi_{\text{tot}}{}^m$, is

$${}^3\psi_{\text{tot}}{}^m = \sum_{j\text{ odd}} {}^3\psi_j^{m(1)} + \sum_{j\text{ even}} {}^3\psi_j^{m(2)}. \quad \ldots\ldots(3.21)$$

The total unpolarized wave, ${}^3\psi_{\text{tot}}$, is obtained by suitably averaging over m. The scattered wave may then be written in the form

$$\begin{aligned}{}^3\psi_{\text{scat}} \sim {}^3\psi_{\text{scat},c} &+ (1/2ir)e^{i(kr-l\pi|2-\alpha\log 2kr)} \sum_{m,\,l\text{ odd}} \{\beta_l{}^m\, {}^3Z_l^{(l)m} \exp i(\gamma^{(l)} + 2\delta_l) \\ &+ [\alpha_{l+1}{}^m \exp i(\gamma^{(l)} + 2\delta_{l+1}{}^{\alpha}) - \gamma_{l+1}{}^m \exp i(\gamma^{(l+2)} + 2\delta_{l+1}{}^{\gamma})]\, {}^3Z_{l+1}{}^{(l)m} \\ &+ [\gamma_{l-1}{}^m\omega_{l-1}{}^{\gamma} \exp i(\gamma^{(l)} + 2\delta_{l-1}{}^{\gamma}) - \alpha_{l-1}{}^m\omega_{l-1}{}^{\alpha} \exp i(\gamma^{(l-2)} + 2\delta_{l-1}{}^{\alpha})]\, {}^3Z_{l-1}{}^{(l)m} \\ &- (2/k)^3 j_m\, {}^3(\sigma)_m[4\pi(2l+1)]^{1/2} i^l Y_l{}^0 \exp 2i\gamma^{(l)}\}. \end{aligned} \quad \ldots\ldots(3.22)$$

In (3.22), ${}^3\psi_{\text{scat},c}$ is the scattered wave when purely Coulomb interactions are considered. The constants $\alpha_j{}^m$, $\beta_j{}^m$, $\gamma_j{}^m$ are fixed, in the usual way, by demanding that asymptotically ${}^3\psi_{\text{tot}} - {}^3\psi_{\text{tot},c}$ be an outgoing wave. The constants ${}^3j_m$ are chosen (for unpolarized waves) $|{}^3j_m|^2 = 1/4$ for $m = 1, 0, -1$. The phase shift δ_l corresponds to the radial wave function $l = j$, j odd (see equation (3.8)). The differential cross section in the triplet state is then

$${}^3dS_{\theta} = {}^3\psi_{\text{scat}} \cdot {}^3\psi_{\text{scat}}{}^* r^2\, d\Omega. \quad \ldots\ldots(3.23)$$

The cross section has been derived taking into account the states ${}^3P_0$, ${}^3P_1$, ${}^3P_2$ and the ${}^3F_2$ coupling. The formulae are quoted in Appendix B.

We turn now to a further inspection of $\delta_j^{\alpha,\gamma}$, $\omega_j^{\alpha,\gamma}$. For this purpose we convert the differential equation (3.9) and (3.10), together with the boundary conditions on u_j, v_j into an equivalent integral equation, namely,

$$u_j = A_j F_{\text{R},j-1} - (1/k)F_{\text{R},j-1}\int_r^{\infty} F_{\text{I},j-1}\phi_1(s)\, ds - (1/k)F_{\text{I},j-1}\int_0^r F_{\text{R},j-1}\phi_1(s)\, ds, \quad \ldots\ldots(3.24)$$

$$v_j = B_j F_{\text{R},j+1} - (1/k)F_{\text{R},j+1}\int_r^{\infty} F_{\text{I},j+1}\phi_2(s)\, ds - (1/k)F_{\text{I},j+1}\int_0^r F_{\text{R},j+1}\phi_2(s)\, ds, \quad \ldots\ldots(3.25)$$

where $F_{\text{R},j-1}$, $F_{\text{I},j-1}$, $F_{\text{R},j+1}$, $F_{\text{I},j+1}$ are the Coulombian functions and are the independent solutions of the auxiliary equations (3.9) and (3.10) with $P \equiv Q \equiv 0$;

$$\phi_1(s) = \left[P(s) - \frac{2(j-1)}{2j+1}Q(s)\right]u_j - \frac{6[j(j+1)]^{1/2}}{2j+1}Q(s)v_j, \quad \ldots\ldots(3.26)$$

$$\phi_2(s) = \left[P(s) - \frac{2(j+2)}{2j+1}Q(s)\right]v_j - \frac{6[j(j+1)]^{1/2}}{2j+1}Q(s)u_j. \quad \ldots\ldots(3.27)$$

Comparing now the asymptotic forms of (3.24) and (3.25) with (3.12), we have

$$A_j = -\cot\delta_j{}^u \int_0^\infty k^{-1} F_{\mathrm{R},\,j-1}\phi_1(s)\,ds, \qquad \ldots\ldots(3.28)$$

$$B_j = -\cot\delta_j{}^v \int_0^\infty k^{-1} F_{\mathrm{R},\,j+1}\phi_2(s)\,ds. \qquad \ldots\ldots(3.29)$$

The phase shifts may be conveniently defined as follows. In (3.28), choose $A_j = 1$. Then

$$C_{j-1}{}^{-2}k^{-2j+1}\tan\delta_j{}^\alpha = -\int_0^\infty k^{-j}C_{j-1}{}^{-1}F_{\mathrm{R},\,j-1}[k^{-j}C_{j-1}{}^{-1}\phi_1(s)]\,ds, \qquad \ldots\ldots(3.30)$$

where C_{j-1} is the normalization factor for the Coulomb wave functions. A similar definition for $\tan\delta_j{}^\gamma$ may be arrived at by choosing in (3.29) $B_j{}^\gamma = 1$. These choices of the normalization constants would be convenient if equations (3.24) and (3.25) are solved, for instance, using the iteration procedure.

The energy expansions for quantities closely related to the phase shifts may also be derived by generalizing Bethe's technique. For this purpose we choose

$$A_j{}^\alpha = C_{j-1}\cot\delta_j{}^\alpha. \qquad \ldots\ldots(3.31)$$

Let u, u_0; v, v_0 be the two solutions (3.9) and (3.10) corresponding to the wave numbers k and k_0, and $F_{j-1}{}^\alpha$ the complete solution of the auxiliary equation (i.e. (3.9) with $P(r) \equiv Q(r) \equiv 0$), viz.

$$F_{j-1}{}^\alpha = C_{j-1}[\cot\delta_j{}^\alpha F_{\mathrm{R},\,j-1} + F_{\mathrm{I},\,j-1}]. \qquad \ldots\ldots(3.32)$$

It then follows, as in § 2, that

$$[FF_0' - F_0F']_{r_0} = (k^2 - k_0^2)\int_{r_0}^\infty [uu_0 - FF_0]dr + \frac{6[j(j+1)]^{1/2}}{2j+1}\int_{r_0}^\infty Q(r)[vu_0 - uv_0]dr. \qquad \ldots\ldots(3.33)$$

In the latter derivation we have dropped the subscripts α and j where such omission causes no confusion.

Comparison of (3.33) with (2.10) indicates that the results are similar in form, though the expression (3.33) is of a more general character. The derivation of the phase shift and its expansion in the energy may be achieved in a manner outlined in § 2.

APPENDIX A

ENERGY EXPANSIONS OF THE REGULAR AND IRREGULAR COULOMBIAN WAVE FUNCTION

The functions $S_l \equiv [C_l k^{l+1}]^{-1} F_{\mathrm{R}}{}^{(l)}(r,k)$ and $N_l \equiv C_l k^l F_{\mathrm{I}}{}^{(l)}(r,k)$ are two linearly independent solutions of the equation

$$\frac{d^2G}{dr^2} - [l(l+1)/r^2 + 1/Rr]G = -k^2G. \qquad \ldots\ldots(A\,1)$$

Their expansions in the series

$$\left.\begin{aligned} S_l &= S_0{}^{(l)}(r) + k^2 S_1{}^{(l)}(r) + k^4 S_2{}^{(l)}(r) + \ \ldots \\ N_l &= N_0{}^{(l)}(r) + k^2 N_1{}^{(l)}(r) + k^4 N_2{}^{(l)}(r) + \ \ldots \end{aligned}\right\} \qquad \ldots\ldots(A\,2)$$

have been investigated by Yost, Wheeler and Breit (1936) for S_l and recently by Breit and Hull (1950) for N_l. The terms of these expansions have been

derived explicitly by other means for certain particular cases, and in our notation are, for all l,

$$\left.\begin{aligned} S_0^{(l)}(r) &= R^{l+1}\Gamma(2l+2)\,(r/R)^{1/2}I_{2l+1}, \\ N_0^{(l)}(r) &= 2R^{-l}\{1/\Gamma(2l+2)\}(r/R)^{1/2}K_{2l+1};* \end{aligned}\right\} \quad \ldots\ldots(\text{A}\,3)$$

$$\text{for } l=0,\quad \left.\begin{aligned} S_1^{(0)}(r) &= (-1/3)r^2RI_2, \\ S_2^{(0)}(r) &= (1/18)(r/R)^{1/2}R^2r^3I_3-(1/45)R^2r^3I_4, \\ N_1^{(0)}(r) &= (2/3)r^2K_2, \\ N_2^{(0)}(r) &= (2/45)Rr^3K_4+(1/9)(r/R)^{1/2}Rr^3K_3; \end{aligned}\right\} \quad \ldots\ldots(\text{A}\,4)$$

$$\text{for } l=1,\quad \left.\begin{aligned} S_1^{(1)}(r) &= -2r^2R^2[I_4+(R/r)^{1/2}I_5], \\ S_2^{(1)}(r) &= (1/3)r^2R^3[(r/R)^{3/2}I_5+(4/5)(r/R)^{1/2}I_7+(8r/5R)I_6], \\ N_1^{(1)}(r) &= (1/9R)r^2K_2+(2/9)(r/R)^{1/2}K_1, \\ N_2^{(1)}(r) &= (1/54)r^3[(r/R)^{1/2}K_3+(12/5)K_2]. \end{aligned}\right\} \quad \ldots\ldots(\text{A}\,5)$$

In all of the above the argument of the Bessel function is $2(r/R)^{1/2}$.

It will be noticed that in the limit as $R\to\infty$ (i.e. the n–p case), the function S_l reduces to the expansion of

$$[(\pi kr/2)^{1/2}J_{l+1/2}(kr)]2^{l+1}\Gamma(l+3/2)/\pi^{1/2}k^{l+1}=r^{l+1}[1-r^2k^2/2(2l+3)+\ldots] \quad \ldots(\text{A}\,6)$$

It is readily checked that the terms as defined by (A 4) and (A 5) conform to (A6) in this limit. On the other hand N_l does not reduce directly to the corresponding irregular solution of the n–p system in this limit, as may be surmised from inspection of the series defining $F_l(r,k)$.

Blatt and Jackson (1949), in their consideration of the S state, have developed an alternative expansion for N_0 which is slightly less restrictive than the expansion given in (A 2). The essence of this expansion is to separate out of the irregular solution a part which reduces to the solution of the n–p system as $R\to\infty$, i.e.

$$[(\pi kr/2)^{1/2}J_{-l-1/2}(kr)](-)^lk^{2l-1}\pi^{1/2}/\Gamma(l+\tfrac{3}{2})=(2l+1)^{-1}r^{-l}[1-k^2r^2/2(1-2l)+\ldots]. \quad \ldots\ldots(\text{A}\,7)$$

For $l=0$, we write $\qquad N_0=X_0+R^{-1}h_0(\alpha)S_0 \qquad \ldots\ldots(\text{A}\,8)$

in which $\qquad X_0=\psi_0+rR^{-1}[\ln(r/R)-1/2]\Phi_0. \qquad \ldots\ldots(\text{A}\,9)$

Blatt and Jackson's expansion is now written

$$N=X_0^{(0)}+k^2X_1^{(0)}+k^4X_2^{(0)}+\ldots+R^{-1}h_0(\alpha)[S_0^{(0)}+k^2S_1^{(0)}+\ldots] \quad \ldots\ldots(\text{A}\,10)$$

in which the functions are already specified. Observing that the first few terms of the expansion in the energy of $h_0(\alpha)$ are

$$h_0(\alpha)=(\tfrac{1}{3})k^2R^2+(2/15)k^4R^4+\ldots, \quad \ldots\ldots(\text{A}\,11)$$

we have

$$\left.\begin{aligned} X_0^{(0)} &= N_0^{(0)}, \\ X_1^{(0)} &= N_1^{(0)}-(R/3)S_0^{(0)}, \\ X_2^{(0)} &= N_2^{(0)}-(R/3)S_1^{(0)}-(2R^3/15)S_0^{(0)}. \end{aligned}\right\} \quad \ldots\ldots(\text{A}\,12)$$

Similarly, for $l=1$, we write

$$N_1=X_1+(9R)^{-1}(k^2+1/4R^2)h_0(\alpha)S_1 \quad \ldots\ldots(\text{A}\,13)$$

* K_ν is here the function defined by Watson, *Theory of Bessel Functions* (Cambridge, 1922), p. 79. For ν integral, it differs from the function used by Breit by the factor $(-1)^\nu$.

in which

$$X_1=(1/3r)\psi_1+r^2(9R)^{-1}\{k^2+1/4R^2)(\ln(r/R)-11/6)-k^2\}\Phi_1. \quad \ldots\ldots(A\,14)$$

The coefficients $X_n^{(1)}$ of the expansion

$$N_1=X_0^{(1)}+k^2X_1^{(1)}+k^4X_2^{(1)}+\ldots+(9R)^{-1}(k^2+1/4R^2)h_0(\alpha)\{S_0^{(1)}+k^2S_1^{(1)}+\ldots\} \quad \ldots\ldots(A\,15)$$

are then

$$\left.\begin{aligned} X_0^{(1)}&=N_0^{(1)}, \quad X_1^{(1)}=N_1^{(1)}-(1/108R)S_0^{(1)},\\ X_2^{(1)}&=N_2^{(1)}-(1/108R)[S_1^{(1)}+(22R^2/5)S_0^{(1)}],\end{aligned}\right\} \quad \ldots\ldots(A\,16)$$

APPENDIX B

DIFFERENTIAL SCATTERING CROSS SECTION FOR THE ^{3}P STATE AND THE $^3F_2$ COUPLING

The following is the contribution to the triplet differential cross section for scattering due to the states $^3P_0$, $^3P_1$ and $^3P_2$ along with the coupling of the $^3F_2$ state to the $^3P_2$ state. The Coulomb scattering is taken into account completely. We write the cross section in the form

$$(^3dS_\theta/d\Omega)=(^3dS_\theta/d\Omega)_C+(^3dS_\theta/d\Omega)_N+(^3dS_\theta/d\Omega)_{int}, \quad \ldots\ldots(B\,1)$$

in which the subscripts C, N and int denote the purely Coulomb and nuclear scattering and the interference of the two, respectively.

$$(^3dS_\theta/d\Omega)_C=\frac{\alpha^2}{4k^2}\left\{\frac{3}{4}\left(\frac{1}{\sin^4\theta/2}+\frac{1}{\cos^4\theta/2}-\frac{2\cos(\alpha\log\tan^2\theta/2)}{\sin^2\theta/2\cos^2\theta/2}\right)\right\} \quad \ldots\ldots(B\,2)$$

$$\begin{aligned}(^3dS_\theta/d\Omega)_N=\frac{3\pi}{k^2}\Big\{&[\sqrt{2}p_2+(4/3)\sin^2\delta_0+4\sin^2\delta_1+(20/3)b_1\sin^2\delta_2\\
&+(20/3)b_2\sin^2(\gamma^{(3)}-\gamma^{(1)})-c_1\sin^2(\delta_2-\delta_1)+a_2\sin^2(\gamma^{(3)}-\gamma^{(1)}-\delta_0)\\
&-c_2\sin^2(\gamma^{(3)}-\gamma^{(1)}-\delta_1)-(2/3)f\sin^2(\gamma^{(3)}-\gamma^{(1)}-\delta_2)-4a_1\sin^2(\delta_2-\delta_0)](Y_1^0)^2\\
&+2[-p_2-(1/9)f\sin^2(\gamma^{(3)}-\gamma^{(1)}-\delta_2)+d_1\sin^2(\delta_2-\delta_0)\\
&+3c_1\sin^2(\delta_2-\delta_1)+d_2\sin^2(\gamma^{(3)})-\gamma^{(1)}-\delta_0)+3c_2\sin^2(\gamma^{(3)}-\gamma^{(1)}-\delta_1)]Y_1^1Y_1^{1*}\\
&+\frac{1}{\sqrt{21}}\Big[-\frac{6(2+\omega_1+\omega_2)}{2+\omega_1^2+\omega_2^2}-20b_2\sin^2(\gamma^{(1)}-\gamma^{(3)})-20b_2\sin^2\delta_2\\
&-2c_2\sin^2(\gamma^{(1)}-\gamma^{(3)}+\delta_0)+9a_2\sin^2(\gamma^{(1)}-\gamma^{(3)})+\delta_1)-9a_2\sin^2(\delta_1-\delta_2)\\
&-2c_2\sin^2(\delta_0-\delta_2)+4/\sqrt{6}g\sin^2(\gamma^{(1)}-\gamma^{(3)}+\delta_2)\Big]Y_1^0Y_3^0\\
&+\frac{1}{\sqrt{21}}\Big[-\frac{4(2\sqrt{6}+\omega_1+\omega_2)}{3(2+\omega_1^2+\omega_2^2)}+\frac{4}{\sqrt{6}}c_2\sin^2(\gamma^{(1)}-\gamma^{(3)}+\delta_0)\\
&\qquad-\frac{4}{\sqrt{6}}c_2\sin^2(\delta_0-\delta_2)\\
&-\frac{8}{\sqrt{6}}a_2\sin^2(\delta_1-\delta_2)+\frac{4}{3}q\sin^2(\gamma^{(1)}-\gamma^{(3)}+\delta_2)\Big]Y_1^1Y_3^{1*}\\
&+\frac{1}{21}\Big[\frac{4(16-18\omega_1^2+7\sqrt{6}\omega_1-4\sqrt{6}\omega_2)}{2+\omega_1^2+\omega_2^2}(Y_3^0)^2\\
&+\frac{2}{3}\frac{190\sqrt{6}\omega_1-182\sqrt{6}\omega_2-168-160\omega_1^2}{2+\omega_1^2+\omega_2^2}Y_3^1Y_3^{1*}\\
&+\frac{20}{3}\frac{3\sqrt{6}\omega_1-7\sqrt{6}\omega_2-10\omega_1^2-8}{2+\omega_1^2+\omega_2^2}Y_3^2Y_3^{2*}\Big]\sin^2(\gamma^{(1)}-\gamma^{(3)}+\delta_2)\Big\}.\end{aligned} \quad \ldots\ldots(B\,3)$$

In the above we have abbreviated as follows:

$$b_i = \frac{1}{1+\omega_i^2}, \quad a_i = \frac{2b_i}{9}(2+\sqrt{6}\omega_i), \quad c_i = \frac{2b_i}{3}(3-\sqrt{6}\omega_i)$$

$$d_i = \frac{2b_i}{9}(2+\sqrt{3}\omega_i), \quad p_i = \frac{2\sqrt{3}}{9}\omega_i b_i, \quad i=1, 2.$$

$$f = b_1 b_2[\sqrt{6}(\omega_1+\omega_2)-1], \quad g = \frac{9\sqrt{6}+7\omega_1-\omega_2-3\sqrt{6}\omega_1^2}{2+\omega_1^2+\omega_2^2}$$

$$q = \frac{2\sqrt{6}\omega_1^2-3\omega_1-\omega_2-6\sqrt{6}}{2+\omega_1^2+\omega_2^2},$$

and have for convenience written $\omega_1=\omega_2{}^{\alpha}$, $\omega_2=\omega_2{}^{Y}$, $\delta_2=\delta_2{}^{\alpha}$.

$$(dS_0/d\Omega)_{\text{int}} = Y_1{}^0 \frac{\alpha}{2k^2}(12\pi)^{1/2}\left\{t_1+\frac{1}{3}t_0+\frac{5}{3}b_1t_2+\frac{5}{6}b_2 s\right.$$
$$\left.-\frac{5}{6}b_2\left[\frac{\sin\{\alpha\log\cos^2\theta/2+2(\gamma^{(1)}-\gamma^{(0)})\}}{\cos^2\theta/2}-\frac{\sin\{\alpha\log\sin^2\theta/2+2(\gamma^{(1)}-\gamma^{(0)})\}}{\sin^2\theta/2}\right]\right\}$$
$$+Y_3{}^0\frac{5\alpha}{4k^2}(28\pi)^{1/2}b_2\left\{-\frac{1}{7}s+\frac{1}{9}\left[\frac{\sin(\alpha\log\cos^2\theta/2+2(\gamma^{(1)}-\gamma^{(3)}+\delta_2))}{\cos^2\theta/2}\right.\right.$$
$$\left.\left.-\frac{\sin(\alpha\log\sin^2\theta/2+2(\gamma^{(1)}-\gamma^{(3)}+\delta_2))}{\sin^2\theta/2}\right]\right\} \qquad \ldots\ldots(B4)$$

in which, with $i=0, 1, 2$,

$$t_i = \sin\delta_i\left[\frac{\cos\{\alpha\log\cos^2\theta/2+\delta_i+2(\gamma^{(1)}-\gamma^{(0)})\}}{\cos^2\theta/2}\right.$$
$$\left.-\frac{\cos\{\alpha\log\sin^2\theta/2+\delta_i+2(\gamma^{(1)}-\gamma^{(0)})\}}{\sin^2\theta/2}\right]$$
$$s = \frac{\sin\{\alpha\log\cos^2\theta/2+2(\gamma^{(3)}-\gamma^{(0)})\}}{\cos^2\theta/2}-\frac{\sin\{\alpha\log\sin^2\theta/2+2(\gamma^{(3)}-\gamma^{(1)})\}}{\sin^2\theta/2}.$$

In the derivation of the results (B3), (B4), use is made of the fact that the ${}^3P_0$ state is uncoupled, i.e. $\omega_0{}^{\alpha}=1$, $\omega_0{}^{Y}\to-\infty$. The phase shift pertaining to this state was labelled δ_0.

It is readily verified that in the limit of no coupling of the $j=2$ states, i.e. $\omega_1=1$, $\omega_2\to-\infty$, the form of the cross section formula reduces to the usual formula for central forces.

REFERENCES

BETHE, H. A., 1949, *Phys. Rev.*, **76**, 38.
BLATT, J. M., and JACKSON, J. D., 1949, *Phys. Rev.*, **76**, 18.
BREIT, G., and HULL, M. H., Jr., 1950, *Phys. Rev.*, **80**, 392, 561.
CHEW, G. F., and GOLDBERGER, M. L., 1949, *Phys. Rev.*, **75**, 1637.
CHRISTIAN, R. S., 1949, *Phys. Rev.*, **75**, 1675.
HATCHER, R. D., ARFKEN, G. B., and BREIT, G., 1949, *Phys. Rev.*, **75**, 1389.
JACKSON, J. D., and BLATT, J. M., 1950, *Rev. Mod. Phys.*, **22**, 77.
LANDAU, L., and SMORODINSKY, J., 1944, *J. Phys., U.S.S.R.*, **8**, 154.
PEIERLS, R. E., and BARKER, F. C., 1949, *Phys. Rev.*, **75**, 312.
ROHRLICH, F., and EISENSTEIN, I., 1949, *Phys. Rev.*, **75**, 705.
SCHWINGER, J., 1947, Lecture Notes quoted by BLATT and JACKSON, 1949.
YOST, F. L., WHEELER, J. A., and BREIT, G., 1936, *Phys. Rev.*, **49**, 174.

Average Numbers for the Development of the Nucleon Component of the Cosmic Radiation in Air

By H. MESSEL
School of Theoretical Physics, Dublin Institute for Advanced Studies

MS. received 19*th March* 1951

ABSTRACT. Comprehensive results are presented in graphic form for nucleons with energies equal to or greater than 500 MEV., based on calculations using a new cross section for nucleon–nucleon collisions and in the light of recent experimental evidence. The results obtained are in good agreement with existing experimental observations and it is felt that the high-energy nucleon component of the cosmic radiation can now be satisfactorily accounted for by our theory. The basic assumptions underlying the theory are discussed.

§1. INTRODUCTION

In a number of recent works (Messel and Ritson 1950, Jánossy and Messel 1951, Messel 1951 a, b) an attempt was made to account theoretically for the experimentally observed behaviour of the nucleon component of the cosmic radiation in air. The theory of a nucleon cascade was given for both homogeneous nuclear matter (considering the nucleus to be infinite in size) and inhomogeneous matter (a finite absorber) with and without taking ionization losses into account and for various initial conditions. It was shown that the above theory was capable of accounting at least qualitatively for all the salient features of the high energy nucleon component of the cosmic radiation. Since the appearance of more accurate data on the primary spectrum of the cosmic radiation it has been possible to adopt a more accurate cross section for high-energy nucleon–nucleon collisions and thus to obtain a theory for the nucleon cascade which is both in quantitative and qualitative agreement with experiment. We shall present results below on the nucleon component which are in very good agreement with experiment.

Though quantitative agreement is obtained, we do not in any way claim that the cross section used is the *correct* cross section for high energy nucleon–nucleon collisions. At the same time it appears unlikely that, when the true cross section does become known, its energy dependence would differ radically from the one used by us.

Since there has been a good deal of misapprehension regarding the fundamental assumptions underlying our theory we shall endeavour to give these in detail and also to show that the results are valid on either the plural or multiple meson production hypotheses.

§2. ELASTIC AND INELASTIC SCATTERING

Below primary nucleon energies of the order of 1,000 MEV. it appears that elastic scattering of nucleons is the dominant process, with the production of mesons due to inelastic scattering of the nucleons playing a minor role. For energies greater than 1,000 MEV. meson production due to inelastic scattering becomes important. In all the work which follows we shall only consider primary nucleons with energies equal to or greater than 1,000 MEV. and assume that the

scattering for this energy region is inelastic. Thus in a collision of a nucleon of energy E_0 with another nucleon at rest we have $E_0 = E_1 + E_2 + E_m$ where E_1 and E_2 are the energies of the secondary and recoil nucleons and E_m is the energy loss of the primary into a meson or mesons.

Now, following Heitler and Jánossy (1949), we assume that the cross section for a nucleon–nucleon collision leading to secondary energies E_1, $E_1 + dE_1$ and E_2, $E_2 + dE_2$ is a homogeneous function of degree zero of the primary and secondary energies. This assumption is probably equally valid on either scheme of meson production, plural or multiple, for the energy region we are considering. Thus we have for the probability that in a nucleon–nucleon collision a primary nucleon of energy E_0 should give rise to secondary and recoil nucleons of energies E_1 and E_2,

$$w(E_0, E_1, E_2)dE_1dE_2 = w(E_1/E_0, E_2/E_0)E_0^{-2}dE_1dE_2, \quad E_1 + E_2 \leqslant E_0. \quad \ldots\ldots(1)$$

From this it follows that the total probability for a collision is given by

$$\int_0^1 \int_0^{1-E_1/E_0} w\left(\frac{E_1}{E_0}, \frac{E_2}{E_0}\right) E_0^{-2} dE_1 dE_2 = \text{constant}, \qquad \ldots\ldots(1\,a)$$

which is independent of the primary and secondary energies. The function w is so chosen that the total probability is normalized to unity.

We require no further assumptions in order to obtain the solution of the fundamental equations of a nucleon cascade. The actual form of the cross section appearing in (1) is discussed in a later section.

§ 3. THE FUNDAMENTAL EQUATIONS

Denote by $S^{(i,k)}(E, \theta)dE$ the average number of protons or neutrons (according to the suffix k) in the energy range $E, E + dE$ at a depth $\lambda\theta$ gm/cm² in inhomogeneous matter, due to a primary nucleon of energy E_0. λ is the interaction mean free path of nucleons with nuclei in the material concerned. The suffix $i = 1, 2$ refers to the original primary particle and $k = 1, 2$ to the secondary particles. The number 1 refers to protons and 2 to neutrons. The quantities $N^{(i,k)}(E_0, E, \theta)$ denote the corresponding average number of particles with energy greater than E. We denote the ionization loss of nucleons per interaction length by β. Also define $V(E/E')\,dE/E'$ as the probability that a nucleon of energy E' falling on a nucleus gives rise to one or more nucleons such that one of the emerging nucleons has an energy in the interval $E, E + dE$. The fundamental equations are now given by

$$\frac{\partial}{\partial\theta} S^{(i,k)}(E, \theta) + S^{(i,k)}(E, \theta) = \frac{1}{2} \int_0^\infty \{S^{(i,k)}(E', \theta) + S^{(i,3-k)}(E', \theta)\} V(E/E')dE'/E' + \delta_{1,k}\beta \frac{\partial}{\partial E} S^{(i,k)}(E, \theta). \qquad \ldots\ldots(2)$$

The equations (2) and their exact solution were given by Messel (1951 c). Since in the work which follows we shall not be considering secondary energies less than 500 Mev. we may to a good approximation drop the ionization term (Messel 1951 c).

We take for the initial condition a proton integral power law spectrum

$$N^{(1,1)}(E_c, E, \theta = 0) = \begin{cases} (E_c/E)^\gamma & E > E_c \\ 1 & E < E_c \end{cases} \qquad \ldots\ldots(3)$$

(E_c is the cut-off energy).

The average number of particles with energies greater than E is then given by

$$N^{(1,k)}(E_c, E, \theta) = \frac{1}{2\pi i}\int_{s_0-i\infty}^{s_0+i\infty}\left(\frac{E_c}{E}\right)^s P_0^{(1,k)}(s,\theta)\frac{\gamma ds}{s(\gamma-s)}, \quad 0<s_0<\gamma. \quad \ldots\ldots(4)$$

The integration is carried out along a line parallel to the imaginary axis such that the condition $0<s_0<\gamma$ is fulfilled. In (4)

$$P_0^{(1,k)}(s,\theta) = \tfrac{1}{2}\{\exp[-f(D_A\alpha_s)\theta] + (-1)^{k-1}\exp(-\theta)\} \quad \ldots\ldots(5)$$

$$f(\lambda) = 1 - \{1-(1+\lambda)\exp(-\lambda)\}/\lambda^2 \quad \ldots\ldots(5a)$$

$$\alpha_s = \int_0^1\int_0^{1-\epsilon_2}(1-\epsilon_1{}^s-\epsilon_2{}^s)w(\epsilon_1,\epsilon_2)d\epsilon_1 d\epsilon_2. \quad \ldots\ldots(5b)$$

We note that $\alpha_{1\cdot0}$ expresses the average energy loss into a meson or mesons. D_A is the average number of collisions which a nucleon suffers on making a diametrical passage through a nucleus of atomic weight A. Its value will be discussed in the next section.

For the number of nucleons (neutrons plus protons) with energies greater than E at a depth $\lambda\theta$ gm/cm^2, we have

$$N(E_c, E, \theta) = \frac{1}{2\pi i}\int_{s_0-i\infty}^{s_0+i\infty}\left(\frac{E_c}{E}\right)^s \exp\{-f(D_A\alpha_s)\theta\}\frac{\gamma\, ds}{s(\gamma-s)}, \quad 0<s_0<\gamma. \quad \ldots\ldots(6)$$

For $E>E_c$ the solution of (6) is obtained immediately by noting that the integral has a pole at $s=\gamma$, hence

$$N(E_c, E, \theta) = (E_c/E)^\gamma \exp\{-f(D_A\alpha_\gamma)\theta\}, \quad E>E_c. \quad \ldots\ldots(7)$$

For $E<E_c$ (6) may be evaluated using a saddle-point integration (as may be (4)).

§ 4. CHOICE OF CROSS SECTION

The solution of equations (2) was given utilizing so far only the one assumption given by (1). In order to obtain numerical results from the formulae (4) and (6) we must choose explicit values for the probability function (1) and for D_A. Taking the nuclei to be spheres with radius $1{\cdot}37\times10^{-13}A^{1/3}$ cm. we find $D_A = 1{\cdot}5A^{1/3}(R_k/1{\cdot}37\times10^{-13})^2$ where R_k is the range of nuclear forces and A is the atomic weight. We take for the range of nuclear forces $R_k = \hbar/\pi_m c$ with π_m equal to 286 electron masses. Thus for air $D_A = 3{\cdot}7$.

We now proceed to choose our cross section utilizing the following three results, deduced from experiments: (*a*) the interaction mean free path λ for high-energy nucleons in air is of the order of 75 gm/cm^2 (Sitte 1951); (*b*) the absorption length for high-energy nucleons in air is approximately 125 gm/cm^2: this result has been confirmed many times (McMahon *et al.* 1950); (*c*) the integral proton primary power law exponent γ appearing in (3) has the value $\gamma = 0{\cdot}90$ to $1{\cdot}1$. In our previous work we used the value $1{\cdot}7$ which at the time the work was being done appeared to be the accepted value. The results of Van Allen and Singer (1950) and Winckler *et al.* (1950) have shown that the value $1{\cdot}7$ is too high and that a value close to $1{\cdot}1$ is valid for energies up to 15,000 Mev. There has also been mentioned the possibility that γ increases for energies greater than 15,000 Mev. To date there has been little or no evidence to confirm this;* however, in order to take into account this eventuality throughout we shall adopt throughout our work the upper limit $\gamma = 1{\cdot}1$. Our results depend

* See M. Schein and J. J. Lord, *Phys. Rev.*, abstract of meeting of 26th April 1951. Evidence is given for γ not increasing very rapidly for very high energies.

fairly critically upon the choice of γ, consequently it is not surprising that our former work, where the value $\gamma = 1{\cdot}7$ was used, gave only qualitative agreement with experiment.

Using (7) and (*a*), (*b*) and (*c*) above, we must have the following condition fulfilled: $f(3{\cdot}7\,\alpha_{1\cdot1})/75 = 1/125$. From a table of the function f we find

$$\alpha_{1\cdot1} \simeq 0{\cdot}40. \qquad \ldots\ldots(8)$$

Recall that $\alpha_{1\cdot0}$ expresses the average energy loss into a meson or mesons. In other words, if we were to choose $\gamma = 1{\cdot}0$ the average energy loss per collision into the meson component would be immediately defined.

One may now choose a general form for the function $w(\epsilon_1, \epsilon_2)$, (where $\epsilon_i = E_i/E_0$) and adjust it so that the condition (8) is satisfied. We omit the straightforward but laborious detail here and only give the results. It should be pointed out that if one wishes to obtain a reasonable function $w(\epsilon_1, \epsilon_2)$ then the choice is not as broad as one would expect, especially when one takes into consideration the fact pointed out in the previous paragraph. We find that

$$w(\epsilon_1, \epsilon_2) = 120\epsilon_1\epsilon_2(1 - \epsilon_1 - \epsilon_2) \qquad \ldots\ldots(9)$$

satisfies the conditions above and also yields $\alpha_{1\cdot0} = 0{\cdot}33$. This cross section is to be preferred on physical grounds to the type used previously in our work. We note that, for $\epsilon_1 = 0$ or $\epsilon_2 = 0$ or $\epsilon_1 + \epsilon_2 = 1$, $w(\epsilon_1, \epsilon_2)$ now vanishes, thus ensuring that our collisions are inelastic. The value of 33% is sufficiently high to be compatible with either a plural or a multiple meson production hypothesis. However, if one accepts the hypothesis of plural meson production then it is possible immediately to work out the meson spectrum for the energy region we are considering. Since quantitative agreement with experiment for the nucleon component has been obtained using the cross section following from (9), one would expect the same to hold true for the meson component—providing the plural hypothesis is correct. If the results obtained were incompatible with those observed experimentally, then a good deal of doubt would be thrown on the plural hypothesis. On the other hand we cannot hope to disprove a multiple meson producing hypothesis by the above method. One may always argue that the multiplicities to be expected in the energy region we are considering are too low to be critical. We hope to present results shortly along the lines mentioned above on this highly controversial point which at present we feel is far from settled.

§ 5. RESULTS

In Figures 1, 2 and 3 we give the results for the vertical intensity of protons, neutrons and nucleons respectively above a given energy E for various ratios E_c/E. Our results should not be trusted for E less than 500 MEV. We hope to present results shortly for the low energy nucleon component, making use of the high energy results. In Figure 4 we have plotted the ratio of neutrons to protons.

(i) *Latitude Effect*

The latitude effect at any given depth and for any given energy E equal to or greater than 500 MEV. may easily be obtained from our curves. One merely measures the difference between the two curves in question, subtracts it from the logarithm of the normalization factor for the latitudes concerned and takes the antilogarithm.

For instance, we wish to know the latitude effect for protons with E equal to or greater than 500 Mev. at an atmospheric depth of 312 gm/cm² between latitudes 0° and 55° N. where $E_c = 15{,}000$ and 1,000 Mev. respectively: from Figure 1 we measure the difference between the curves for $E_c/E = 30$ and

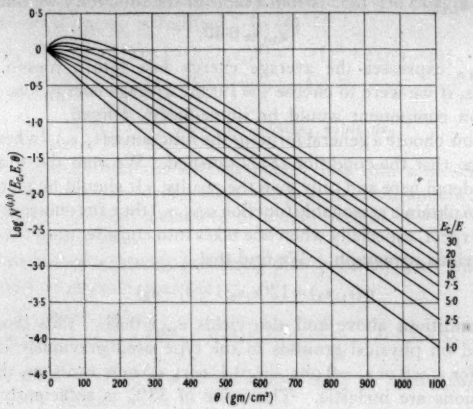

Figure 1. Log $N^{(1,1)}(E_c, E, \theta)$, logarithm of the intensity of vertical protons with energy greater than E due to the primary proton spectrum given by (3), plotted against the atmospheric depth θ for various values of the ratio E_c/E.

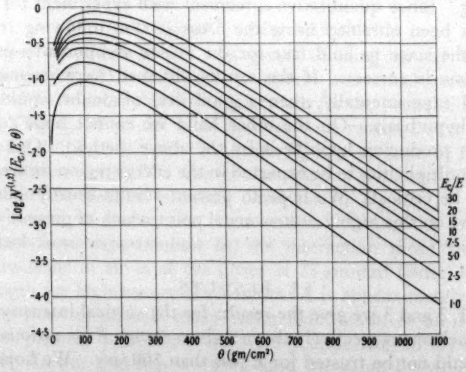

Figure 2 Log $N^{(1,2)}(E_c, E, \theta)$, logarithm of the intensity of vertical neutrons with energy greater than E due to the primary proton spectrum given by (3), plotted against the atmospheric depth θ for various values of the ratio E_c/E.

2 at 312 gm/cm². We find this value to be 0·84. This has now to be subtracted from the normalization factor, $\log (15 \times 10^9/10^9)^{1\cdot1}$, and the antilogarithm taken; the result is 2·9. Conversi (1950), working on protons under corresponding conditions (actually he considers a differential energy spectrum) finds a latitude effect of $3\cdot2 \pm 0\cdot5$. McMahon *et al.* (1950), using an ionization chamber, find for

protons with a minimum energy of about 400 Mev. a latitude effect of 2·0 between latitudes 20° and 55° N. If we apply an inverse Gross transform to our results we also find a value of 2·0.

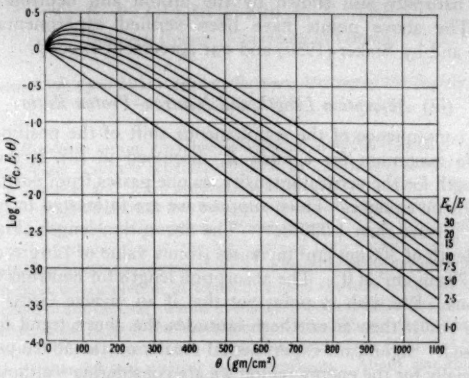

Figure 3. Log $N(E_c, E, \theta)$, logarithm of the intensity of vertical nucleons with energy greater than E due to the primary proton spectrum given by (3), plotted against the atmospheric depth θ for various values of the ratio E_c/E.

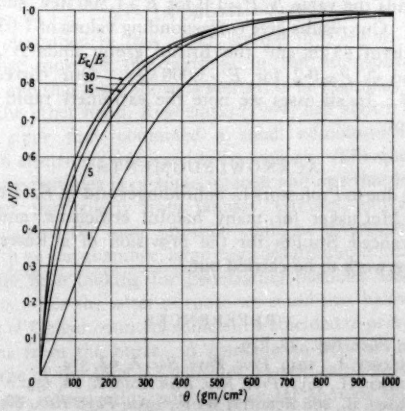

Figure 4. A plot of the ratio of neutrons to protons against the atmospheric depth θ for various ratios E_c/E.

(ii) *Position of Maximum*

From (4) and (6) it is readily seen that the maximum value for protons, neutrons and nucleons is attained when $f(D_A\alpha_\theta)=0$. This occurs for $s\simeq 0{\cdot}55$. Thus, for example, in the case of nucleons $\theta_{\max}=54\log(E_c/E)\,\mathrm{gm/cm^2}$, $E<E_c$. This expression shows that for a fixed E, as one passes from the geomagnetic

equator (large E_c) to northern latitudes (smaller E_c), the position of the cascade maximum shifts from a high to a small value of θ. From Figure 3 it is also evident that the height of the maximum decreases simultaneously. The same behaviour is naturally also shown by the proton and neutron components, separately. The above points have been verified experimentally both by Whyte (1951) and by Staker (1950) and our agreement is good.

(iii) *Absorption Length and Neutron–Proton Ratio*

A natural consequence of the simultaneous shift of the position and height of the cascade maximum for a fixed E, discussed in (ii), is the increase of absorption length for the vertical intensity, as one passes from northern latitudes to the geomagnetic equator. Thus, suppose we are interested in nucleons with E equal to or greater than 1,000 Mev. The absorption length (Figure 3) at an atmospheric depth of 300 gm/cm² increases from a value of 126 gm/cm² at 57° N. to a value of 170 gm/cm² at 0°. The absorption length for neutrons is larger than that for protons. We wish to point out that if an inverse Gross transform is applied to our result then at northern latitudes the above trend for protons is actually reversed. Significant experimental results on the above points are still lacking—especially for the energy region we are considering—although the trend appears to be that given above.

For the neutron–proton ratio our agreement with existing experimental evidence is good. For instance, at an atmospheric depth of 650 gm/cm² the Bristol group * finds the value $N/P=1{\cdot}0$ for $E\geqslant 1{,}500$ Mev. and $N/P\simeq 1{\cdot}0\pm 0{\cdot}1$ for $E>3{,}000$ Mev. Our results give corresponding values of 1·03 and 1·1. At an atmospheric depth of 45 gm/cm² the Bristol group finds $N/P\simeq 0{\cdot}6\pm 0{\cdot}1$ for $E>1{,}500$ Mev. and $N/P\simeq 0{\cdot}2$ for $E>3{,}000$ Mev. Our corresponding values are 0·45 and 0·15. In all cases we note the extremely rapid build-up of the neutron component.

ACKNOWLEDGMENTS

My thanks are due to Professors E. Schrödinger and H. S. Green and Assistant Professor C. B. McCusker for many helpful criticisms, and to the Dublin Institute for Advanced Studies for the provision of a Research Fellowship, enabling the above work to be carried out.

REFERENCES

Conversi, M., 1950, *Phys. Rev.*, **79**, 749.
Heitler, W., and Jánossy, L., 1949, *Proc. Phys. Soc.* A, **62**, 374.
Jánossy, L., and Messel, H., 1951, *Proc. Roy. Irish Acad.* A, **54**, 245.
McMahon, A. J., Rossi, B., and Burditt, W. F., 1950, *Phys. Rev.*, **80**, 157.
Messel, H., 1951 a, *Comm. Dublin Institute for Advanced Studies*, Series A, No. 7; 1951 b, *Proc. Roy. Irish Acad.* A, **54**, 125; 1951 c, *Phys. Rev.*, two papers in the press.
Messel, H., and Ritson, D. M., 1950, *Proc. Phys. Soc.* A, **63**, 1359.
Sitte, K.,† 1951, *Phys. Rev.*, in the press.
Staker, W. P., 1950, *Phys. Rev.*, **80**, 52.
Van Allen, J. A., and Singer, S. F., 1950, *Phys. Rev.*, **78**, 819.
Whyte, G. N.,† 1951, *Phys. Rev.*, **82**, 204.
Winckler, J. R., Stix, T., Dwight, K., and Sabin, R., 1950, *Phys. Rev.*, **79**, 656.

* I am indebted to U. Camerini for communicating these results to me.
† I am indebted to these authors for communicating their results before publication.

Penetrating Bursts of Cosmic Radiation

By E. P. GEORGE and P. T. TRENT
Birkbeck College, University of London

MS. received 6th April 1951; *read at Summer Meeting of the Society at Belfast on 6th July* 1951

ABSTRACT. Bursts in an ion chamber, accompanied by the discharge of one or more of 18 surrounding Geiger counters separated from it by 15 cm. Pb, have been studied at the Jungfraujoch, at sea level and below ground at a depth of 60 m. water. With 15 cm. Pb over the chamber the bursts at altitude were separated into those associated with air showers (accompanied bursts), and the remainder (local bursts). The accompanied penetrating bursts appear to be associated with the incidence of high density regions of air showers. The local penetrating burst size increases with the number of penetrating particles recorded consistent with their interpretation in terms of mixed showers involving the simultaneous production of charged and neutral mesons in energetic nuclear collisions of the N-component.

Underground, about 10% of the bursts under 15 cm. Pb are of the mixed shower type. These underground bursts are attributed to nuclear excitations produced by fast μ-mesons, resulting again in charged and neutral meson emission. About one-third of the bursts observed below ground with no Pb over the chamber appear to be produced by single penetrating particles which release, by an unidentified process, 20 Mev. and more in the ion chamber.

§ 1. INTRODUCTION

The work described in this paper started in 1946 in this way. It was known that most of the particles in the atmospheric showers were electrons, and that these showers seemed to be examples of electron–photon cascades. On the other hand, Rogozinski (1944) had shown that they were not pure cascades since they contained a small admixture of particles more penetrating than electrons, presumed to be mesons. The question of the origin of the penetrating particles is of some interest and one that has received a good deal of attention, particularly from Jánossy, Greisen, and their collaborators. It occurred to us that the same question could be investigated in another way by selecting, with an ion chamber, large cascades produced locally in an absorber, and at the same time looking for penetrating particles associated with these ionization bursts. For the latter purpose we could use, below the ion chamber, an arrangement of Geiger counters sufficiently shielded to prevent their discharge by the electrons from the burst. A coincidence between an ionization burst and the discharge of the shielded counters we will call a penetrating burst.

A preliminary investigation with a pilot set showed the feasibility of the experiment (George and Jánossy 1946) and a more elaborate scheme was prepared. The first results obtained with the latter arrangement were described by George and Trent (1948). Later, an experiment along similar lines was proposed by Greisen (1948).

A parallel investigation of penetrating bursts was also carried out by Rossi and his collaborators (Bridge and Rossi 1949) with a different experimental emphasis. Their results were in agreement with ours in suggesting that at high altitude the majority of the bursts recorded under thick absorbers are due to nuclear interactions of the N-component of the cosmic radiation.

Our observations fit into the picture that has now come to be accepted of high-energy nuclear collisions giving rise to the emission of charged and neutral mesons. On this view, the latter quickly decay into photons, giving rise to a soft cascade shower which registers, in our experiments, in the ion chamber. The former discharge the counters set to detect the associated penetrating particles. The use of an ion chamber has the advantage that it is possible to investigate showers that are too large for quantitative study with a cloud chamber.

§ 2. SCOPE OF THE PRESENT INVESTIGATION

Observations were made first at the Scientific Station, Jungfraujoch, at an altitude of 3,457 m. Bursts under 15 cm. Pb only were recorded. These were found to be frequently associated with groups of penetrating particles, and size–frequency distributions of these groups were determined separately for bursts associated and not associated with air showers. The multiplicity of penetrating particles was found to increase with burst size for the unaccompanied bursts.

A comparison of the frequency of bursts at the Jungfraujoch with that at sea level gives the fraction of bursts produced by the hard and the N-component at these two places.

The observations were repeated in our underground laboratory in London, at a depth equivalent to 60 metres of water. Bursts observed here must be attributed to the penetrating component, i.e. the μ-mesons. We found that the proportion of bursts associated with groups of penetrating particles is much reduced, but that this type of burst still occurs at these large depths. On analysis, the results indicate that probably about 90% of the cascade bursts at this depth arise from bremsstrahlung and knock-on electrons produced by the energetic μ-mesons, while the remaining 10% appear to arise from nuclear interactions of fast μ-mesons resulting in charged and neutral π-meson emission. The frequency of this latter type of burst is consistent with other recent results on the nuclear interactions of fast μ-mesons (George and Evans 1950).

Further observations enabled us to separate out experimentally those bursts produced by stars occurring in the gas or the walls of the ion chamber.

§ 3. APPARATUS

The main part of the apparatus is shown in Figure 1. It consists of a $1\frac{1}{2}$-litre duralumin ion chamber I filled with 99·9% pure argon at 40 atmospheres,

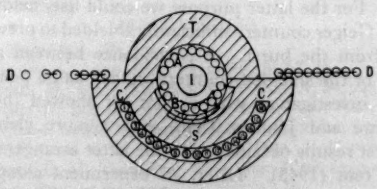

Figure 1. General arrangement.

surrounded by lead screens S and T and several banks of Geiger counters A.... D. The ends were closed by lead screens 12 cm. thick. The ion chamber was kindly lent to us by Dr. H. Carmichael, and has been described by Chou (1948). Negative ions were collected, the collection time being approximately 0·1 sec.

The burst pulses were amplified and recorded by means of a cathode-ray oscilloscope and a continuously moving film camera. The smallest size of burst measured corresponded to the passage of 20 minimum ionization particles through the chamber.

Counter banks A and D were alternative arrangements not employed simultaneously. A hodoscope was used to record coincidences between the ionization bursts and the discharge of the Geiger counters. The hodoscope possesses no novel features and need not be described. The frequencies of accidental coincidences were determined experimentally and shown to be negligibly small.

§4. OBSERVATIONS AT THE JUNGFRAUJOCH

At the Jungfraujoch the lead screen T was permanently in position, and its thickness was not varied. Counter bank A was not used, while counter bank D was. The requirement for operating the hodoscope was an ionization burst, plus a threefold coincidence in B plus one or more counters discharged in C, which may be written (I, B_3, $C_{\geqslant 1}$). On the occurrence of such an event, the hodoscope indicated which other counters in C or counter groups in D were also discharged.

The counter banks D were designed to indicate those events associated with air showers, and bursts in coincidence with counters D (I, D) will be referred to as 'accompanied bursts', while anticoincidences (I, $-$D) will be called 'local bursts'.

The apparatus was operated at the Jungfraujoch during September and October 1947. The integral size–frequency distribution of the different types of burst that we classified are given in Figure 2. More detailed results are given separately for the local and accompanied bursts.

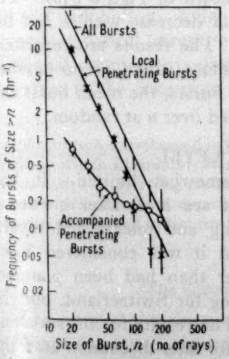

Figure 2. Size–frequency distributions under 15 cm. Pb at the Jungfraujoch.

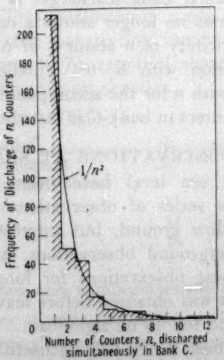

Figure 3(*a*). Local penetrating bursts.

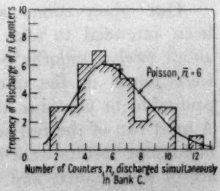

Figure 3 (*b*). Accompanied penetrating bursts.

4.1. *Local Bursts*

From Figure 2 it is seen that a good proportion of the bursts are in fact penetrating bursts. A differential size–frequency distribution of the discharge of groups of counters in bank C is shown for the local bursts in Figure 3(*a*).

The frequency of discharge of n screened counters in coincidence with local bursts $F(n)$ shows a rapid decline with increasing n, and may be approximately represented by $F(n) \propto n^{-2}$.

Another feature of interest concerning the local bursts is the fact that there is a marked correlation between n, the number of counters discharged in bank C, and the size of the associated ionization burst. This is illustrated in Table 1,

Table 1

No. of counters n discharged in C	2	3	4	5	6	7	8, 9
Mean size of bursts in coincidence with n counters (rays)	23	31	41	51	103	106	161

from which the steady increase of burst size with n will be seen.

One notable feature of the events associated with the discharge of more than one counter in bank C was the frequent occurrence of wide separations between the discharged counters. Details are given in Table 2. This suggested that in these events we were not dealing with knock-on electrons in bank C.

Table 2

No. of counters n discharged in bank C	Events with q intervening undischarged counters					
	$q=0$	$q=1$	$q=2$	$q=3$	$q=4$	$q \geqslant 5$
2	16	10	8	5	6	15
3	4	6	8	8	6	11
4	5	0	3	4	2	8
5, 6	1	1	5	4	1	5
>6	0	3	4	3	3	2

4.2. *Accompanied Bursts*

The situation is different for the accompanied bursts. The size–frequency distribution of the C counter bank discharges is shown in Figure 3 (*b*). The distribution for these bursts no longer shows a rapid decrease with n, but has a flat maximum in the vicinity of n about 5 or 6. The results are consistent with a Poisson distribution with $\bar{n}=6$. Furthermore, there is no marked correlation of burst size with n for the accompanied bursts, the mean burst size in coincidence with n counters in bank C is distributed over n at random.

§ 5. OBSERVATIONS AT SEA LEVEL

Our observations at sea level have been somewhat limited. It had been intended to take a series of observations at sea level after a run of about twelve months below ground, but interesting and unexpected results were found in the underground observations, and it was considered more profitable to continue these observations for longer than had been planned. A brief run of the full set was obtained before leaving for Switzerland, but the hodoscope results were too few to be significant. The results for bursts alone are of significance, and those which will be useful for later discussion are: the burst frequency with no lead absorber over the ion chamber, $2{\cdot}7 \pm 0{\cdot}25$ hr^{-1}, and that under 15 cm. Pb, $4{\cdot}6 \pm 0{\cdot}3$ hr^{-1}.

§ 6. OBSERVATIONS BELOW GROUND

The apparatus was moved to the laboratory on Holborn underground station, at a depth equivalent to 60 metres of water, and has been operated there since the summer of 1948.

6.1. $T = 15$ *cm. Pb*

A preliminary test with $T = 15$ cm. Pb showed that few, if any, of the underground bursts were accompanied bursts. In a run lasting 14 days, 208 bursts were observed, none of which was in coincidence with counter discharges in bank D. Frequent checks of the satisfactory operation of the apparatus were made. The use of counter bank D was therefore discontinued, and the hodoscope channels used to indicate the operation of the counters in bank A. The next observations were made with $T = 15$ cm. lead with the same requirement for the production of a hodoscope master-pulse as in the high altitude measurements, viz. (I, B_3, $C_{\geq 1}$). In a run lasting 1,550 hours, 846 bursts were observed ($0{\cdot}54 \pm 0{\cdot}02\,hr^{-1}$), of which 382 were penetrating bursts. Of these 382, 336 occurred with the discharge of only one of the lower counters C. Of the remaining 46 events, 33 discharged 2 counters in bank C, 9 discharged 3, and 4 discharged 4.

The penetrating bursts underground show an increase of size with the number of counters discharged simultaneously in C, as already noted for the Jungfraujoch observations. Table 3 gives the details.

Table 3

No. of counters n discharged in C	1	2	3	4
Mean size of bursts in coincidence with n counters (rays)	40	42	52	66

The distribution of the intervals between the discharged counters is given in Table 4. The frequent wide separation of the discharged counters was taken to indicate that in these events the C counters were not operated frequently by knock-on electrons. It was felt important to confirm this for the underground penetrating bursts, and this was achieved in the following way: about half-way through the run we placed vertical lead slats, 3 mm. thick, between each of the counters C. These slats ran the entire length of the counter slot, and touched the top and bottom walls. This modification made no detectable difference, beyond statistical errors, to the penetrating burst type of event, although additional counter experiments, to be reported separately, showed a marked reduction in the frequency of knock-on showers.

Table 4

No. of counters n discharged in bank C	2	3	4
Events in which all counters were adjacent	22	2	1
Events with 1 intervening undischarged counter	8	4	3
Events with 2 or more intervening	3	3	3
Counters discharged in last row	1, 11	14, 16, 18	1, 3, 4, 9
	7, 19	6, 7, 12	7, 12, 14, 18
	3, 18	3, 8, 13	8, 16, 17, 18

(The C counters were numbered serially 1 . . . 18.)

The integral size–frequency distribution of the underground bursts is shown in Figure 4, plotted logarithmically, and may be represented by an expression of the form $F(N) = AN^{-S}$ with $S = 1{\cdot}6 \pm 0{\cdot}15$ for all bursts, and $1{\cdot}75 \pm 0{\cdot}15$ for penetrating bursts. The former result is consistent with the observations of Chou (1948) at the same station.

6.2. $T = 45$ *cm. Pb*

Also indicated on Figure 4 are the results for a run of 273 hours with $T = 45$ cm. Pb. Increasing the lead screen from 15 to 45 cm. was found to reduce

all the readings by about 5%. The proportion of penetrating bursts associated with one or more than one discharged counter in bank C did not differ significantly from the proportion observed with $T=15$ cm. Pb.

The counter bank A was only employed for a fraction of the two runs with $T=15$ and 45 cm. Pb. For such time as it was employed, the A bank record of counter discharges always indicated the high degree of multiplicity expected from the large cascade bursts required to operate the hodoscope.

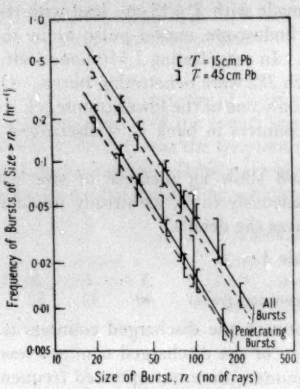

Figure 4. Integral size–frequency distribution of underground bursts.

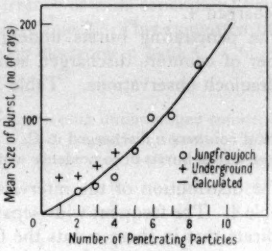

Figure 5.

6.3. $T=0$ *cm. Pb*

It is well known that most of the smaller bursts observed in an unscreened ion chamber at sea level are caused by nuclear fragments from 'stars' produced in the gas, walls or surrounding material of the ion chamber (Euler 1940, Carmichael 1948). The hodoscope used above was intentionally made insensitive to this type of event. For the run with $T=0$ it was decided to modify the requirement for hodoscope master-pulses, making the system less selective for showers. The master-pulse requirement decided on was an ion chamber pulse in coincidence with at least one counter in A, B and C, which may be written $(I, A_{\geq 1}, B_{\geq 1}, C_{\geq 1})$.

In a run of 580 hours, 89 bursts were observed, the exponent in the size distribution being again 1·6. Nineteen bursts were associated with operations of the hodoscope, and four of these events showed multiple counters discharged in banks A and B, and were classified as incident showers produced in the overlying earth. The breakdown of the remaining fifteen events is given in Table 5.

Table 5

No. of counters discharged in	A	1	1	1
,, ,, ,,	B	1	2	3
,, ,, ,,	C	1	1	1
No. of events		12	2	1

These events were all associated with the discharge of single counters in banks A and C. They could not be classified as showers, since the ion chamber

walls, of thickness 1·2 cm. aluminium, were far too thin to allow the development of cascade showers from a single incident particle. Their classification is discussed further below.

§7. DISCUSSION

7.1. *Contribution from Stars*

Before discussing the burst results in detail, we first estimate the contribution to the observed burst frequencies which may be attributed to nuclear fragments from stars. We base this estimate on the burst frequency, 2·7 hr^{-1}, observed with the unscreened chamber at sea level. It is known (Euler 1940, Carmichael 1948) that for the size-group in question these bursts are almost entirely due to star processes. From the known ratio (300 : 1) of the frequency of stars at sea level to that at the same underground laboratory (George and Evans 1950) we get immediately the frequency of bursts due to nuclear fragments in the ion chamber below ground, 0·01 hr^{-1}. The required burst frequencies under Pb due to stars at sea level and at the Jungfraujoch may be determined from the known decrease under Pb of the frequency of stars, and its increase with altitude (Bernardini *et al.* 1948, George and Jason 1949). The results are collected together in Table 6.

Table 6

	Bursts per hour due to stars
Jungfraujoch (15 cm. Pb)	15·2
Sea level: 0	2·7
15 cm. Pb	1·6
Underground: 0	0·01
15 cm. Pb	0·01

7.2. *Bursts at the Jungfraujoch*

(*a*) *Local bursts.*

The observed frequency of local bursts after subtraction of the star contribution is 14·0 hr^{-1}. The stars are predominantly low energy events, and will only rarely be associated with particles capable of crossing the absorber S and discharging one of the counters C. In any case they would not be expected to give a three-fold coincidence in bank B. The observed frequency of local penetrating bursts is 10·3 hr^{-1}. Since this is approximately equal to the frequency of all local bursts with stars subtracted, we may conclude that the majority of those bursts under 15 cm. Pb not produced by nuclear disintegration fragments are produced by electron cascades which contain penetrating particles increasing with the size of the electron cascade (Table 1). These observations are consistent with the assumption that they arise from the simultaneous production of charged and neutral mesons in energetic nuclear collisions of the N-component of the cosmic radiation. On this view, the neutral mesons decay rapidly, with a lifetime less than 2×10^{-15} sec., into photons (Kaplon *et al.* 1949, Carlson *et al.* 1950, Lord *et al.* 1950), giving rise to the cascade shower recorded as the burst in our ion chamber. The charged mesons of sufficient energy produced simultaneously that escape nuclear absorption in the screen S are those that are recorded in the counter bank C.

Sufficient data now exist to put these ideas on a more quantitative basis. Thus, assume that a nuclear excitation of energy E is produced. From the data of Powell (1950, Figure 29), we obtain—by extrapolation if necessary—the

mean number of charged mesons $n(\pi^{\pm})$ emitted, and hence, from Carlson *et al.* (1950), the mean number of neutral mesons, $n(\pi^0) = \frac{1}{2}n(\pi^{\pm})$. We also have available from Camerini *et al.* (1950), and Carlson *et al.* the energy spectrum of the charged and neutral mesons. This enables us to calculate, in a straightforward manner, the maximum size of the cascade shower produced by the neutral mesons and the number of charged mesons able to penetrate the lead screen S. In calculating the penetration of the charged mesons we have assumed they suffer nuclear absorption with a probability determined by the geometric nuclear cross section. For the purpose of our approximate calculation it is sufficient to assume that the bursts are produced by cascade showers near their maximum, and to neglect fluctuations. By repeating for various values of E, it is possible to determine the number of charged mesons penetrating S as a function of the size of burst in the ion chamber. The results, so calculated, are given in the full curve in Figure 5, and are seen to be in reasonable agreement with the observations.

The fact that at high altitude most of the bursts under thick lead are produced by the N-component has been well established by the work of Bridge and Rossi (1949). The remaining bursts can be understood in terms of electromagnetic interactions of μ-mesons resulting in knock-on electrons and bremsstrahlung. Taking the absorption mean free path of the N-component producing these mixed showers to be 120 gm/cm^2, we obtain, from a comparison of the sea level and Jungfraujoch results, the following contributions to the observed burst frequency under 15 cm. Pb at the Jungfraujoch: stars, 51%; mixed showers, 40%; μ-mesons (knock-on electrons and bremsstrahlung), 9%.

Our results and conclusions concerning the penetrating bursts at altitude appear to be in agreement with those of Hudson (1949).

(*b*) *Accompanied bursts.*

Here we confine ourselves to a demonstration that a reasonable interpretation of the accompanied penetrating bursts lies in the assumption that they are produced by the high-density regions of air showers incident on the apparatus. A more detailed analysis is precluded at present by the very complexity of these events, possessing, as seems probable, a high density of all the known fundamental particles.

Cocconi *et al.* (1949) have used an arrangement of counters comparable in size to our arrangement to select high-density regions in air showers. They found the frequency of these events at Echo Lake, 3,500 m. altitude, to be 1·4 hr^{-1}, which may be compared with our observed frequency of accompanied penetrating bursts at the same altitude, 0·8 hr^{-1}.

Further, McCusker (1950) has shown that of the penetrating particles in an extensive shower, about one-quarter show the strong interaction characteristic of the N-component. As a rough approximation, we assume this same ratio holds in the high-density region, and that the total number of penetrating particles striking our apparatus is proportional to the energy of the primary particle causing the shower. Then we would expect the frequency of events in Figure 3(*b*) to increase with decreasing number of counters n simply on account of the power spectrum of the primary radiation. We would not, however, expect this increase to be maintained indefinitely, since the requirement of an ionization burst entails a low energy cut-off. The fact that the cut-off sets in for n about 5 or 6,

indicating the incidence of between one and two nucleons per event, does not seem unreasonable. Thus the frequency of the events, and the number–frequency distribution of the associated counter discharges in the bank C, do not seem inconsistent with the assumption that they are produced by the high-density regions of air showers. In view of the complexity of the events, it does not seem profitable to attempt to push the analysis further.

7.3. *Bursts at Sea Level*

The same analysis used for the bursts at altitude gives the following results for the contributions to the bursts observed at sea level under 15 cm. Pb: stars, 35%; mixed showers, 15%; μ-mesons (knock-on electrons and bremsstrahlung), 50%. These observations are consistent with the cloud-chamber observations of Fretter (1948) at sea level. They suggest that arguments for μ-meson spin based on burst observations under thick lead (Christy and Kusaka 1941) are rendered a little uncertain unless the contributions to the observed burst frequency from components other than the μ-mesons of the cosmic radiation are taken into account. Actually, the main conclusion of Christy and Kusaka was that the value of the (μ) meson spin was not unity. This conclusion is not modified when we allow for the fact that only about one-half of the bursts at sea level are due to μ-mesons.

7.4. *Bursts Underground*

(*a*) *Bursts under thick lead, $T=15$ and 45 cm.*

We shall assume that all the bursts observed below ground are produced by the energetic μ-mesons of the hard component. The very small reduction in burst frequency on increasing T from 15 to 45 cm. Pb is consistent with this assumption.

The results in §6.1 show that approximately 50% of the bursts are accompanied by the discharge of a single counter in the bank C. These events may be simply interpreted as those in which the fast μ-meson causing the event passes through one of the lower counters. The fact that the μ-meson is only detected in about 50% of the cases may be attributed to the geometry of the counter arrangements.

Of more interest is the fact that 12·5% of the penetrating bursts discharged more than one counter in bank C. While we may attribute some of these events to the production of knock-on electrons in the screen S, the frequency and spatial distribution of the discharged counters (Table 4) shows that they may not all be explained in this way. Observations on the frequency of knock-on electrons were made with the same apparatus, the frequency observed being 2·5%. Subtracting this from the 12·5% mentioned above, we conclude that 10% of the bursts observed underground are associated with penetrating showers containing two or more penetrating particles. These results do not agree with those of Hudson (1949). Working in a tunnel under 2,000 gm/cm^2, Hudson reports that none of the bursts were associated with penetrating showers.

In Figure 5 we have also plotted the mean burst size associated with the discharge of n of the screened counters C for the underground observations. The results are seen to lie close to the calculated curve, and to the results obtained at the Jungfraujoch, which is consistent with the viewpoint that the penetrating bursts observed above and below ground are essentially of the same nature,

and arise from the emission of charged and neutral π-mesons from energetic nuclear collisions.

We have calculated the cross sections for the production of bursts below ground for the following interactions of μ-mesons: knock-on electrons, bremsstrahlung and neutral meson production, and the results are shown in Figure 6. In all cases we have averaged the cross sections over the μ-meson

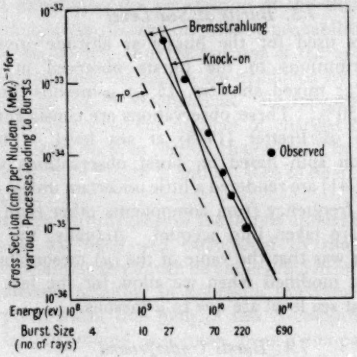

Figure 6. Cross sections for bursts produced underground by μ-mesons.

spectrum, assumed to be of the form $N(E)dE \propto dE(E+E_0)^{-3}$, where E_0 is the energy lost in ionization in the overlying material, equal to $1{\cdot}2\times10^{10}$ ev. The values of the cross sections for knock-on electrons and bremsstrahlung production by mono-energetic μ-mesons of spin $\frac{1}{2}$ were taken from Christy and Kusaka (1941). The figures for neutral meson emission were obtained in the following way. We assume that the excitation is produced by the electromagnetic interaction of fast μ-mesons in passing through atomic nuclei (cf. George and Evans 1950). The mechanism can be understood in terms of the Williams–Weizsäcker photon spectrum of a fast-charged particle of energy E,

$$N(\nu)d\nu = \frac{2\alpha}{\pi}\frac{d\nu}{\nu}\log\frac{E}{\hbar\nu},$$

where ν is the photon frequency and α is $e^2/\hbar c = 1/137$. If σ is the cross section for star production by photons, assumed constant in the following, then the cross section for the production of a star of energy in the interval W, dW is, when averaged over the μ-meson spectrum,

$$\Phi(W)\,dW = \frac{2\alpha}{\pi}\frac{dW}{W}\left[\log\left\{\frac{W+E_0}{W}\right\} - \frac{E_0}{W+E_0}\right]. \qquad \ldots\ldots(1)$$

The value of σ was fixed by normalizing to the frequencies of stars observed in nuclear plates exposed below ground. The resulting value of σ was found to be 2×10^{-28} cm² per nucleon, a value close to that derived by Miller (1951) from observations of stars formed in nuclear emulsions exposed directly to the γ-ray beam of the 340 Mev. electron synchrotron at Berkeley. At large excitations most of the energy is liberated in the form of charged and neutral mesons

(Powell 1950). The required cross section for the emission of neutral mesons of energy W, dW was then taken to be $\Phi(3W)d(3W)$ (equation (1)), since Carlson *et al.* report that only one-third of the energy liberated as mesons is in the form of neutral mesons. The results of the calculation performed in this way are indicated in Figure 6.

In order to express the observed burst frequencies in the same units, we assumed that the experimental cross section for the production of an energetic electron or photon of energy E, $\bar{\sigma}(E)$ varied in the same way as the total theoretical cross section (Figure 6) with E when averaged over the μ-meson spectrum, but was not necessarily equal to it numerically. This then enabled us to perform the integral giving the number of bursts of size greater than N rays/cm^{-2} sec^{-1}:

$$F(N) = ILA \int_0^\infty \int_0^\infty \bar{\sigma}(E) P(E, N, x)\, dE\, d\alpha, \qquad \ldots\ldots(2)$$

where I = frequency of μ-mesons cm^{-2} sec^{-1}, L = number of atoms gm^{-1} cm^2, A = atomic number, x = absorber thickness in gm. cm^{-2}; $P(E, N, x)$ is the probability that an energetic photon or electron of energy E gives a shower of more than N particles after a thickness x of absorber. $P(E, N, x)$ was obtained from the results of Bhabha and Chakrabarty (1943), assuming the number of electrons to follow a Poisson distribution. Equating the integral (2) to the observed burst frequency enabled us to fix the numerical values of $\bar{\sigma}(E)$. The observed burst frequency agrees well with the sum of the various calculated contributions. The calculated frequency of bursts of the mixed shower type arising from nuclear interactions of μ-mesons is 6% of that arising from the production of knock-on electrons and bremsstrahlung, and this is reasonably consistent with the observed proportion, 10%.

In calculating the frequency of the mixed shower bursts, we have assumed that the characteristics of meson emission do not depend on the mechanism of nuclear excitation. There is some evidence from recent observations at Berkeley that nuclear excitation by photons results in the emission of a higher proportion of neutral mesons than is found for excitation by nucleons. If the proportion of neutral mesons is increased to, say, 50%, as indicated by these experiments, then this would improve the agreement between theory and observation by increasing the calculated proportion of mixed showers in the underground bursts, and would account for the underground points lying above the curve in Figure 5.

The observed proportions of the various events giving rise to bursts under thick lead below ground are: stars, 2%; mixed showers, 10%; knock-on electrons and bremsstrahlung of μ-mesons, 88%.

(*b*) *Bursts with lead removed, i.e.* $T = 0$.

The observed frequency of bursts with $T = 0$ is 0·15 hr^{-1}, and the upper limit to the possible contribution from stars is 0·01 hr^{-1}; hence we conclude that, contrary to the conditions at sea level, with only air above the ion chamber, the bursts observed underground with $T = 0$ are not due to stars. Although there was no lead above the ion chamber, there was a considerable thickness of earth, 3 m., above the apparatus, and the majority of the bursts were probably produce by electron cascades incident from the roof. This explanation cannot apply to those 15 events in coincidence with the hodoscope counters in Table 5, since only one counter in bank A was discharged. The frequency of these events is 0·025 ± 0·006 hr^{-1}, and since the hodoscope efficiency is approximately 50%

(§ 7.4(*a*)), we may infer that the actual frequency of these events is $0{\cdot}05 \pm 0{\cdot}01$ hr^{-1}. The hodoscope records clearly indicate that most of these events are associated with the passage of a single particle through the banks of counters and, from their frequency, we know that not more than 20% of these events can be due to stars produced by fast μ-mesons. A few of the hodoscope records may have been produced by accidental coincidences, but the majority indicate that bursts of more than 20 MEV. of ionization in the chamber were produced by single penetrating particles by a process so far unidentified.

§ 8. CONCLUSIONS

From our observations we have drawn the following conclusions:

(i) 90% of the local bursts observed under 15 cm. Pb in our ion chamber at the Jungfraujoch are produced by the N-component of the cosmic radiation, 50% being produced by heavily ionizing fragments from nuclear disintegrations, and 40% from electron cascades containing penetrating particles (mixed showers); the remaining 10% are produced by μ-mesons.

(ii) The number of penetrating particles in a local penetrating burst under 15 cm. Pb increases with the burst size, the proportion being about 1 per 50 electrons at the shower maximum.

(iii) The observations of penetrating bursts at the Jungfraujoch are consistent with the assumption that they are produced by energetic nuclear disintegrations resulting in the simultaneous emission of charged and neutral mesons, the latter decaying to form cascade showers.

(iv) About 3% of the bursts observed under 15 cm. Pb at the Jungfraujoch are produced by the incidence of high-density regions of energetic air showers on the apparatus.

(v) Under 15 cm. Pb at sea level only about 50% of the bursts are produced by fast μ-mesons.

(vi) At a depth equivalent to 60 m. of water about 10% of the bursts under 15 cm. Pb are of the mixed shower type, and presumably arise from energetic nuclear disintegrations emitting charged and neutral mesons produced by fast μ-mesons.

(vii) The frequency of these mixed-shower events below ground is consistent with observations of nuclear disintegrations observed in nuclear emulsions at the same depth.

(viii) The remaining bursts under lead are produced by the knock-on electrons and bremsstrahlung produced by fast μ-mesons.

(ix) With no lead immediately above the ion chamber, two-thirds of the bursts are due to cascade showers produced in the earth above the apparatus.

(x) About one-third of the bursts observed underground with no lead above the apparatus are produced by single penetrating particles crossing the ion chamber and releasing 20 MEV. or more of ionization in the chamber. The mechanism of this energy release has not been identified.

ACKNOWLEDGMENTS

We are grateful to Professor J. D. Bernal for his support of the investigation and his interest in its progress. We would like to thank Professor von Muralt, Director of the Jungfraujoch Scientific Station, for the excellent facilities provided, and Herr Hans Wiederkehr for much assistance there. We also

gratefully acknowledge the help of Arnold Müller, of Basle University, during the Jungfraujoch observations.

The work below ground was made possible thanks to the kind co-operation of the London Transport Executive. We are grateful for stimulating discussions with Dr. J. C. Barton and for helpful criticism from Dr. J. G. Wilson. Our thanks are due also to the Department of Scientific and Industrial Research, and the Central Research Fund of the University of London for research grants.

REFERENCES

BERNARDINI, G., CORTINI, G., and MANFREDINI, M., 1948, *Phys. Rev.*, **74,** 1878.
BHABHA, H. J., and CHAKRABARTY, S. K., 1943, *Proc. Roy. Soc.* A, **181,** 267.
BRIDGE, H., and ROSSI, B., 1949, *Phys. Rev.*, **75,** 810.
CAMERINI, U., FOWLER, P. H., LOCK, W. O., and MUIRHEAD, H., 1950, *Phil. Mag.*, **41,** 413.
CARLSON, A. G., HOOPER, J. E., and KING, D. T., 1950, *Phil. Mag.*, **41,** 701.
CARMICHAEL, H., 1948, *Phys. Rev.*, **74,** 1667.
CHOU, C. N., 1948, *Phys. Rev.*, **74,** 1659.
CHRISTY, R. F., and KUSAKA, S., 1941, *Phys. Rev.*, **59,** 414.
COCCONI, G., COCCONI-TONGIORGI, V., and GREISEN, K., 1949, *Phys. Rev.*, **76,** 1020.
EULER, H., 1940, *Z. Phys.*, **116,** 73.
FRETTER, W. B., 1948, *Phys. Rev.*, **73,** 41.
GEORGE, E. P., and JÁNOSSY, L., 1946, *Phys. Rev.*, **70,** 773.
GEORGE, E. P., and JASON, A. C., 1949, *Proc. Phys. Soc.* A, **63,** 243.
GEORGE, E. P., and TRENT, P. T., 1948, *Nature, Lond.*, **161,** 249.
GEORGE, E. P., and EVANS, J., 1950, *Proc. Phys. Soc.* A, **63,** 1248.
GREISEN, K., 1948, *Phys. Rev.*, **73,** 521.
HUDSON, D. E., 1949, *Echo Lake Conference on Cosmic Rays*, Paper No. 23, p. 85.
KAPLON, M. F., PETERS, B., and BRADT, H. L., 1949, *Phys. Rev.*, **76,** 1735.
LORD, J. J., FAINBERG, J., and SCHEIN, M., 1950, *Phys. Rev.*, **80,** 970.
MCCUSKER, C. B. A., 1950, *Proc. Phys. Soc.* A, **63,** 1240.
MILLER, R. D., 1951, *Phys. Rev.*, **82,** 260.
POWELL, C. F., 1950, *Rep. Prog. Phys.*, **13,** 350 (London : Physical Society).
ROGOZINSKI, A., 1944, *Phys. Rev.*, **65,** 291.

Observations of the Latitude Effect of Penetrating Showers

BY J. W. STURGESS

Birkbeck College, University of London

Communicated by E. P. George; MS. received 13th February 1951

ABSTRACT. The latitude effect of the local penetrating showers of cosmic radiation produced in paraffin has been measured at sea level and found to be in the ratio of $1{\cdot}8 \pm 0{\cdot}4$ between London and Dakar, French West Africa. The extensive penetrating showers showed no latitude effect, which is consistent with the greater energy of these showers. The background frequency of local showers, i.e. those recorded with no absorber above the counter system, was found to be insensitive to latitude and reasons for this are discussed.

§1. INTRODUCTION

RECENTLY the latitude dependence of the nucleon component of the cosmic radiation has attracted some attention. Simpson and Uretz (1949) and Yuan (1949) have studied the latitude effect for low energy neutrons, while observations on disintegration 'stars' observed in photographic plates have been

reported by Salant *et al.* (1950) and Lattimore (1950). Results for the more energetic type of event, the penetrating showers, observed with systems of lead-screened Geiger counters have been given by Walsh and Piccioni (1950) at altitude and by Appapillai and Mailvaganam (1950) at sea level. In addition a series of theoretical papers has been published by the Dublin School of Cosmic Physics (see Messel and Ritson (1950) for a list of references).

In the present paper, results are given of observations of the penetrating showers produced in paraffin at sea level at Dakar, 21·6° N and London 54·2° N geomagnetic latitude.

Paraffin was chosen in order to minimize the response of the apparatus to the extensive showers (cf. Broadbent and Jánossy 1948) which, being events of considerable energy, were expected to show negligible latitude effect.

Since it seemed probable that the latitude effect would be larger the smaller the energy required to discharge the counter system, it was decided to reduce to a minimum the lead screening while still maintaining the system insensitive to cascade electron showers. A thickness of 15 cm. Pb between extreme counters was used, and separate experiments are reported which show that this screening was adequate.

§ 2. APPARATUS

The apparatus is shown in Figure 1. It is similar to that used by Broadbent and Jánossy (1947), except for the reduction in the lead thickness from 30 cm. to 15 cm., as stated above. Sevenfold coincidences were recorded between the discharges of the three counter groups in the top bank, and the two groups in

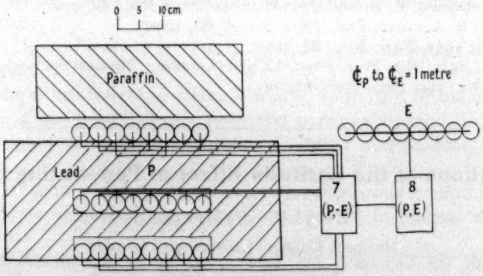

Figure 1. The apparatus.

each of the middle and the bottom banks of counters. Butler *et al.* (1950) have shown that the mean energy of the showers detected by the Broadbent–Jánossy arrangement is 10^{10} ev., whereas the latitude cut-off energy at Dakar is $1{\cdot}15 \times 10^{10}$ ev. in the vertical direction. The mean energy of the showers detected in the present experiment may be taken as 5×10^{9} ev., well below the cut-off energy.

The unscreened tray E was used in the usual way to detect events associated with extensive air showers, and was connected in coincidence with the main shower set P. The resolving time of the coincidence circuits was 10^{-5} sec. and the accidental rate was negligible. The paraffin absorber was cast in blocks 45 cm. × 45 cm. × 15 cm.

§ 3. RESULTS

(i) *Extensive Showers*

Table 1 gives the frequencies of extensive showers (coincidences (P, E)) at London and Dakar, for various absorber thicknesses. It is seen that there is no significant difference between the results at the two latitudes.

Table 1

Paraffin absorber thickness (cm.)		0	15	30
Extensive penetrating showers per hour	London	$0{\cdot}17 \pm 0{\cdot}02$	$0{\cdot}18 \pm 0{\cdot}02$	$0{\cdot}15 \pm 0{\cdot}02$
	Dakar	$0{\cdot}17 \pm 0{\cdot}02$	$0{\cdot}16 \pm 0{\cdot}04$	$0{\cdot}17 \pm 0{\cdot}03$

(ii) *Local Showers*

Table 2 gives the frequencies of occurrence of local showers (anticoincidences (P, $-$E)) corrected for differences in barometric pressure (Jánossy and Rochester 1944).

Table 2

Paraffin absorber thickness (cm.)		0	15	30
Local penetrating showers per hour	London	$0{\cdot}40 \pm 0{\cdot}03$	$0{\cdot}73 \pm 0{\cdot}04$	$0{\cdot}85 \pm 0{\cdot}04$
	Dakar	$0{\cdot}41 \pm 0{\cdot}04$	$0{\cdot}51 \pm 0{\cdot}07$	$0{\cdot}66 \pm 0{\cdot}05$

The two straight lines of best fit relating the shower frequency to paraffin thickness were found by the usual procedure of minimizing the value of χ^2. The latitude effect determined from the ratio of the slopes of these two lines is $1{\cdot}8 \pm 0{\cdot}4$.

(iii) *Local Showers produced in Pb at London*

In order to verify that the coincidences were mostly caused by penetrating and not by electron cascade showers, the frequency of showers under various Pb absorbers was determined at London. The results, corrected for barometric fluctuations and the effect of the geometry of the top absorber (cf. George and Jason 1950), are plotted in Figure 2. Fitting an inverse exponential curve to

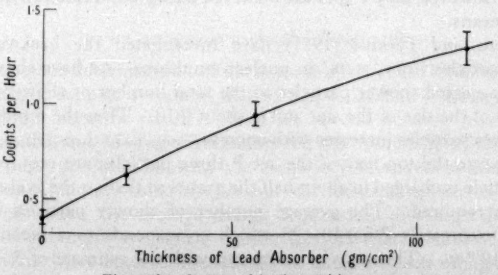

Figure 2. Corrected lead transition curve.

the results, in the manner indicated by these authors, gave the value of the collision length in Pb of the particles generating the showers as $L_c = 150 \pm 70$ gm/cm^2, consistent with recent results.

Thus, from the transition curves obtained in paraffin and in lead, it appears that in spite of the reduction in the amount of Pb absorber between the counters of the set P, the events recorded were still of the penetrating shower type, and the latitude effect measured is that for events generally accepted as penetrating showers.

§4. DISCUSSION

(i) *Extensive Showers*

The lack of latitude effect for the extensive showers is not unexpected, since the mean energy of the extensive showers recorded must have been in the region of 10^{15} ev., well beyond the geomagnetic cut-off energies.

(ii) *The Background Frequency of Showers with no Material above the Counter System*

Table 2 shows that the background frequency of penetrating showers, with no material above the top tray, is the same at both latitudes. One might expect these background rates to show the same ratio as the measured latitude effect. As possible explanations of this latitude-insensitive background, the following mechanisms have been considered: (*a*) low density extensive air showers, whose penetrating particles discharge the main set but miss the unscreened counter tray E, or (*b*) the discharge of the top trays by back-ejected shower particles from an event in the lead below, such events being of a higher energy than the normal showers recorded, and hence less latitude-sensitive.

The contribution of extensive air showers has been estimated numerically in the following manner. For showers of density greater than $10\,m^{-2}$ the density spectrum and proportion of penetrating particles have been taken from Cocconi *et al.* (1949). For lower density showers, where few measurements have been made the density spectrum and proportion of penetrating particles have been calculated from the primary spectrum and the known cross section for meson production. It was found that below densities of $1m^{-2}$ the proportion increases markedly beyond the 2% observed for denser showers, because these low density and therefore low energy showers are well beyond their cascade maxima and the associated mesons are being absorbed much less rapidly than the cascade electrons. However, only 1% of the observed background rate can be accounted for by this means.

Franzinetti and Perkins (1951) have investigated the backward ejected relativistic particles from 'stars' in nuclear emulsions, and have shown that the ratio of back-ejected shower particles to the total number of shower particles is independent of the size of the star and is about 0·10. Thus the number of back-ejected shower particles increases with energy.

To discharge the top tray of the set P three particles are required, but the incident particle is charged in about half the events so that on the average 2·5 back particles are required. The average number of shower particles in such an event is approximately $2{\cdot}5/0{\cdot}10 = 25$ which corresponds to a mean energy of about $2{\cdot}5 \times 10^{10}$ ev. This may be compared with the estimate of 5×10^{9} ev. for a shower generated in the top absorber. The nucleons causing the apparatus to discharge will have energies greater than these values. If the energy spectrum of these high energy nucleons is taken as $N(>E) \propto E^{-1{\cdot}6}$ (cf. Barton *et al.* 1951), the ratio of the frequencies of nucleons above these two energies will be $5^{1{\cdot}6}$ or about 12:1.

Table 2 shows that the frequency of showers produced in 30 cm. paraffin is comparable with the background rate of showers. As the collision length in paraffin is about 80 gm/cm² (George and Jason 1950), the chance of a collision in 30 cm. paraffin is about 0·25. But the efficiency of recording showers in

paraffin is about one-third from geometric considerations, whereas for the background showers produced in lead it is nearer unity. Therefore the chance of recording those showers produced in lead with sufficient back-ejected particles is probably so much greater that it compensates for the lower frequency of nucleons of sufficient energy ($\geqslant 2{\cdot}5 \times 10^{10}$ ev.), and the shower frequency from 30 cm. paraffin is approximately equal to the background rate.

It seems probable therefore that the small latitude effect in the background rate may be understood in terms of the higher energy required to produce the background coincidences.

(iii) *Local Showers*

The latitude effect observed was $1{\cdot}8 \pm 0{\cdot}4$, a value somewhat larger than other recent determinations discussed below. A nucleon of energy 5×10^9 ev. which will discharge the penetrating shower set must have had an energy of 7×10^9 ev. at the top of the atmosphere. The cut-off energy at Dakar is $1{\cdot}15 \times 10^{10}$ ev., and if the penetrating showers arise from primaries only, the index γ of the primary spectrum in this energy region will be given by $(11{\cdot}5/7)^{\gamma} = 1{\cdot}8 \pm 0{\cdot}4$, whence $\gamma = 1{\cdot}2 \pm 0{\cdot}4$. This figure is in good agreement with the results of Van Allen and Singer (1950) who obtained a value of 1·1 for the primary spectrum in the energy range 3 to 15×10^9 ev. from rocket experiments. At a residual depth of 15 gm/cm^2, Winckler, Stix, Dwight and Sabin (1950) obtained a value of 0·9 in the same energy range. If secondary nucleons are also considered to discharge the set, the energy of the primary nucleons from which these arise must be greater and the index will be greater.

Messel (private communication) has extended the original work of Heitler and Jánossy (1949) by including the effect of nucleon recoils and ionization loss, thus giving, in effect, a theory of the nucleon cascade. He gives a value of 1·7 for the latitude effect for nucleons at sea level with energy greater than 5×10^9 ev., using $\gamma = 1{\cdot}1$.

(iv) *Comparison with other Observations*

The only other determination of the latitude effect at sea level for penetrating showers using a counter system is that of Appapillai and Mailvaganam (1950) who obtained a negative result. There are several possible reasons for this. First, Appapillai and Mailvaganam compared the frequency of showers determined by them at Colombo with the frequency observed at Manchester by Broadbent and Jánossy, using similar but not identical apparatus. Secondly, as mentioned above, the average energy required to discharge this particular equipment is about 10^{10} ev., and a smaller latitude effect would be expected in any case. Thirdly, a small difference existed in the two sets of apparatus which would tend to reduce the observed effect. The top absorber used by Broadbent and Jánossy was 45 cm. square, whereas that used by Appapillai and Mailvaganam was 50 cm. square. Thus, from the null effect reported by Appapillai and Mailvaganam, one may conclude that the latitude effect was probably of the order of $(50/45)^2$ or 1·2, a not unreasonable value for showers of 10^{10} ev. energy. In the present experiment, the same apparatus was used at the two latitudes, though it had necessarily to be dismantled for transport between them.

A latitude effect of 1·1 was observed at sea level and at altitudes of 25,000 and 30,000 feet by Walsh and Piccioni (1950) between 21° and 55° N. These

authors estimate the mean energy of the penetrating showers discharging their apparatus at 2×10^{10} ev., which is above the latitude cut-off energy.

Observations of the nuclear component made with photographic plates and with neutron detectors have in general shown a bigger latitude effect than that reported here; this is reasonable in view of the smaller energy of these events.

§ 5. CONCLUSIONS

The conclusions resulting from this investigation are as follows: (i) the latitude effect of local penetrating showers of mean energy about 5×10^9 ev. is $1{\cdot}8 \pm 0{\cdot}4$ between 20° N and 54° N geomagnetic latitudes. From this the index of the integral energy spectrum for primary nucleons for energies between 5×10^9 ev. and $1{\cdot}15 \times 10^{10}$ ev. is found to be $1{\cdot}2 \pm 0{\cdot}4$. (ii) The range in lead of the particles producing the showers investigated is 150 ± 70 gm/cm². (iii) The local showers observed with no material above the top counter tray show a negligible latitude effect. This implies that the mean energy of the particles producing the showers under this condition is higher than with material above the top counter tray, consistent with the assumption that in the former case the top tray is discharged by back-ejected particles. (iv) The extensive showers show no detectable latitude effect. This is consistent with the large value, of the order of 10^{15} ev., of the energy of these showers.

ACKNOWLEDGMENTS

The author is grateful to Professor J. D. Bernal for providing the facilities for carrying out this work and for his great interest in its progress, and to Professor M. G. E. Cosyns of Brussels University and Professor T. Monod (of the Institut Français d'Afrique Noire) for enabling him to carry out measurements at Dakar. The investigation was carried out under the supervision of Dr. E. P. George, whom the author thanks for many helpful discussions, and was supported by a grant from the Department of Scientific and Industrial Research.

REFERENCES

Appapillai, V., and Mailvaganam, A. W., 1950, *Proc. Phys. Soc.* A, **63,** 856.
Barton, J. C., George, E. P., and Jason, A. C., 1951, *Proc. Phys. Soc.* A, **64,** 175.
Broadbent, D. A., and Jánossy, L., 1947, *Proc. Roy. Soc.* A, **190,** 497; 1948, *Ibid.*, 192, 364.
Butler, C. C., Rosser, W. G. V., and Barker, K. H., 1950, *Proc. Phys. Soc.* A, 63, 145.
Cocconi, G., Cocconi-Tongiorgi, V., and Greisen, K. I., 1949, *Phys. Rev.*, 75, 1063.
Franzinetti, C., and Perkins, D. H., 1951, *Phil. Mag.*, **42,** in the press.
George, E. P., and Jason, A. C., 1950, *Proc. Phys. Soc.* A, **63,** 1081.
Heitler, W., and Jánossy, L., 1949, *Proc. Phys. Soc.* A, **62,** 374.
Jánossy, L., and Rochester, G. D., 1944, *Proc. Roy. Soc.* A, **183,** 186.
Lattimore, W. S., 1950, *Phil. Mag.*, **41,** 961.
Messel, H., and Ritson, D. M., 1950, *Proc. Phys. Soc.* A, **63,** 1359.
Salant, E. O., Hornbostel, J., Fisk, C. B., and Smith, J. E., 1950, *Phys. Rev.*, 79, 184.
Simpson, J. A., and Uretz, 1949, *Phys. Rev.*, **76,** 569.
Van Allen, J., and Singer, F., 1950, *Phys. Rev.*, **78,** 819.
Walsh, T. G., and Piccioni, O., 1950, *Phys. Rev.*, **80,** 619.
Winckler, J. R., Stix, T., Dwight, K., and Sabin, R., 1950, *Phys. Rev.*, **79,** 656.
Yuan, L., 1949, *Phys. Rev.*, **76,** 1267.

LETTERS TO THE EDITOR

Investigation of Superconductivity in Lead Compounds

Meissner, Franz and Westerhoff (1933) have made electrical resistivity measurements on lead sulphide down to 1·3° K. and concluded that the very pure substance is a semiconductor, whilst the occasional appearance of superconductivity in specimens showing a metallic characteristic must be due to small amounts of excess lead. Dunaev and Maslakovitz (1947) have worked with specimens containing small amounts of lead impurity (carrier concentration of the order 10^{19} per cm^3) and find a metallic behaviour below 450° C. but no superconductivity down to 2·15° K.

Quite recently Darby, Hatton and Rollin (1950) reported superconductivity in PbS, PbSe, and PbTe all at about 5° K., as measured by a magnetic method. The materials were prepared by fusion together of the constituents *in vacuo*; no X-ray investigation was made, apparently, to look for excess lead. The figure 5° K. is most interesting, being relatively far removed from the normal lead transition temperature of 7·3° K. Lark-Horovitz, in a discussion of these results pointed out that it is now generally accepted that the chemically very pure lead compounds behave as semiconductors. If they should become superconducting at low temperatures this would be the only known case of such behaviour and would be of great interest from the theoretical point of view. On the other hand, X-ray investigations of lead compounds in the Purdue laboratories have shown that frequently lead is found if the material is electrically n-type (excess conduction).

We have investigated the problem using the ballistic-throw magnetic method of detection; this enables one to distinguish most readily between a bulk effect and an impurity effect. The specimen under investigation is enclosed in the bulb of a gas thermometer, which is surrounded by a vacuum case immersed in a bath of liquid helium. It was hoped to reproduce the results of Darby *et al.* and then to show that the specimens were impure, but we were unable to obtain a 5° transition and the results are essentially a confirmation of Meissner's work.

Pure lead sulphide may be prepared in the form of a fine powder by precipitation from solutions of, for example, lead acetate and sodium sulphide. Care must be taken in the method of fusing together lead and sulphur, for the reaction is strongly exothermic and some of the sulphur is vaporized. This difficulty may be overcome by heating the mixture in a graphite crucible inside an evacuated, sealed-off quartz tube. After the reaction has taken place the temperature of the furnace is raised to the melting-point of the sulphide (1,120° C.) and held there for a time before cooling again. Ingots may also be prepared by using the precipitated powder instead of the lead sulphur mixture.

We have made measurements on ingots prepared by fusion and on the precipitated powder both finely divided and sintered.* In most cases no transition could be observed down to 1·3° K. and the X-ray photographs contained only PbS lines.† In a few specimens a very small (partial volume) effect was found at 7·3° K., the normal lead transition temperature, and the X-ray patterns for these specimens included a very weak extra line presumably due to excess lead.

Crystals of natural lead sulphide (galena) and of the pure commercial product also gave negative results. A fusion sample of lead telluride became superconducting at 7·3° K., the magnitude of the effect indicating that it was confined to a small fraction of the total volume of the specimen, and the presence of lead was confirmed by X-ray. A single crystal of lead telluride (kindly supplied by Mr. R. A. Smith of Telecommunications Research Establishment, Malvern) showed no transition down to 1·3° K.

These experiments, in essentially reproducing Meissner's results—and extending them to lead telluride—strongly suggest that these lead compounds are not superconductors. We feel that the results of Darby and his co-workers may be explained by the presence of excess lead in their specimens (a possibility admitted by the authors) since their transition temperatures and critical field curves are nearly the same for the three different compounds. A few per cent of excess lead could easily form a superconducting network of lead veins that would give an apparently complete volume effect (cf. Hudson 1950) and the stated

* We are indebted to L. M. Roth for assistance in the preparation of these specimens.
† We are indebted to I. G. Geib for all the X-ray investigations connected with these experiments.

procedure of rapidly cooling the melt to room temperature might result in internal strains sufficient to alter the transition temperature appreciably. We have, however, tried to obtain such a strain effect without success.

These experiments were carried out at the suggestion of K. Lark-Horovitz. Since their completion, Dr. Rollin has sent us an account (to be published later) of more recent experiments with very pure specimens which are in agreement with the above results.

Department of Physics,
Purdue University,
Lafayette, Indiana.
22nd May 1951.

R. P. HUDSON.

DARBY, J., HATTON, J., and ROLLIN, B. V., 1950, *Proc. Phys. Soc.* A, **63**, 1181.
DUNAEV, U. A., and MASLAKOVITZ, U. P., 1947, *J. Exp. Theor. Phys. U.S.S.R.*, **17**, 901.
HUDSON, R. P., 1950, *Phys. Rev.*, **79**, 883.
MEISSNER, W., FRANZ, H., and WESTERHOFF, H., 1933, *Ann. Phys Lpz.*, **17**, 593.

Effect of Temperature on the Height of Potential Barriers and on the Breakdown Voltage of Contact Rectifiers

Theoretical calculations (Kimball 1935) have indicated a widening of the energy gap of covalent lattices, such as diamond and silicon, with decreasing lattice parameter. This is confirmed by Taylor (1950) who finds the intrinsic resistivity of germanium to increase by $10{\cdot}2\times10^{-5}$/atm. With the values of volume compressibility and of the coefficient of thermal expansion this corresponds to a change in the gap of $-0{\cdot}87\times10^{-4}$ ev/°c. This is confirmed by Shockley and Bardeen (1950), who obtain a value of $-0{\cdot}9\times10^{-4}$ ev/°c. from the change of mobility of electrons and holes in germanium with temperature. On the other hand, Fan (1950) finds a value of $-4{\cdot}0\times10^{-4}$ ev/°c. from the long-wave limit of the optical absorption band; this high value may be caused by increased line width (Radkowsky 1948).

Apart from these effects in the semiconductor itself, it might be expected that the height of the potential barrier arising at the interface when in contact with a metal would also be affected by a change in gap width. Such changes in barrier height would affect certain characteristics of barrier cells very sensitively and would thus make the changes highly susceptible to measurement. Some such effects have recently been observed here on rectifiers and photocells (Billig and Ridout 1951). Measurements of the contact resistance of standard selenium, germanium and silicon rectifiers and of selenium photocells over a large range of temperatures indicate that the height of the barrier in all these cells remains constant above room temperature, but gradually decreases as the temperature is lowered. Extrapolation beyond the lowest temperature reached so far (78°K.) seems to indicate a complete disappearance of the barrier around absolute zero temperature. Such a drop in barrier height is supported by an analysis of the inverse current–voltage characteristic of contact rectifiers at low temperatures. As has recently been shown (Billig 1951), electrical breakdown in rectifiers is mainly due to the onset of thermal instability and is critically dependent on the height of the potential barrier as well as on the cooling. As these two effects operate in opposite directions, a lowering of the temperature may lead to either an increase or a decrease in the breakdown voltage. This is actually borne out by experience: selenium rectifiers, for instance, when cooled considerably below room temperature break down at a lower voltage, whilst in germanium point contact rectifiers the turnover voltage actually increases at low temperatures, at least down to liquid air temperature (Benzer 1949, confirmed by unpublished measurements of the present author).

Quantitatively, the results obtained could not so far be correlated with the effects reported above in the semiconductor material itself: taking Taylor's value of $-0{\cdot}87\times10^{-4}$ ev/°c., a drop of 100°c. in the temperature should increase the gap width in the germanium by 0·0087 ev., whilst, according to our measurements, cooling the germanium rectifier by 100°c. depresses the height of the barrier by 0·125 v.

According to the simple model of Schottky (1942), the height of the potential barrier—the ' diffusion voltage '—should be equal to the difference in work functions of the contacting metal and semiconductor. Very little information is available on the change with temperature of the work function, particularly in semiconductors; it is, therefore, impossible at this stage to decide in what way, according to Schottky's model, the observed change in barrier height should be correlated with the change in width of the energy gap. Further measurements, particularly a study of the effect of large hydrostatic pressures on the characteristics of barrier cells, should provide useful evidence for or against that simple model of the potential barrier. Such experiments are being planned and will be reported in due course.

Research Laboratory, E. BILLIG.
Associated Electrical Industries Ltd.,
Aldermaston, Berkshire.
4th May 1951.

BENZER, S., 1949, *J. Appl. Phys.*, **20**, 804.
BILLIG, E., 1951, *Proc. Roy. Soc.* A, in the press.
BILLIG, E., and RIDOUT, M. S., 1951, *Nature, Lond.*, **167**, 1028.
FAN, H. Y., 1950, *Phys. Rev.*, **78**, 808.
KIMBALL, G. E., 1935, *J. Chem. Phys.*, **3**, 560.
RADKOWSKY, A., 1948, *Phys. Rev.*, **73**, 749.
SCHOTTKY, W., 1942, *Z. Phys.*, **118**, 539.
SHOCKLEY, W., and BARDEEN, J., 1950, *Phys. Rev.*, **77**, 407.
TAYLOR, J. H., 1950, *Phys. Rev.*, **80**, 919.

K Capture in ^{128}I

The nucleus ^{128}I lies between two stable isobars : ^{128}Te and ^{128}Xe. It has long been known to decay by β-emission to ^{128}Xe; more recently Reynolds (1950) has shown by mass spectrometric analysis of an old neutron-irradiated iodine sample that 5% of ^{128}I nuclei decay to ^{128}Te. This alternative decay process must consist principally of K capture, since less than one in a thousand positrons are emitted (Barber 1947).

We have observed X-rays emitted by ^{128}I by means of a NaI (Tl activated) crystal and photomultiplier. They consist of Te K-radiation and are not emitted in coincidence with the ^{128}I β-ray. By comparing with the X-rays from ^{114}In we have estimated the K capture branching ratio.

Sources of ^{128}I were prepared by the Szilard–Chalmers method from neutron irradiated ethyl iodide. Owing to the fact that the K absorption edge of Ag lies below the X-ray energies involved, the use of silver iodide precipitate was avoided in the extraction, and active iodine was prepared as cuprous iodide.

Beta-rays were screened off with 1 cm. of plastic, and the sources were placed in front of a thin slice of sodium iodide crystal mounted on an E.M.I. photomultiplier tube. An analysis of the pulse height spectrum with a single channel kicksorter showed a peak at an energy 1·15 times that corresponding to the peak found with ^{114}In. This may be compared with the ratio of 1·13 : 1 to be expected for Te and In K X-rays. Further experiments with absorber foils identified these X-rays as predominantly characteristic of Te.

To support this conclusion an experiment was devised to distinguish X-rays which were in coincidence with β-particles from those which were not. An ^{128}I source was sandwiched between two crystals of naphthalene–anthracene and mounted on a photomultiplier tube. This formed a β-counter of 4π solid angle. The 4π counter and source were then brought in contact with the X-ray counter. A coincidence circuit generated a pulse which could be used either to block or to pass counts through the kicksorter. In this way the kicksorter could be used to analyse the spectrum in coincidence with β-decay, or not in coincidence with β-decay, or simply the total spectrum due to the source.

Curves obtained with and without β-decay anticoincidence are shown in the Figure to the same scale. The ^{114}In X-ray peak is added as a calibration mark. Beyond the peak, anticoincidence reduces the count rate to 16%, this remainder presumably representing the inefficiency of the 4π counter; in view of the thickness of the source and the consequent β-absorption and loss of light, this is a plausible figure. The reduction within the X-ray

peak is due to the removal of bremsstrahlung and of small pulses produced by the 428 kev. γ-ray line of ^{128}I, both of these being in coincidence with β-decay. Observation of the x-ray spectrum in coincidence with β-decay showed the same type of spectrum as that obtained from the bremsstrahlung of a ^{32}P (pure β) source. No significant quantity of characteristic x-radiation could be detected.

With the 4π counter and anticoincidence circuit we hope to proceed with the examination of other nuclei; it is possible that in some cases bremsstrahlung and γ-ray emission have hitherto obscured any x-rays arising from K capture.

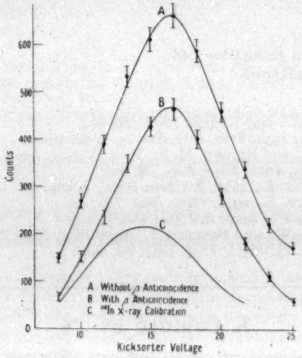

In order to estimate the proportion of ^{128}I nuclei decaying by K capture, a comparison of β-ray emission and of x-ray emission was made between sources of ^{114}In and ^{128}I. A highly converted isomeric level of ^{114}In decays with a 48-day half-life to the ground state of ^{114}In, and this in turn decays 97% by β-ray emission to ^{114}Sn and 3% by K capture to ^{114}Cd. K capture and K shell conversion of the isomeric level lead to a fraction $(45 \pm 4) \times 10^{-2}$ of K shell vacancies per β-ray emitted (Boehm and Preiswerk 1949). Since both β-ray and x-ray energies lie near one another in these two cases, a comparison is particularly easy to make. The correction for Auger effect need not be made since a similar fraction of K shell vacancies will be thus filled in both types of atom. A branching ratio, K capture to β-decay, of $(6{\cdot}3 \pm 0{\cdot}7) \times 10^{-2}$ was found.

The authors would like to thank Dr. P. F. D. Shaw for his assistance with the Szilard–Chalmers separation, and Lord Cherwell for putting at their disposal the facilities of this Laboratory.

The Clarendon Laboratory,
Oxford.
21st May 1951.

W. B. Mims.
H. Halban.

Barber, W. C., 1947, *Phys. Rev.*, **72**, 1156.
Boehm, F., and Preiswerk, P., 1949, *Helv. phys. Acta*, **22**, 331.
Reynolds, J. H., 1950, *Phys. Rev.*, **79**, 745.

Magnetic Analysis of α-Particle Groups from (d, α) Reactions

A heavy-particle magnetic focusing spectrometer has been used to measure the energy spectrum of α-particles emitted during the bombardment of light elements with the deuteron beam from the Liverpool 37 inch cyclotron. The spectrometer is similar to those described by Ringo (1940) and by Burcham and Freeman (1949), and uses a 50° sector field to give focusing in the horizontal plane. Particles emitted within $\pm 1\frac{1}{2}°$ of the normal to the field boundary enter the field and those with a 25 cm. radius of curvature in the field are focused at

an adjustable slit. The target and slit are symmetrically placed with respect to the 50° sector on a line through the intersection of the effective field boundaries. A proportional counter is used as a detector. Thus different types of particle of equal momenta may be distinguished and α-particle energies up to 4 MeV. may be measured. The vertical separation of the pole faces is 1 cm., giving a $\frac{1}{2}$° angle of collection in this plane, and a total solid angle for collection of about 1/2400.

The thin targets used (~1 mm. air equivalent) were deposited on strips of gold foil 1·2 cm. wide supported vertically with their faces making an angle of 30° with the deuteron beam. In the target chamber the beam was about 2 cm. wide and $\frac{1}{2}$ cm. high, so that a target area of about $\frac{1}{4}$ cm² was illuminated. The analyser was arranged to measure particles emitted at a mean angle of 90°. A proportional counter was used to monitor the beam passing through the target by counting elastically scattered deuterons in a small solid angle at 45° to the deuteron beam. Absorbers could be placed in an air gap between the cyclotron extension tube and the target chamber to reduce the incident beam energy. The energy resolution was limited to 10% by the energy spread of the incident deuterons, the spread in angle between incident and emitted particles, and the width and thickness of the targets.

The current to the high resistance windings of the spectrometer magnet was supplied from a 1,200 v. rectifier set and was stabilized electronically. To measure the magnetic field, the charge generated in a flip coil was compared with that stored in a condenser charged to a voltage known by comparison with that of a standard cell. As the spectrometer was in the stray field of the cyclotron magnet it was calibrated *in situ* by slowing down α-particles from Thorium C in an air absorption cell.

The α-particle spectra observed from thin deposits of carbon and zinc oxide are shown in Figures 1 and 2. The higher energy peak (2·81 MeV.) in the carbon spectrum corresponds

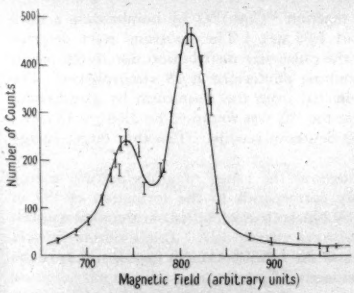

Figure 1. Spectrum of α-particles from $^{12}C(d, \alpha)^{10}B$.

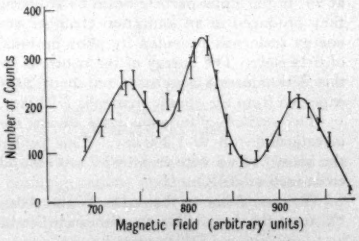

Figure 2. Spectrum of α-particles from $^{16}O(d, \alpha)^{14}N$.

to the ground state of ^{10}B, giving an incident beam energy of 6·77 MeV. using the Q value −1·44 MeV. for this reaction. This beam energy has been used to calculate the Q values and energy levels given in the Table. The accuracy of the excitation energies is estimated to be closer than ±0·08 MeV.

Reaction	$^{12}C(d, \alpha)^{10}B$	$^{16}O(d, \alpha)^{14}N$	$^{16}O(d, \alpha)^{14}N$	$^{16}O(d, \alpha)^{14}N$
α-particle energy (MeV.)	2·31	2·28	2·83	3·70
Q (MeV.)	−2·15	−2·64	−1·95	−0·89
Excitation energy of residual nucleus (MeV.)	0·71	5·70	5·01	3·95

The α-particle group corresponding to the known level in ^{10}B at 0·71 MeV. (Hornyak *et al.* 1950) has also been observed in photographic plates by Berlman (1950). A range of energy levels of ^{10}B up to 1·3 MeV. would be covered by our measurements, but they show no α-particle groups corresponding to levels at 0·41 and 1·02 MeV. suggested to explain γ-ray lines from $^{10}B^*$ (Hornyak *et al.* 1950).

There is a possibility that the 2·28 and 2·83 MeV. groups from oxygen might be due to carbon contamination although measurements with freshly prepared zinc oxide targets indicate that this is unlikely. The α-groups corresponding to known levels of ^{14}N at 3·95

and 5 MeV. (Hornyak *et al.* 1950) have also been reported by Berlman (1950), while the 2·28 MeV. group would correspond to the suggested level at 5·5 MeV. (Hornyak *et al.* 1950). A range of energy levels of ^{14}N from 3·4 to 6·1 MeV. would be covered by the spectrum shown and this range has been extended to 2·0 MeV. by using a reduced deuteron beam energy of 5·31 MeV. No further groups were discovered. There is no sign of α-particle groups corresponding to the known levels at 2·3 and 3·4 MeV. or the doubtful level at 6·1 MeV. (Hornyak *et al.* 1950).

Using the reduced beam energy of 5·31 MeV. we have also observed a 4·32 MeV. α-particle group from magnesium. As this element has three isotopes, this could correspond to excited states of 2·90, 8·06 and 3·05 MeV. for ^{22}Na, ^{23}Na, ^{24}Na respectively. Since ^{24}Mg is considerably the most abundant isotope, ^{22}Na is the most probable residual nucleus.

A more detailed account of this work will be published elsewhere.

George Holt Physical Laboratory,
University of Liverpool.
3rd May 1951.

A. Ashmore.
J. F. Raffle.

Alburger, D. E., and Hafner, E. M., 1950, *Rev. Mod. Phys.*, **22**, 373.
Berlman, J. B., 1950, *Phys. Rev.*, **80**, 775.
Burcham, W. E., and Freeman, J. M., 1949, *Phil. Mag.*, **40**, 807.
Hornyak, W. E., Lauritsen, T., Morrison, P., and Fowler, W. A., 1950, *Rev. Mod. Phys.*, **22**, 291.
Ringo, R., 1940, *Phys. Rev.*, **58**, 942.

The Reaction $^{13}C(\alpha n)^{16}O$

We have established the existence of the reaction $^{13}C(\alpha n)^{16}O$ by bombarding a thick target of separated ^{13}C with alpha-particles of 1·05 MeV. The neutrons were detected at 90° to the alpha-particle beam by studying the pulse-size distribution due to the recoils they produced in an ionization chamber containing deuterium at 38 atmospheres. The energy scale was provided by photoprotons ejected from the deuterium by gamma-rays of 6·14 MeV. The energy of the neutrons from the ^{13}C was found to be $2{\cdot}68 \pm 0{\cdot}15$ MeV.; this determination was based on about 20,000 deuteron recoils. The thin target energy expected from the atomic masses is 2·92 MeV.

The excitation function rises slowly throughout the range of alpha-particle energy investigated—up to 1,200 kev. This probably corresponds to the formation of ^{17}O in the known broad state around 7·7 MeV. found by Nuckolls *et al.* (1946) in the total neutron cross section of ^{16}O.

We should like to thank Dr. W. D. Allen and Sir John Cockcroft for the supply of the ^{13}C from the Atomic Energy Research Establishment, Harwell.

Cavendish Laboratory,
Cambridge.
24th May 1951.

G. A. Jones.
D. H. Wilkinson.

Nuckolls, R. G., Bailey, C. L., Bennett, W. E., Bergstralh, T., Richards, H. T., and Williams, J. H., 1946, *Phys. Rev.*, **70**, 805.

Angular Distributions of the Two Long-Range Neutron Groups of the Reaction $^{16}O(d, n)^{17}F$

The angular distributions of charged particles emitted by certain light elements subject to deuteron bombardment have recently been published by several authors. Previous to this communication there have been no reports on the angular distributions of separated neutron groups. Using the photographic plate technique, we have investigated the neutron spectra and angular distributions of a number of light elements bombarded by 8 MeV. deuterons. In this note we present the angular distributions of the two long-range neutron groups from the reaction $^{16}O(d, n)^{17}F$. A detailed account of the experiment will be published elsewhere.

A lead peroxide target of thickness 0·15 MeV. deposited on a thick gold backing was bombarded by the 8 MeV. deuteron beam of the Liverpool 37-in. cyclotron. Twenty photographic plates, of emulsion thickness 400 μ, were orientated at 5° intervals about the target, and simultaneously irradiated. From measurements on the pjates ranging from angles of $-5°$ to 55° with respect to the incident deuteron direction, we were able to establish the existence of two long range neutron groups. These correspond to the ground state and a level of the residual nucleus ^{17}F at $0{\cdot}53 \pm 0{\cdot}06$ MeV. The Q-value for this reaction was found to be $-1{\cdot}51 \pm 0{\cdot}05$ MeV., and from this the mass of ^{17}F was calculated to be $17{\cdot}007398 \pm 0{\cdot}00005$ mass units using the mass of the neutron and deuteron as given by Bethe (1947).

The angular distributions of the neutron groups were determined by measuring the total number of tracks belonging to these two groups in a known volume of emulsion. After correcting for the variation with energy of the n–p scattering cross section, the results were transferred to the centre-of-mass system and plotted as shown in the Figure. The

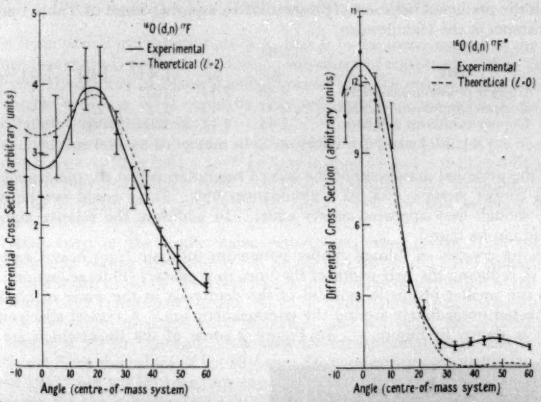

theoretical curves were calculated by H. Newns on the basis of the theory of Bhatia and Huang (unpublished). Also, Butler (private communication) obtained similar curves by applying his theory (Butler 1950). In both cases the agreement was achieved only by assuming the angular momentum l of the absorbed proton to be 2 in the case of the ground state and zero for the first excited state. Since the ground state of ^{16}O has spin zero and even parity, then the ground state of ^{17}F must have spin 3/2 or 5/2 and even parity, and the first excited state must have spin $\frac{1}{2}$ and even parity.

We conclude by pointing out the similarity between the mirror nuclei ^{17}O and ^{17}F. The observed level (0·53 MeV.) in ^{17}F presumably corresponds to the 0·876 MeV. level in ^{17}O. The experiment of Burrows, Gibson and Rotblat (1950) on the angular distribution of the protons from the reaction ^{16}O(d, p)^{17}O led them to exactly similar conclusions regarding the spins and parities of the ground and first excited state of ^{17}O. Recently the spin of the ground state of ^{17}O has been reported by Alder and Yu (1951) using the nuclear induction method to be 5/2; it therefore appears likely that the spin of the ground state of ^{17}F may also be 5/2.

George Holt Physics Laboratories,
University of Liverpool.
22nd May 1951.

F. A. El-Bedewi.
R. Middleton.
C. T. Tai.

Alder, F., and Yu, F. C., 1951, *Phys. Rev.*, **81**, 1067.
Bethe, H. A., 1947, *Elementary Nuclear Theory* (New York: Wiley and Sons).
Burrows, H. B., Gibson, W. M., and Rotblat, J., 1950, *Phys. Rev.*, **80**, 1095.
Butler, S. T., 1950, *Phys. Rev.*, **80**, 1095.

Quadrupole Moments of Copper 63 and 65

Hyperfine structure in the paramagnetic resonance spectrum of the copper Tutton salts has been extensively studied in this laboratory since its discovery by the late Dr. R. P. Penrose (1949). Ingram (1949) found that in addition to magnetic interaction between the electrons and the nucleus, another effect was present which was interpreted as due to an electric quadrupole interaction. Abragam and Pryce (1951) have shown how both this and the anomalous magnetic interaction can be accounted for theoretically. A brief review of the experimental results is presented in this letter.

The observed spectra have been interpreted in terms of the usual Hamiltonian

$$\mathcal{H}=\beta\{g_{\parallel}H_zS_z+g_{\perp}(H_xS_x+H_yS_y)\}+AS_zI_z+B(S_xI_x+S_yI_y)+Q\{I_z^2-\tfrac{1}{3}I(I+1)\}-\gamma\beta_N H.I.$$

By the use of crystals where most of the copper ions are replaced by diamagnetic zinc ions, the half-width at half intensity of the lines can be reduced to about six gauss. Although the spectrum is by no means fully resolved (cf. Ingram 1949), its principal features are in accord with the predicted behaviour (Bleaney 1951), and the values of Table 1 are obtained for the constants in the Hamiltonian.

Table 1

Salt	$g_{\parallel}$	$g_{\perp}$	$\lvert A\rvert$	$\lvert B\rvert$	$\lvert Q\rvert$
Copper potassium sulphate	2·45	2·14	103	35	11
Copper ammonium sulphate	2·47	2·13	132	20	9
Copper rubidium sulphate	2·45	2·12	120	9	11

$\lvert A\rvert$, $\lvert B\rvert$ and $\lvert Q\rvert$ values are to be multiplied by 10^{-4} cm^{-1}.

One of the principal drawbacks of the lack of resolution is that the quadrupole moments of the two copper isotopes (63, 65 : abundances 69%, 31%) could not be determined accurately, though they appeared nearly equal. In addition, the relative signs of A, B and Q could not be found.

By growing crystals of diluted copper potassium sulphate from heavy water we have succeeded in reducing the half-width of the lines to 2 gauss. This reduction is achieved because of the smaller magnetic moment of the deuterons in the water of crystallization, which is located immediately around the paramagnetic ion. A typical spectrum at 3 cm. wavelength is shown in Figure 1. In Figure 2 some of the lines which are normally

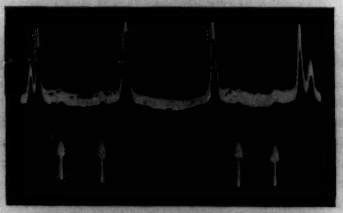

Figure 1. Hyperfine structure of the electronic $\frac{1}{2}\leftrightarrow-\frac{1}{2}$ transition showing the strong transitions $(\frac{1}{2}, m)\leftrightarrow(-\frac{1}{2}, m)$ in which the nuclear magnetic quantum number m does not change. The $m=3/2$ and $m=-3/2$ lines of the less abundant isotope 65 are clearly resolved at each end of the spectrum. Weak transitions (see Figure 2) in which m changes by 1 are indicated by arrows.

Figure 2. The $(\frac{1}{2}, 3/2)\leftrightarrow(-\frac{1}{2}, \frac{1}{2})$ and $(\frac{1}{2}, \frac{1}{2})\leftrightarrow(-\frac{1}{2}, 3/2)$ transitions at high resolution and intensity. The lines due to the less abundant isotope 65 are displaced to higher fields owing to its larger nuclear magnetic moment.

forbidden (if $Q=0$) are shown, the smaller lines being due to the isotope 65. These are shifted outwards owing to its larger nuclear magnetic moment. From a number of such spectra we have determined the ratio of the quadrupole terms Q_{63}/Q_{65} as $1{\cdot}08\pm0{\cdot}02$, all the values lying within this range. This is in agreement with the value $1{\cdot}081\pm0{\cdot}003$ obtained by Becker and Krüger (1951) from the quadrupole splitting of the nuclear resonance spectrum of copper in a diamagnetic salt. The ratio of the magnetic hyperfine splittings parallel to the tetragonal axis of the copper ion is $1 : 1{\cdot}069\pm0{\cdot}003$, in agreement with the nuclear resonance ratio $1 : 1{\cdot}0711\pm0{\cdot}0002$ (Pound 1948).

The relative signs of A, B and Q have been found through the direct effect of the external magnetic field on the nuclear magnetic moment, which produces a small asymmetry in the spectrum (see Bleaney 1951). To obtain a more pronounced effect, measurements were made at 1·2 cm. wavelength (higher field). These showed that B and Q had the same sign for both isotopes, and were opposite in sign to A. This is in agreement with the theory of Abragam and Pryce and we may adopt their actual signs for these coefficients. The results on the heavy water crystal are summarized in Table 2; the values of the coefficients are more accurate than those in Table 1, as the magnetic field was calibrated by means of a proton resonance.

Table 2. Coefficients for $CuK_2(SO_4)_2 \cdot 6D_2O$

Isotope	$g_{\parallel}$	$g_{\perp}$	A	B	Q
63	2·42	2·12	−96·9	+34·0	+10·3±1
65	2·42	2·12	−103·5	+36·3	+9·5±1

A, B and Q values are to be multiplied by 10^{-4} cm^{-1}.

There is some variation in the values of $g_{\perp}$ and B in the plane normal to the tetragonal axis, showing that there is present a rhombic component of anisotropy. The values given refer to the crystallographic *ab*-plane, which coincides with the magnetic K_1K_2 plane in this salt. No similar variation in Q could be detected, and the error given is such that all measurements lay within this range.

Application of the theory of Abragam and Pryce shows that the values of the nuclear quadrupole moments are $-0{\cdot}12_7 \pm 0{\cdot}01 \times 10^{-24}$ cm^2 for isotope 63 and $-0{\cdot}11_7 \pm 0{\cdot}01 \times 10^{-24}$ cm^2 for isotope 65. Previous values were $-0{\cdot}1 \pm 0{\cdot}1$ (Schuler and Schmidt 1936), later re-calculated as $-0{\cdot}26 \pm 0{\cdot}10$, $-0{\cdot}15 \pm 0{\cdot}10$ (Brix 1949) for the isotopes 63 abd 65 respectively.

The crystals used in the heavy water experiments were grown from two different solutions containing copper and zinc in the ratios 1 : 1,000 and 1 : 200 respectively. No difference in line width could be observed, indicating that the contribution to the half-width from other copper ions is less than 1 gauss. At 90° K. a small increase in line width, compared with 20° K. is attributed to sign–lattice relaxation, and the value hence obtained for the relaxation time τ is 5×10^{-8} second. Allowing for experimental error, this is not significantly different from the values of 9×10^{-8} sec., for copper potassium sulphate (Broer and Kemperman 1947) and 6×10^{-8} sec., for copper ammonium sulphate (Gorter 1947). The latter values are for the concentrated salts; it appears therefore, that in this case there is no great change in γ on dilution, unlike the results of Benzie (1951) at helium temperatures.

Clarendon Laboratory,
Oxford.
13th June 1951.

B. Bleaney.
K. D. Bowers.
D. J. E. Ingram.

Abragam, A., and Pryce, M. H. L., 1951, *Proc. Roy. Soc.* A, **206**, 164.
Becker, G., and Krüger, H., 1951, *Naturwissenschaften*, **38**, 121.
Benzie, R. J., 1951, *Proc. Phys. Soc.* A, **64**, 507.
Bleaney, B., 1951, *Phil. Mag.*, **42**, 441.
Brix, P., 1949, *Z. Phys.*, **126**, 725.
Broer, L. J. F., and Kemperman, J., 1947, *Physica*, **13**, 465.
Gorter, C. J., 1947, *Paramagnetic Relaxation* (New York: Elsevier).
Ingram, D. J. E., 1949, *Proc. Phys. Soc.* A, **62**, 664.
Penrose, R. P., 1949, *Nature, Lond.*, **164**, 116.
Pound, R. V., 1948, *Phys. Rev.*, **73**, 523.
Schuler, H., and Schmidt, T., 1936, *Z. Phys.*, **100**, 113.

REVIEWS OF BOOKS

Molecular Spectra and Molecular Structure: Vol. I. *Spectra of Diatomic Molecules*, by GERHARD HERZBERG. Pp. xv+658. 2nd Edition. (New York: Van Nostrand; London: Macmillan, 1950.) $9.75; 73*s*. 6*d*.

The first edition of Professor Herzberg's book on the spectra and structure of diatomic molecules appeared in 1939 and is well known as an excellent text and reference book on the subject. The new edition has been revised, extended and brought up to date, not simply by the addition of new paragraphs, but by a most thorough process of alterations and improvements affecting almost every page.

In spite of the considerable increase in the material, the book has fortunately retained its character as a textbook. The author has achieved this by making a clear distinction between paragraphs dealing with fundamentals and paragraphs dealing with less essential details, and by marking this distinction by means of different types of print. An outstanding feature of this book is the extreme thoroughness and care with which it has been written, and the attention given to every detail.

New sections on microwave spectra, hyperfine structure in molecular spectra and intensities of electronic transitions have been added. The list of references has been brought up to date, and an appendix covering 80 pages contains a complete table of molecular constants for excited as well as for normal states.

The new edition of this work by one of the first authorities on the subject will be warmly welcomed by many physicists and chemists, and will prove invaluable to all those whose work is connected with molecular spectra and molecular structure. H. K.

Negative Ions, by H. S. W. MASSEY. (Cambridge Monographs on Physics.) Pp. x+136. 2nd Edition. (Cambridge: University Press, 1950.) 12*s*. 6*d*.

The first edition of this excellent monograph was reviewed in the *Proceedings of the Physical Society* in 1938. This second edition is better bound with hard covers, has a bibliography, and is nearly 30% larger, the increase being due mainly to the complete re-writing of the last chapter on modern developments in the study of negative ions.

The first four chapters closely follow those of the first edition apart from small modifications due to later work. Chapter I discusses the theory and structure of negative atomic ions and describes experimental determinations of electron affinities. (There are two small misprints in the last paragraph: 10^{12} being printed for 10^{-12}, and O^- being printed for O^{--}.) Chapter II discusses the nature of molecular ions in general, and of the simple cases H_2^-, O_2^-, halogen ions and OH^- in particular. Chapter III deals with modes of formation of negative ions: it discusses fully the various processes of electron attachment. Calculations are given of free-electron radiative capture by atoms of hydrogen and of oxygen, and capture by Na, Hg, Cl is also considered: then follows a discussion of the possibility of experimental confirmation of these theoretical results. Attachment in three-body collisions is next examined, and attachment by molecules (a form of three-body problem) is discussed. The two groups of experiments on electron attachment are then described: (i) the homogeneous electron beam method of Tate and Lozier and the mass spectrograph of Hagstrum and Tate at low pressures; (ii) the electron group methods such as the filter method of Loeb and Cravath and the diffusion method of Bailey at higher gas pressures. A good review of the main results is given. This important chapter closes with a survey of other modes of ion formation by capture of bound electrons from neutral atoms or metals. The next chapter discusses processes of electron detachment in the light of the principle of detailed balancing. This discussion is mainly theoretical, and reflects the lack of experimental data in this field: in fact, one of the features of this book is the emphasis it lays on the need for more experimental data on these collisional processes, since many of the views now held are, of necessity, conjectural.

Detachment is more difficult to study experimentally than attachment, as the main desideratum is a high value of the ratio of negative ion to electron concentration, whereas for attachment the more readily obtained low values of this ratio are required.

The last chapter occupies more than a quarter of the book, and deals with applications of negative ions and interpretation of collisional processes, whether in glow discharge tubes or in the terrestrial or stellar atmospheres. Some possible effects of negative ions in glow discharges are outlined qualitatively. Many new data on the earth's upper atmosphere are included, and a careful summary of its properties is given in tabular form. The Chapman theory of ionized layer formation is outlined. The influence of negative ions in solar and stellar atmospheres is discussed, and it is shown in some detail how negative ions of hydrogen practically determine the spectral distribution of solar continuous radiation over the observable frequency range.

This book is very readable, and can be highly recommended for its treatment of the subject.

F. LLEWELLYN JONES.

CONTENTS FOR SECTION B

	PAGE
Dr. M. BLACKMAN. Diffraction from a Bent Crystal	625
Dr. M. BLACKMAN. Diffraction from a Curved Linear Lattice	631
Dr. J. M. COWLEY, Dr. A. L. G. REES and Mr. J. A. SPINK. The Morphology of Zinc Oxide Smoke Particles	638
Dr. J. CORNER and Mr. E. D. PENDLEBURY. The Coagulation and Deposition of a Stirred Aerosol	645
Dr. R. Q. TWISS. On Oscillations in Electron Streams	654
Dr. R. E. B. MAKINSON, Dr. P. C. THONEMANN, Mr. R. B. KING and Mr. J. V. RAMSAY. Dielectric Constant and Electron Density in a Gas Discharge	665
Dr. K. W. PLESSNER. Conductivity, Hall Effect and Thermo-electric Power of Selenium Single Crystals	671
Dr. K. W. PLESSNER. Conductivity and Hall Effect of Micro-crystalline Selenium containing Iodine Impurities	681
Dr. C. A. HOGARTH. Some Conduction Properties of the Oxides of Cadmium and Nickel	691
Dr. W. EHRENBERG and Dr. J. HIRSCH. The Conductivity–Temperature Characteristics of Lead Sulphide: The Influence of Oxygen and of the Rate of Heating	700
Dr. R. BECHMANN and Mr. P. L. PARSONS. Piezoelectric Behaviour of Partially Plated Square Plates Vibrating in Contour Modes	706
Dr. R. S. LONGHURST. The Astigmatic Correction of Telescopes	713
Letters to the Editor:	
Dr. J. A. CLEGG and Mr. R. L. CLOSS. Plasma Oscillations in Meteor Trails	718
Dr. J. M. CASSELS, Mr. J. M. DICKSON and Dr. J. HOWLETT. Multiple Traversal of Cyclotron Targets: an Extension to the Theory	719
Reviews of Books	720
Contents for Section A	726
Abstracts for Section A	727

ASTRACTS FOR SECTION B

Diffraction from a Bent Crystal, by M. BLACKMAN.

ABSTRACT. The diffraction of plane waves by a bent crystal is considered. It is shown that the peak of the diffracted ' intensity ' can be represented in reciprocal space by an arc, the limits of the arc being the total angle of bend of the crystal. The ' intensity ' function in reciprocal space has been studied numerically in a particular case, and it is shown that both ' intensity ' and shape change with order.

Diffraction from a Curved Linear Lattice, by M. BLACKMAN.

ABSTRACT. The diffraction of plane waves by a curved linear lattice is studied by calculating the ' intensity ' in reciprocal space. It is shown that the regions of high intensity are arc-shaped in character. Further, the intensity associated with a particular order of diffraction (considered as a function of the cylindrical radial coordinate in a plane parallel to that containing the curved lattice) can be represented by the square of a Bessel function of high index in the neighbourhood of the main peak, but dies off sharply on that side of the peak furthest from the origin. This ' cut-off ' is characteristic of the total angle of bend as long as this angle of bend is less than 180°. The zero order diffraction peak is of a different type from the others, but is similar to the peak characteristic of a straight chain except for angles of bend greater than 180°.

The Morphology of Zinc Oxide Smoke Particles, by J. M. COWLEY, A. L. G. REES and J. A. SPINK.

ABSTRACT. Single-crystal electron diffraction patterns with doubled spots obtained from zinc oxide smoke particles originate from pairs of thin sheets which are commonly seen in electron micrographs of this material joining up the members of a group of four spines. The plane of each sheet is parallel to a $(10\bar{1}0)$-type lattice plane. The sheets are continuous with one of the spines and spaced at 120° intervals around this spine. The other three spines, and additional spines which grow from corners of the sheets, are related to this one spine and the sheets by twinning on $(11\bar{2}2)$ planes. Intensity measurements of single-crystal patterns allow the shape-transform and thickness of the sheets to be deduced. Sharp lines and extra spots indicate the occasional presence of lattice imperfections in the form of parallel faults. Electron micrographs show wide deviations from the idealized group of spines and sheets.

The Coagulation and Deposition of a Stirred Aerosol, by J. CORNER and E. D. PENDLEBURY.

ABSTRACT. Langstroth and Gillespie have determined experimentally the rate of change of particle number in ammonium chloride smokes in still and moving air, and have analysed their results into deposition on the walls and coagulation inside the aerosol cloud. It is shown here that the empirical constants describing these processes can be explained on theoretical grounds, both in order of magnitude and as regards their variation with the rate of stirring.

On Oscillations in Electron Streams, by R. Q. TWISS.

ABSTRACT. A critical discussion is given of the conventional procedure for determining whether a particular electron stream is unstable. It is shown that in some cases where this analysis suggests instability the stream is stable, while in others, where instability does occur, neither the frequency nor the rate of build up of oscillations are as predicted. The physical causes of instability in an electron stream are also considered.

Dielectric Constant and Electron Density in a Gas Discharge, by R. E. B. MAKINSON, P. C. THONEMANN, R. B. KING and J. V. RAMSAY.

ABSTRACT. Measurements have been made of the impedance at frequencies of the order 1,000 Mc/s. of a coaxial transmission line terminating in a small electrode immersed in the plasma of a low pressure discharge in mercury vapour. The frequencies f chosen were in the neighbourhood of that for which the real part ϵ_1 of the dielectric constant of the space near the electrode, as given by $\epsilon_1=1-ne^2/(\pi mf^2)$ where n is the local electron density, was near zero. The effect of making a small change in the size of the electrode was also studied. The electron density in the neighbourhood of the electrode was measured by Langmuir probes. A minimum in reactance and a maximum in resistance (when plotted against discharge current) were found to indicate $\epsilon_1=0$ near the electrode, in agreement with a qualitative argument given. The possible use of such impedance measurements as a means of measuring electron density is discussed.

Conductivity, Hall Effect and Thermo-electric Power of Selenium Single Crystals, by K. W. PLESSNER.

ABSTRACT. Single crystals of selenium have been grown from the vapour phase and their conductivity and thermo-electric power were measured over a range of temperatures. The Hall effect was determined for one crystal. The conductivity obeys a relatively simple exponential law $\sigma=\sigma_0 \exp(-eE/kT)$, with $eE=0{\cdot}13$ ev. and the room temperature conductivity between 10^{-5} and $0{\cdot}5\times10^{-6}$ ohm^{-1} cm^{-1}. Both thermo-electric power and Hall effect rise slightly with increasing temperature, indicating a fall in the current carrier concentration. Values calculated from thermo-power and Hall effect agree reasonably well, and give about 10^{14} positive holes per cm^3. Because of an experimentally established correlation between thermo-power and conductivity, differences in conductivity between various crystals are ascribed to different hole concentrations. Deviations from Ohm's law, the rapid increase in mobility with temperature and its low absolute value (about $0{\cdot}14$ cm^2/v.sec. at room temperature) all point to the existence of potential barriers within the crystals. It is shown that a range of barriers of different heights could explain the observed behaviour. The conductivity is anisotropic (ratio about 10 : 1), whereas the thermo-power is not.

Conductivity and Hall Effect of Micro-crystalline Selenium containing Iodine Impurities, by K. W. PLESSNER.

ABSTRACT. The conductivity and Hall effect of micro-crystalline selenium have been measured as a function of iodine content under two different conditions of crystallization, over a range of temperatures. The conductivity increases with iodine concentration, a maximum being reached at a concentration of about $0{\cdot}03$ atomic per cent. The Hall effect shows this increase to be due to an increasing mobility, the carrier concentration remaining nearly constant. The effect of carrying out the first crystallization of the amorphous Se at 175° c. instead of 110° c. is to reduce the conductivity by a factor of ten. This is due to reductions in both mobility and current carrier concentration. With increasing temperature the mobility rises and the carrier concentration falls, the product of the two resulting in a rising conductivity with samples crystallized at 175° and a slightly falling conductivity with samples crystallized at 110° c. The results are discussed in terms of the grain structure of the material. Microscopic examination has shown that the grain size is different for different crystallization temperatures and it is suggested that larger crystals contain a smaller density of acceptor centres. The fall in carrier concentration with increasing temperature is thought to be due to the relief of stress set up due to anisotropic contraction when the material is cooled from the annealing temperature. The low absolute value of the mobility and its rise with temperature are ascribed to intergranular high resistance barriers.

Some Conduction Properties of the Oxides of Cadmium and Nickel, by C. A. HOGARTH.

ABSTRACT. The electrical conductivity and thermo-electric power of specimens of cadmium oxide and nickel oxide are measured as functions of temperature and of oxygen pressure, and the results are found to agree in general form with theories previously proposed by C. Wagner and by the present author. The results are used to verify Wagner's concept of a differential thermo-electric circuit, and a band model for CdO is proposed.

The Conductivity–Temperature Characteristics of Lead Sulphide: The Influence of Oxygen and of the Rate of Heating, by W. EHRENBERG and J. HIRSCH.

ABSTRACT. In general, the conductivity–temperature curves of impurity semiconductors should be affected by the rate of heating. An arrangement is described by which such curves can be recorded with rates of heating up to 5,000 centigrade degrees per second. Extensive tests made on lead sulphide films in an oxygen atmosphere lead to conclusions about the stages of oxidation.

Piezoelectric Behaviour of Partially Plated Square Plates Vibrating in Contour Modes, by R. BECHMANN and P. L. PARSONS.

ABSTRACT. In extension of a previous paper, the piezoelectric behaviour of partially plated square plates vibrating in contour modes is used to check the theoretical solution for the motion. For the longitudinal mode 2 recently described by Ekstein a particularly sensitive test of the theory is possible. A critical electrode arrangement should cause the piezoelectric excitation to vanish. This is confirmed by experiment.

The Astigmatic Correction of Telescopes, by R. S. LONGHURST.

ABSTRACT. It is shown theoretically that if a telescope has positive field curvature the best possible image on the Gaussian plane is obtained by making the tangential field flat.

Magnification = 58·5 ×

(*a*) Maze pattern found after electrolytic polishing but before annealing.

(*d*) (111) plane.
Field 26·5 oersteds.

(*b*) Line pattern on (111) plane.
Field 16·3 oersteds along [110] direction→

(*e*) Complicated closure pattern on side of crystal, i.e. (112) plane.
Field parallel to [110] direction→

(*c*) (111) plane.
Field 25·0 oersteds→

(*f*) Pattern on (112) plane showing branching at grain boundary.

Figure 1.